NASA Technical Paper 1736

Evaluation of a Computer-Generated Perspective Tunnel Display for Flight-Path Following

Arthur J. Grunwald, James B. Robertson,
and Jack J. Hatfield

DECEMBER 1980

NASA

NASA Technical Paper 1736

Evaluation of a Computer-Generated Perspective Tunnel Display for Flight-Path Following

Arthur J. Grunwald, James B. Robertson,
and Jack J. Hatfield
Langley Research Center
Hampton, Virginia

National Aeronautics
and Space Administration

**Scientific and Technical
Information Branch**

1980

SUMMARY

The purpose of this study was to evaluate the use of a computer-generated perspective tunnel display for following a strongly curved flight path. The display was evaluated by monitoring pilot performance in a fixed-base simulator with the vehicle dynamics of a CH-47 tandem-rotor helicopter, linearized about a 33.5-m/sec (110 ft/sec) forward velocity and a level flight trim condition. Superposition of the predicted future vehicle position on the tunnel image was also investigated to determine whether, and to what extent, it contributes to better system performance (the best predicted future vehicle position was sought).

Three types of simulator experiments were conducted: following a desired trajectory in the presence of disturbances; entering the trajectory from a random position, outside the trajectory; and detecting and correcting failures in automatic flight. Two other display configurations were considered for comparison: a tracking display which incorporates future trajectory information by displaying the predicted future error, and combined vertical and horizontal situation displays containing aircraft attitude information and trajectory map information, respectively.

The tunnel display with superimposed predictor/director symbols was shown to be a very successful combination, which outperformed the other two displays in all three experiments. A prediction time of 4 to 7 sec was found to optimize trajectory tracking for the given vehicle dynamics and flight condition. Pilot acceptance of the tunnel plus predictor/director display was found to be favorable, and the time the pilot needed for familiarization with the display was found to be relatively short.

The simulator study was conducted on the Langley Real-Time Simulation System using a fixed-base simulator cabin with helicopter controls. An Adage Graphics Terminal, the AGT/130, was programmed to generate the various display configurations. The Control Data CYBER 175 computer system at the Langley Research Center was used in the real-time mode for simulating the vehicle dynamics and for the on-line and off-line data processing.

The feasibility of the tunnel display for operation in actual flight was demonstrated at NASA Wallops Flight Center, Wallops Island, Va. A modified CH-47 helicopter served as the flight vehicle. The tunnel image provided sufficient control information for following the trajectory smoothly, and the deviations from the desired trajectory remained within reasonable limits.

INTRODUCTION

In a conventional helicopter approach under instrument flight rules (IFR), control information (such as position, rate, and attitude information) is presented to the pilot by a set of electromechanical flight instruments. On most instruments, the control variable is explicitly displayed as the deviation of a pointer from an indicated reference line. However, this information is rather symbolic and shows little resemblance with the visual world the pilot is used to. Furthermore, several instruments are used, and the pilot must derive the control information by scanning them. Thus, the conventional IFR approach requires a high level of pilot proficiency and imposes a high workload. In order to minimize the probability of human errors, the approach path generally is kept simple, with a limited number of straight and curved sections.

In the advanced display concept under investigation, control information is presented to the pilot in a format similar to the "through-the-windshield" visual field. A simplified computer-generated perspective image of the visual field is presented to the pilot as if it were a "tunnel in the sky," in which the three-dimensional (3-D) approach path is to be followed. In contrast with conventional instrument displays, the control information is integrated into one format, natural to the pilot. This characteristic makes the display very suitable for following, with great accuracy, approaches which are complicated, strongly curved, and steep. This type of approach might become a necessity in heavily congested fixed-wing and helicopter traffic areas.

Use of trade names or names of manufacturers in this report does not constitute an official endorsement of such products or manufacturers, either expressed or implied, by the National Aeronautics and Space Administration.

SYMBOLS AND ABBREVIATIONS

A_ℓ, A_v lateral or vertical not-augmented system matrix

$\hat{A}_\ell, \hat{A}_v$ lateral or vertical augmented system matrix, SAS engaged

a_ℓ, a_v inertial accelerations of vehicle along y_b-axis and z_b-axis, respectively, m/sec^2

a_t centripetal trajectory acceleration, m/sec^2

B_ℓ, B_v lateral or vertical input matrix

cov( )	autocovariance
D	predictor distance, m
d_ℓ, d_v	lateral or vertical deviation from trajectory, m
d_p	preview term, m, see equation (A34)
d_γ	lateral intercept angle of velocity vector and trajectory direction, rad
d_θ	vertical intercept angle of vehicle axis and trajectory direction, rad
d_ψ	lateral intercept angle of vehicle axis and trajectory direction, rad
F_ℓ, F_v	lateral or vertical feedback matrix
f(t)	lateral trajectory curvature, m^{-1}
f_p, g_p	roll rate on cyclic SAS gain and feedback, respectively
f_{pr}, g_{pr}	roll rate on differential, cyclic SAS gain and feedback, respectively
f_q, g_q	pitch rate on SAS gain and feedback, respectively
f_r, g_r	yaw rate on SAS gain and feedback, respectively
f_u, g_u	perturbed forward-velocity SAS gain and feedback, respectively
f_v, g_v	sideslip SAS gain and feedback, respectively
f_θ, g_θ	pitch SAS gain and feedback, respectively
g	acceleration due to gravity, m/sec^2
$H_{\delta_s}^{d_\ell}(s), H_{\delta_c}^{d_v}(s)$	transfer function relating deviation to control input
I_{xx}, I_{yy}, I_{zz}	vehicle moments of inertia about x_b-axis, y_b-axis, and z_b-axis, respectively, $kg\text{-}m^2$

I_{xz}	vehicle product of inertia in $x_b z_b$-plane, kg-m^2
K_{d_ℓ}	lateral gain, stability augmentation system
K_{d_v}	vertical gain, stability augmentation system
$k_{b\ell}, k_{bv}$	gain of biases on estimates of v and w, respectively, see equations (7) and (8)
k_{br}	undesired rudder input gain, see equation (9)
k_ℓ, k_v	lateral or vertical automatic control system gain, see equations (3) and (4)
$k_{\ell p}$	simulated roll-rate feedback failure gain, see equation (10)
k_{pv}	gain for reduction of vertical acceleration in computing vertical prediction, see equation (B5)
L, M, N	total rolling, pitching, and yawing moments about center of gravity of vehicle, N · m
m	vehicle mass, kg
p, q, r	vehicle angular velocity about x_b-axis, y_b-axis, and z_b-axis, respectively, rad/sec
R_ℓ, R_v	radius of curvature of lateral or vertical vehicle path, m
R_t	radius of curvature of lateral trajectory, m
s	Laplace operator
sc( )	deviation score for entry maneuvers, m
T_c	time elapsed between moment of manual takeover and moment of reengagement of automatic control system (correction time), sec
T_f	time of occurrence of automatic control failure, sec
T_p	prediction time, sec

T_r time elapsed between occurrence of automatic control failure and moment of manual takeover (reaction time), sec

T_{sf}, T_{sv} lateral or vertical settling time, sec

T_1, T_2 starting point and end point, respectively, of run-time range (used for computation of deviation scores)

t time

u,v,w velocity of vehicle along x_b-axis, y_b-axis, and z_b-axis, respectively, m/sec

u_N, w_N nominal trim values of u and w, m/sec

V ground speed, m/sec

$\vec{V}$ vehicle velocity vector

v_g, w_g lateral or vertical gust component, m/sec

W_f, W_v lateral or vertical disturbance matrix

X,Y,Z total aerodynamic, thrust, and gravitational forces along x_b-axis, y_b-axis, and z_b-axis, respectively, N

x_b, y_b, z_b orthogonal body-axis coordinate system, with x_b-axis pointing toward front of vehicle, y_b-axis pointing to right, and z_b-axis pointing downward

x_i, y_i, z_i orthogonal inertial coordinate system, with x_i-axis pointing to north, y_b-axis to east, and z_b-axis downward

$\vec{x}_f, \vec{x}_v$ lateral or vertical state vector

$\delta_b, \delta_c, \delta_s, \delta_r$ differential-collective, collective, cyclic, and differential-cyclic control inputs, cm

$\delta_{b,a}, \delta_{c,a}, \delta_{s,a}, \delta_{r,a}$ differential-collective, collective, cyclic, and differential-cyclic actuator inputs, cm

$\vec{\delta}_\ell, \vec{\delta}_v$	lateral or vertical control input vector
$\vec{\delta}_{s,a}, \vec{\delta}_{v,a}$	lateral or vertical actuator input vector
$\epsilon_\ell, \epsilon_v$	lateral or vertical predicted deviation from trajectory, m
ζ	damping factor
θ, ϕ, ψ	pitch, roll, and yaw attitude angles, rad
θ_N	nominal trim value of pitch attitude, rad
θ_t	downslope of trajectory, rad
λ_ℓ, λ_v	lateral or vertical displacement of predictor on screen, in screen coordinates
σ	standard deviation (root-mean-square deviation from mean)
ω_n	natural frequency, rad/sec

Abbreviations:

EADI	electronic attitude director indicator
FDRS	flight display research system
HSI	horizontal situation indicator
IFR	instrument flight rules
SAS	stability augmentation system
VAC	vehicle axis cross
VALT	VTOL approach and landing technology

An arrow over a symbol denotes a vector quantity. A dot over a symbol denotes the first derivative with respect to time. A prime denotes values generated by the automatic control system.

DISPLAY CONFIGURATION

The conceptual tunnel display is shown in figure 1. The trajectory to be followed is presented as a perspective image of a tunnel with a square cross section. The perspective appearance of the tunnel changes with the vehicle position. Positional cues are derived from this perspective appearance, while rate cues are derived from the rate of change in the appearance.

The tunnel cross section is constant and square with a scale width of 45.7 m (150 ft), which corresponds to the width of a typical runway. The Adage Graphics Terminal is programmed to draw (see fig. 2(a)) tunnel squares (1) and cornerlines (2). An experimental configuration was chosen in which the tunnel squares are drawn a scale distance of 91.4 m (300 ft) apart. In order to augment the impression of forward velocity, the cornerlines are dashed. Only the five squares nearest to the vehicle are drawn. Thus, the number of lines drawn is substantially reduced, which prevents cluttering of the display. The tunnel is shown in the viewing range from 0 to 762 m (2500 ft). The maximum horizontal and vertical field of view is from $+45^{o}$ to -45^{o}. The tunnel image generated is square and is shown on the 33-cm (13-in.) display monitor, with aspect ratio 4:3 (horizontal:vertical). The tunnel image magnification is 0.165 for an average viewing distance of 76.2 cm (30 in.) from the monitor. Pitch scales (3) and pitch pointers (5) are located at the left and right sides of the image, and a roll scale (4) is located at the top. Pitch motion is also visualized by an equivalent rotation of the optical axis. For small angles, this is equivalent to a vertical displacement of 0.22 cm per degree pitch angle of the tunnel image. The pitch pointer and the tunnel image are displaced, while the pitch scales remain vertically fixed.

Digital readouts of magnetic heading (MAG) (10) and airspeed (TAS) (11) are displayed in boxes on the vertical centerline at the top and bottom of the image, respectively. (See fig. 2(a).) These boxes also provide a reference for estimating the center of the image. Note that a large area in the center of the display is kept clear of symbology to prevent cluttering the tunnel image.

In addition to the basic tunnel display, several other displays were used in the evaluation, either as additions to the tunnel display to improve pilot performance or as primary displays for purposes of comparison. The following display configurations were investigated.

Roll-Stabilized Tunnel (Configuration A)

In visualizing the roll motion, two versions were considered. In the first version (fig. 2(a)), the tunnel image, pitch scales, horizon, and roll scales are roll-stabilized, and the bank angle ϕ is visualized by rotating the wing bars (7) and the roll pointer (9), in fixed-wing aircraft. This image does not conform to the through-the-windshield visual field and can only be used in head-down type displays.

Rolling Tunnel (Configuration B)

In the second version (see fig. 2(b)), the tunnel image is rotated with the pitch and roll scales, and the aircraft reference symbology remains stationary. Note that, in this configuration, the pitch motion results in an image displacement perpendicular to the rotated horizon represented by the pitch pointers.

Predictor/Director Display (Configuration C)

In order to obtain the rate information required, it is necessary to estimate the predicted vehicle path. As discussed in references 1 and 2, peripheral vision is utilized in estimating the vehicle path from the apparent motion in the visual field. Since peripheral vision is partially missing due to the limited size of the monitor, this estimation process is expected to be limited. A possible solution for this problem is to display the predicted vehicle position explicitly on the tunnel image. A display was designed in which a flight-path predictor and a flight-path director are displayed. (See fig. 2(c).) The predictor is displayed as a cross located on the predicted flight path at a distance D ahead of the vehicle. The director is displayed as a square with its center located on the desired flight path a distance D ahead of the vehicle. The outer dimensions of the cross and the square are equal (i.e., width: 45.7 m (150 ft)). The distance D can be varied, and the apparent size of the cross and square on the image varies accordingly. The predictor cross remains parallel to the vehicle wing line at all times, and thus, will remain upright in the roll version and rotate in the roll-stabilized version. With this display, the control task reduces to a simple tracking task.

In a well-defined trajectory-following task, in the presence of random disturbances, and for a well chosen prediction time T_p, this predictor/director (i.e., predictor cross plus director square) display is expected to perform equally well as a more complex tunnel plus predictor/director (i.e., tunnel plus predictor cross plus director square) display. However, the predictor/director display yields the following shortcomings:

(1) Without the tunnel image, the pilot has no knowledge of the position or attitude of the vehicle with respect to the tunnel. Thus, the pilot has no way of judging how well the predictor/director performs in following the trajectory.

(2) With the predictor/director display, the pilot is forced to use the control error between the cross and the square. With the tunnel plus predictor/director display, the pilot has the option of partially or fully rejecting the information provided by the predictor/director and relying more on the tunnel image.

(3) It is clear from shortcoming (2) that the predictor/director display will perform adequately only in the well-defined stationary control task for which T_p is adjusted correctly. However, the control task generally is not stationary and is subject to large variations in velocity, disturbance spectrum, stability derivatives, etc.

Tunnel Plus Predictor/Director (Configuration D)

This configuration (see fig. 2(d)) is a combination of the roll-stabilized tunnel (configuration A) and a superimposed predictor/director (configuration B). The predictor cross (12) shows the predicted vehicle position at a distance D ahead of the vehicle. The bright director square (13) represents the desired future vehicle position at distance D. In contrast with the squares of the tunnel, this square moves along with the vehicle at a fixed distance D ahead.

Vehicle Axis Cross (VAC)/Director (Configuration E)

In this display (see fig. 2(e)), the cross represents the vehicle axis at a distance D ahead. The cross is locked in the center of the image and rolls with the vehicle. The director square is identical to the director square of configuration C.

Tunnel Plus Vehicle Axis Cross/Director (Configuration F)

This configuration (see fig. 2(f)) is a superposition of the tunnel (configuration A) and the VAC/director (configuration E).

Combination Vertical and Horizontal Situation (CVHS) Displays (Configuration G)

In this configuration (see figs. 2(g) and 2(h)), the information of conventional electromechanical instruments is presented on two monitors. The configuration is not intended as a new development, but serves rather as a baseline for comparing conventional with more advanced display concepts. The upper monitor (fig. 2(g)) shows the horizon bar (1), pitch scales (2), roll scale (3), fixed vehicle axis reference cross (4), wing line (5), vertical speed indicator (6), actual altitude (7), commanded altitude (8), and digital read outs of magnetic heading (9) and airspeed (10). In addition to this, the actual lateral and vertical deviation is visualized by the square (11), which is of the same size as the vehicle reference cross (4) and which corresponds to the apparent size of the tunnel cross section 137 m (450 ft) ahead of the vehicle. A displacement of the square, equal to the width of the square, corresponds to a deviation of 45.7 m (150 ft).

On the lower monitor (fig. 2(h)), the horizontal situation is shown with vehicle reference symbol (12), which remains stationary, and a moving map (13), which shows a plan view of the desired trajectory.

VEHICLE MODEL

A linear time-invariant vehicle model, derived from reference 3, was used in the calculation of vehicle motion. The longitudinal and lateral dynamics and kinematics were assumed to be fully decoupled and linearized. The stability derivatives used in this model are valid for relatively small perturbations about a trim condition in which the vehicle is in a level flight with a commanded null velocity of $V = 33.5$ m/sec (110 ft/sec). A detailed description of the vehicle model and the state equations for the nonaugmented lateral and longitudinal dynamics are given in appendix A. The lateral and longitudinal stability derivatives are given in table 1.

EXPERIMENTAL EVALUATION

Objectives of the Experimental Program

The objectives of the experimental program are:

(1) To determine whether the three-dimensional tunnel image provides sufficient positional, rate, and attitude information for entering and following a steep and curved trajectory in a moderate to heavy gust environment

(2) To investigate the effect of predictive information

(3) To compare the performance of the tunnel display with the performance of displays based on conventional approach instrumentation

(4) To investigate the effect of roll cues

(5) To investigate the abilities of the tunnel display in monitoring automatic approaches

Description of the Experimental System

The experimental program was carried out on the Langley Real-Time Simulation System. A functional diagram of the experimental system is shown in figure 3. A Control Data CYBER 175 computer system at the Langley Research Center was used on a time-sharing basis for the real-time digital simulation of the vehicle dynamics. The computed vehicle motions were imparted to an Adage Graphics Terminal, the AGT/130, which was programmed to generate images of the various display configurations. These images were displayed on two display monitors, mounted one above the other, in a fixed-base simulator cabin equipped with helicopter controls (fig. 4). Vehicle motions, thus presented on the cabin display monitors, were utilized by the pilot to generate the control commands, which were imparted to the CYBER computer system.

Prior to each experimental run, the experimental conditions, such as display parameters, run control parameters, initial conditions, and disturbances, were set at the CYBER 175 console. On-line data processing included the computation of actual and predicted deviations from the trajectory as well as the computation of running averages of these deviations, of the vehicle motions, and of the control commands.

Note that all display computations have been performed by the Adage Graphics Terminal on a stand-alone basis, without interfacing with the CYBER 175 computer. The only variables transferred from the AGT/130 to the CYBER 175 were the vehicle motions and the control parameters which defined the display to be generated.

The reasons for operating the AGT/130 on a stand-alone basis are twofold:

(1) It enabled direct implementation of the display in the Flight Display Research System (FDRS) at the NASA Wallops Flight Center (ref. 4), where a real flight vehicle was used and measurements of actual vehicle motions were fed to the AGT/130.

(2) Stand-alone graphics techniques, thus developed, prepared the way for the development of techniques for onboard generation of the display with special purpose microprocessors.

The real-time simulation program was written in Fortran and used 102_8 K memory storage. A fourth-order Runge-Kutta integration scheme was used for solving the equations of motion. Integration, sampling, and averaging was at a rate of 32 Hz. Data could be recorded at 32 Hz as well. Overall computation time of one iteration amounted to 40 percent of the time interval. Data were transferred from the CYBER 175 to the AGT/130 at a rate of 32 Hz in 15-bit fixed-point format. The images generated by the AGT/130 were refreshed at 30 Hz, but the tunnel image was updated at 12 Hz.

The simulator cabin was equipped with a two-axis electrohydraulic control stick, spring loaded rudder pedals, and an unloaded, balanced, collective control lever. The range of the two-axis control stick was from +12.7 to -12.7 cm (+5 to -5 in.), and the spring torque was 0.0848 N · m (0.75 lbf · in.) for both axes. The range of the collective level was from +12.7 to -12.7 cm (+5 to -5 in.). As discussed previously, the zero-stick-force velocity of the vehicle was kept constant at 33.5 m/sec (110 ft/sec), and the forward and aft control stick motion generated a command to increase or decrease the velocity about 0.75 m/sec per cm stick deflection (6 ft/sec per in. stick deflection). The lateral control stick motion generated a roll-rate command, resulting in an initial roll rate of about 0.058 rad/sec per cm stick deflection (8.5 deg/sec per in. stick deflection). Turn coordination was carried out automatically, and the rudder pedals were not used. The vertical speed was controlled by the collective lever, geared to a vertical speed at 2.04 m/sec per cm lever deflection (17 ft/sec per in. lever deflection). Null position of the collective lever corresponded to zero vertical velocity.

The electromechanical instruments of figure 4 were not connected, and all control information was derived from the two display monitors. On the upper monitor (measuring 33 cm (13 in.) diagonally), a raster-scan image of the tunnel, or of an electronic attitude director indicator (EADI), was shown. On the lower monitor (measuring 22.9 cm (9 in.) diagonally), a horizontal situation indicator was shown in part of the experiments. The average distance from the subjects eye to the monitors was about 76.2 cm (30 in.).

Description of the Experiments

All experiments were concerned with the approach phase of the flight in the range from 4570 to 152 m (15 000 to 500 ft) from the landing point. A plan view of the desired trajectory is shown in figure 5, and the desired vertical descent profile along the trajectory is shown in figure 6. In all experiments, the forward velocity was set at 33.5 m/sec (110 ft/sec) with vertical speed, bank angle, and pitch angle initially set to zero.

The experiments were designed to cover a broad range of frequently occurring control situations. Following are discussions of the three types of experiments that were chosen.

Trajectory following in the presence of random, lateral, and vertical gust disturbances.- The pilot was instructed to minimize the lateral and vertical deviations from the trajectory with minimum control effort. Each run started from initial location 7 (see fig. 5) with a lateral deviation of 30.5 m (100 ft) to the right of the trajectory, a vertical deviation of zero, and an intercept angle of zero. Thus, control action was required from the pilot immediately after starting the run, to bring the vehicle back on the trajectory. Gust disturbances were generated by passing band-limited white noise through a first order filter with a break frequency of 0.2 rad/sec. The root-mean-square value of the lateral gusts was 5.33 m/sec and of the vertical gusts 4.57 m/sec.

Each run lasted 120 sec, during which time the means and autocovariances of deviations, vehicle motions, and control commands were computed according to the equation

$$\mathrm{cov}(x) = \frac{1}{t}\int_0^t x^2\,dt \qquad (1)$$

where cov(x) is the autocovariance of variable x, and x can be p, d_ℓ, d_f, d_v, ϵ_f, ϵ_v, $\dot{\epsilon}_f$, $\dot{\epsilon}_v$, δ_s, or δ_c.

Entering the trajectory from a randomly chosen, unknown location outside the tunnel.- This experiment attempted to simulate the situation in which the pilot, after not viewing the display for some time, was at once confronted with the situation of being located outside the tunnel. The pilot was instructed to bring the vehicle back on the

desired trajectory as fast as possible, as smoothly as possible, and with minimum control effort. Gust disturbances were not present in this experiment. In order to prevent the pilot from knowing his initial position before the start of a simulation run, the tunnel image, the tunnel cross-sectional square, the map, and the altimeter scale were initially blanked and were only made visible immediately after starting the simulation run.

Each run started randomly from one of the six initial locations shown in figure 5. For all locations, the initial lateral deviation was 305 m (1000 ft) to the left or to the right of the trajectory, and the initial vertical deviation was 45.7 m (150 ft) above or below the trajectory. The initial intercept angle was set between 0^{o} and 72^{o}.

Each entry run lasted 50 sec, during which the following performance scores were computed: the lateral settling time $T_{s\ell}$ – defined as the time from the start of the run to the moment the lateral deviation remains within a ±15.2-m (50-ft) settling tolerance about the desired trajectory – and the vertical settling time T_{sv} – for which the settling tolerance is ±10.7 m (35 ft); the autocovariances of the roll rate p, of the intercept angle d_{ψ}, of the predicted lateral and vertical deviations ϵ_{ℓ} and ϵ_{v} and their rates $\dot{\epsilon}_{\ell}$ and $\dot{\epsilon}_{v}$, and of the control commands δ_{s} and δ_{c}; the lateral deviation score – defined as the averaged absolute value of the lateral deviation computed between $t = T_1$ and $t = T_2$, where $T_1 = 10$ sec and $T_2 = 50$ sec according to

$$sc\left(d_{\ell}\right) = \frac{1}{\left(T_2 - T_1\right)} \int_{t=T_1}^{t=T_2} \left|d_{\ell}\right| dt \qquad (2)$$

The vertical deviation score was computed in the same way, with $T_1 = 6$ sec and $T_2 = 50$ sec. The lateral and vertical deviation scores were chosen to be averaged absolute values rather than averaged squared values, in order to prevent these scores from being dominated by the large initial deviation. For the same reason, the averaging process only starts at $t = T_1$ sec. Starting point T_1 was chosen to be 25 percent less than the best previously recorded settling time.

Monitoring experiment.- The purpose of this experiment was to investigate the abilities of a pilot, using the various display configurations, to detect and correct control system failures in automatic approaches. Each run started as an automatic flight. At a random chosen time $t = T_f$ (between 5 and 20 sec), a failure occurred in the automatic control system. After detecting the failure, the pilot responded by pressing one of two buttons on the control stick. This disengaged the automatic control system and engaged the manual control mode. The control mode, automatic or manual, was indicated on the display by AUTO or MAN, respectively. The pilot was instructed to bring the vehicle back on the desired trajectory as fast as possible and with minimum control activity. After returning the vehicle to the desired trajectory, the pilot had to reengage the

automatic control system by pressing the second button on the control stick. The control failure was assumed to be eliminated by the use of a backup automatic control system. The condition for the successful reengagement of the automatic control system was that the lateral and vertical deviations and the intercept angle must be within preset tolerances. These tolerances were ±19.8 m (65 ft) for the lateral deviation, ±15.2 m (50 ft) for the vertical deviation, and ±0.15 rad for the intercept angle.

Each run lasted 50 sec, during which the following performance scores were measured: the reaction time T_r – defined as the time elapsed between the occurrence of the failure and the moment of manual takeover; the correction time T_c – defined as the time elapsed between the moment of manual takeover and the moment of reengagement of the automatic control system; the autocovariances of d_ℓ, d_v, ϵ_ℓ, ϵ_v, d_ψ, p, δ_s, and δ_r measured over the total 50-sec interval of combined automatic and manual control.

Based on the predicted lateral and vertical deviations at 229 m (750 ft) ahead of the vehicle, the lateral and vertical automatic control laws were

$$\delta_s' = -k_\ell \epsilon_\ell \tag{3}$$

$$\delta_c' = -k_v \epsilon_v \tag{4}$$

where automatic control inputs δ_s' and δ_c' replaced the manual control inputs δ_s and δ_c to the system with SAS engaged. The gains of the automatic control system were set to 0.018 for k_ℓ and 0.045 for k_v, and the vertical predictor gain k_{pv} was 0.2.

During each run, a control failure would occur, chosen at random from the four failures described hereafter:

(1) Lock of control inputs, where

$$\delta_s'(t) = \delta_s'\left(T_f\right) \tag{5}$$

$$\delta_c'(t) = \delta_c'\left(T_f\right) \tag{6}$$

for $t \geqq T_f$.

(2) Error estimates for v and w, which were used in computing the predicted vehicle position. In this study v and w were assumed to be perfect estimates. However, a control failure would occur when incorrect values of v and w were used in computing the predicted vehicle position. Additive errors, linearly increasing with time, were introduced. The error estimate values $\hat{v}$ and $\hat{w}$ are then given by

$$\hat{v} = v + k_{b\ell}\left(t - T_f\right) \tag{7}$$

$$\hat{w} = w + k_{bv}\left(t - T_f\right) \tag{8}$$

where $k_{b\ell} = k_{bv} = 0$ for $t < T_f$ with $k_{b\ell} = \pm 5$ and $k_{bv} = \pm 2$ for $t \geq T_f$.

(3) Undesired linearly increasing rudder input, according to

$$\delta_r' = k_{br}\left(t - T_f\right) \tag{9}$$

where $k_{br} = 0$ for $t < T_f$ and $k_{br} = \pm 0.1$ for $t \geq T_f$.

(4) Roll-rate feedback failure, simulated by

$$\delta_s' = -k_\ell \epsilon_\ell + k_{\ell p} p \tag{10}$$

where $k_{\ell p} = 0$ for $t < T_f$ and $k_{\ell p} = 7$ for $t \geq T_f$.

Results

Four subjects participated in the evaluation program. The background of the subjects is listed in table 2. Subject training consisted of two to four simulator sessions of 1 to 3 hours duration each, in which the subjects familiarized themselves with the various display configurations. In addition to this, 3 to 12 training runs were made, prior to the production runs, for each experimental condition. The four subjects completed a total of about 1640 production runs, totaling 28.6 hours of net simulation time. Each subject performed at least four repetitions for each experimental condition. The results for the four subjects were treated separately and are summarized in tables 3 to 12. The result for each experimental condition represents the average and standard deviations of a set of four or more repetitions.

Significance tests on the difference between averages were performed with a Student-t test at a 5-percent level of significance. Although significant differences between the results of the four subjects were observed, the general trends were rather similar. Therefore, only the results of subject 1 were plotted.

A 40-min motion picture was made, in which the most characteristic results of the three experiments are recorded. Since the motion picture was made in real time directly from the display monitor and during actual simulation runs, it accurately reproduces the simulator experiments.

Results for the trajectory following experiment.- The results of the trajectory following experiment for the four subjects are summarized in tables 3 to 7. The results for subject 1 are shown in figures 7 to 22. From these results, the following can be concluded.

Comparison of the conventional EADI/map display with the basic tunnel display: For all four subjects, the tunnel display yielded a markedly better accuracy in following the trajectory than the EADI/map display, as can be seen from the significantly lower values for the autocovariances of d_ℓ and d_V for the tunnel display. (See tables 3 to 5 and figs. 7 and 8.) The autocovariance of d_ψ was also significantly lower for the tunnel display, indicating a less oscillatory lateral response. No significant difference in the roll activity, as indicated by cov(p), was found between the two displays. (See fig. 9.)

These results are confirmed by the time histories of the lateral and vertical responses, shown in figures 10 and 11. Note the stepwise character of the collective control input for the EADI/map display in figure 11. This might result from the fact that the pilot intermittently controls the lateral and vertical situations.

Comparison of the basic tunnel with the tunnel/vehicle axis cross (VAC): The effect of adding a VAC and a director to the tunnel image was investigated for subjects 1 and 2 with the cross and director at $D = 305$ m (1000 ft).

No significant difference in the results was found between the basic tunnel and the tunnel plus VAC/director. (See tables 3 and 4 and figs. 7 to 9.) Thus, a VAC/director does not contribute to a better performance.

Comparison of the tunnel plus VAC/director with the VAC/director: The VAC/director at $D = 305$ m (1000 ft) was investigated for subjects 1 and 2. The autocovariances of the lateral and vertical deviations were significantly larger for the VAC/director than for the tunnel plus VAC/director. (See tables 3 and 4 and figs. 7 and 8.) This means that the error between the VAC and the director does not provide the correct control information for this task. Thus, with the tunnel plus VAC/director, all control cues are derived from the tunnel image and the VAC is ignored. This assumption is confirmed by the significantly larger value for the autocovariance of ϵ_ℓ for the tunnel plus VAC/director.

Comparison of the basic tunnel with the tunnel plus predictor/director: For all four subjects, performance was found to improve significantly with the addition of predictor/director symbols to the basic tunnel display, as can be concluded from the markedly reduced roll activity and smaller lateral and vertical deviations. (See tables 3 to 5 and figs. 7 to 9.)

In figures 10 and 11, the time histories for the tunnel plus predictor/director are compared with those for the basic tunnel. Note the lower roll and pitch activity and the smaller vertical deviations for the tunnel plus predictor/director.

The effect of the predictor distance D: The effect of the predictor distance D was investigated for subjects 1 and 2 for the predictor with $k_{pv} = 1$ and D = 91.4 m (300 ft), 137 m (450 ft), 229 m (750 ft), and 305 m (1000 ft). Lateral and vertical deviations were found to increase strongly with D. (See figs. 12 and 13 and tables 6 and 7.) On the other hand, the roll activity decreased with increasing D. (See fig. 14 and tables 6 and 7.) These results indicate that at D = 91.4 m (300 ft) the system is more oscillatory, indicating lower damping, and at D = 305 m (1000 ft) the system is too inaccurate. For this task and airspeed of 33.5 m/sec (110 ft/sec), the optimum predictor distance tends to be between D = 137 m (450 ft) and D = 229 m (750 ft).

Note that the autocovariance for the predicted vertical error rate $\dot{\epsilon}_v$ strongly increases with D. (See tables 6 and 7.) This results from the fact that the vertical disturbances are less filtered by the vehicle dynamics than the horizontal ones, which results in rapid vertical predictor motions.

The time histories for the tunnel plus predictor/director at D = 91.4 m (300 ft) and D = 229 m (750 ft) are shown in figures 15 and 16 and confirm the results mentioned previously.

Comparison of the tunnel plus predictor/director with the predictor/director: The predictor/director was investigated for subjects 1 and 2 and for D = 91.4 m (300 ft), 229 m (750 ft), and 305 m (1000 ft). At D = 229 m (750 ft) and 305 m (1000 ft), the autocovariances of the lateral and vertical deviations for the tunnel plus predictor/director were found to be generally smaller than for the predictor/director. (See tables 6 and 7 and figs. 12 and 13.) At D = 305 m (1000 ft), the differences were found to be significant. The autocovariance of the predicted lateral deviation ϵ_ℓ was significantly larger with the tunnel plus predictor/director than with the predictor/director. (See tables 6 and 7.) This indicates that, for a wrongly adjusted predictor distance, the pilot relies on the tunnel image rather than on the error between predictor and director. Note also the significantly lower roll activity for the predictor/director at D = 305 m (1000 ft).

The time histories for the tunnel plus predictor/director and for the predictor/director, both at D = 305 m (1000 ft), are shown in figures 17 and 13 and confirm these findings.

The simplified predictor and the effect of a reduced predictor gain: The simplified predictor, based on the bank angle ϕ, was investigated for subjects 1 and 2 with D = 229 m (750 ft). The autocovariance of the lateral deviation was significantly larger with the simplified predictor than with the regular one, but it was still significantly smaller than with the tunnel without predictor/director. (See tables 3 and 4.) No significant difference in roll activity was found between the simplified predictor and the regular one. These results indicate that the simplified predictor yields a somewhat less accurate

but adequately damped system. Thus, the roll angle may very well be used for the lateral prediction, in those situations where the lateral acceleration is not available.

In the vertical control, the simplified predictor with $k_{pv} = 0$ yielded vertical deviations similar to those of the predictor with $k_{pv} = 0.2$ and with $k_{pv} = 1$. However, because of the rapid vertical predictor motions, the rate of the vertical error between the predictor and the director $\dot{\epsilon}_v$ was found to be very large for $k_{pv} = 1$. The test subjects objected to these rapid predictor motions. On the other hand, the vertical accelerations were completely disregarded for $k_{pv} = 0$, which resulted in overcontrolling because of the lack of quickening in the display. A compromise between sufficient quickening and acceptable vertical predictor motions was found for $k_{pv} = 0.2$.

The effect of roll cues: The effect of roll cues was investigated for subjects 1 and 2 with the tunnel plus predictor/director at $D = 229$ m (750 ft) and $k_{pv} = 0.2$. No significant difference was found in the results between the roll version and the roll-stabilized version. (See tables 3 and 4.) This indicates that, for this control task, the roll version and the roll-stabilized version perform equally well in a fixed-base simulator.

Results for the trajectory entry experiments.- The entry experiments were conducted in a series of six runs. For each run, the initial location was chosen at random from one of the six positions given in figure 5. No position was used more than once. Significant differences between the scores were observed for the various initial locations. In order to rate the general entry performance, the results of the six runs in each series were averaged in order to obtain the series scores. For each display configuration, two to six series of runs were performed. The experimental results for the four subjects are summarized in tables 8 to 11. Each result represents the average and standard deviation of a set of four to six series scores. From these results, the following can be concluded.

Comparison of the EADI/map display with the basic tunnel display (roll version): For all four subjects, the entry performance for the basic tunnel was found to be markedly better than for the conventional EADI/map display. With the basic tunnel, significantly smaller lateral and vertical deviation scores, as well as smaller lateral and vertical settling times, were found (see tables 8 to 11 and figs. 19 to 22), indicating a faster and more accurate entry. For the tunnel display, the roll activity was found to be significantly lower as well, indicating better system damping. (See fig. 23.)

Shown in figures 28 and 29 are the time histories for the entry from location 3, for the EADI/map, and for the basic tunnel. Both displays yielded considerable roll activity, as shown in figure 24. However, the tunnel display yields a more gradual and accurate entry, as can be seen from the time history of the lateral deviation. Similar results in the vertical control are shown in figure 25. Note the stepwise character of the collective

control input, for the EADI/map. This phenomenon was discussed earlier for the trajectory following experiment.

Comparison of the basic tunnel with the tunnel plus predictor/director: The effect of the predictor is noticed mainly in the markedly lower roll activity, as seen in figure 23. For the tunnel plus predictor/director, lateral and vertical deviation scores, as well as lateral and vertical settling times, were found to be significantly lower also. (See figs. 19 to 22.) Thus, the tunnel plus predictor/director yields a more accurate and better damped entry.

The effect of the predictor distance D: Lateral and vertical deviation scores, as well as lateral and vertical settling times, were found to increase with increasing D. The increase of these scores was not significant in the range between D = 91.4 m (300 ft) and D = 229 m (750 ft). However, a significant increase in these scores was found between D = 229 m (750 ft) and D = 305 m (1000 ft). This trend is shown in figures 26 to 29. On the other hand, the roll activity was found to decrease with increasing D. (See fig. 30.) This decrease in roll activity was found to be significant between D = 91.4 m (300 ft) and D = 137 m (450 ft). These results indicate that, at D = 91.4 m (300 ft), the system lacks damping and, at D = 305 m (1000 ft), the system is too inaccurate. It is clear that, for the given forward velocity of V = 33.6 m/sec (110 ft/sec), a predictor distance in the range from D = 137 m (450 ft) to D = 229 m (750 ft) yields the best compromise.

In figures 31 and 32, the time histories for the entry from location 2 are shown for the tunnel plus predictor at D = 91.4 m (300 ft), 137 m (450 ft), and 229 m (750 ft). The time histories of the lateral deviation and intercept angle indicate a smoother entry for larger D. (See fig. 31.) The time histories of the roll rate for D = 91.4 m (300 ft) indicate a considerable increase in roll activity at the point of intercept with the tunnel. The lack of damping at D = 91.4 m (300 ft) was less pronounced in the vertical control. It was noticed in a slightly increased pitch rate. (See fig. 32.)

Comparison of the tunnel plus predictor/director with the predictor/director: The predictor/director display was investigated for D = 229 m (750 ft) and 305 m (1000 ft). Predictor distances smaller than D = 229 m (750 ft) were not attempted, since the tunnel square was not visible during the first part of the entry.

At D = 229 m (750 ft) and 305 m (1000 ft), lateral and vertical deviation scores, as well as lateral and vertical settling times, were found to be significantly larger for the predictor/director than for the tunnel plus predictor/director. (See figs. 26 to 29.) This proves that the tunnel image contributes significantly to the entry accuracy, particularly for a badly adjusted predictor (e.g., D = 305 m (1000 ft)). The roll activity for the tunnel plus predictor/director was somewhat larger than for the predictor/director. When the tunnel image was shown in addition to the predictor/director, the pilot relied on the tunnel

image rather than on the error between predictor and director square. This is seen in the fact that the autocovariance of the predicted lateral error ϵ_{ℓ} was significantly larger for tunnel plus predictor/director than for predictor/director.

In figures 33 and 34, the time histories for the entry from location 4 are shown for the tunnel plus predictor/director and for the predictor/director. It is shown in figure 33 that, for the tunnel plus predictor/director, the pilot allows a rather large predicted lateral error, while the time history of the actual lateral deviation shows a smooth and accurate response. On the other hand, the predicted lateral error was kept small for the predictor/director; whereas, the time histories of the actual lateral deviation show a large overshoot.

Similar results were obtained for the vertical control, as can be seen from the time histories in figure 34.

The effect of roll cues: The roll and roll stabilized versions of the tunnel plus predictor/director at D = 137 m (450 ft) were compared, and the results are shown in tables 8 and 9. The differences between the scores were not significant, even at a 10-percent confidence level. This indicates that, in the entry task, the roll and roll-stabilized versions perform equally well for fixed-base simulation.

Results for the monitoring experiment.- The monitoring experiments were conducted in a series of four runs of 50 sec each. In each run, one control failure appeared, chosen at random from the set of four failures discussed earlier. The polarity of the failure biases were chosen at random as well. The results of four runs in a series were averaged, in order to obtain averaged failure scores for the series (series scores). Sets of at least 12 series of four runs were conducted, for each experimental condition.

The monitoring experiment included the tunnel plus predictor/director at D = 229 m (750 ft), the predictor/director at D = 229 m, and the EADI/map. The results for subjects 1 and 2 are summarized in table 12. Each result represents the average and standard deviation of a set of 12 to 19 series scores. These results show that, for the lateral deviation, the vertical deviation, as well as the intercept angle, the tunnel plus predictor/director yielded significantly smaller overall autocovariances than the other two displays. The EADI/map performed worst in this respect. The same trend is noticeable for the reaction time T_r and the correction time T_c. The values of T_r and T_c were found to be significantly smaller for the tunnel plus predictor/director than for the EADI/map. Thus, the tunnel plus predictor/director enabled the best failure discovery and failure correction.

Qualitative Flight Test Validation

The feasibility of the tunnel display for operation in actual flight was demonstrated at the NASA Wallops Flight Center. A CH-47C helicopter (fig. 35) served as the flight

vehicle. A special version of a tunnel/map display was developed for operation at Wallops. The displays were generated by a ground-based Adage Graphics Terminal, scan converted, transmitted by TV link to the vehicle, and displayed on two monitors mounted in the CH-47C cockpit. On the upper display, the roll version of the tunnel plus predictor/director was shown; on the lower display, an HSI combined with an altimeter and a vertical speed scale. This configuration, which was specially designed for the VTOL approach and landing technology (VALT) program, served primarily as a display for conducting and monitoring automatic control system experiments.

However, to validate the tunnel display, a limited number of manual approaches were conducted. Subject 3 was the research pilot, and he used the same approach trajectory as used in the simulator experiments. The CH-47C was flown with the SAS engaged, but the velocity hold system used in the simulator was not available. Although the approach trajectory was the same as in the simulator experiments, the control task was considerably more demanding, since the pilot also had to keep the forward velocity constant. Furthermore, the predictor/director was less effective than in the simulator experiments, since not all variables necessary to drive the predictor/director were available. The lateral prediction was based on the bank angle ϕ according to equation (B6). (See appendix B.) Since v was not available, it was set to zero in equation (B3). (See appendix B.) In the vertical prediction, k_{pv} was set to zero.

In spite of the task difficulty and the lack of training runs, the trajectory was followed smoothly, while the lateral and vertical deviations from the trajectory remained within ± 30.5 m (100 ft) and 15.2 m (50 ft), respectively.

The pilot commented that, due to the lack of a velocity hold system, the workload was rather high. However, the tunnel image provided sufficient information for following the trajectory. Since the predictor/director did not provide the correct control cues, the pilot chose to utilize the tunnel image rather than the predictor/director. However, the predictor/director did provide the damping cues to some extent. The pilot also commented that, in spite of the task difficulty, the display was acceptable and that solving the problems mentioned would reduce the workload considerably.

CONCLUSIONS

The tunnel display with a superimposed predictor/director symbol was found to be a very successful combination. It outperformed the other two displays in all three experiments. A prediction time of 4 to 7 sec was found to optimize trajectory tracking for the given vehicle dynamics and flight conditions. Pilot acceptance of the tunnel plus predictor/director display was favorable, and the time for familiarization was relatively short.

Specifics:

1. The perspective tunnel image provides adequate positional and directional information and yields markedly better accuracy in trajectory following and trajectory entry than the conventional EADI/map display.

2. The basic tunnel display yields poor damping, due to the lack of rate information (caused by the narrow visual field).

3. Predictor/director symbols superimposed on the tunnel image provide the rate information which is vital for an adequately damped system. For the given vehicle dynamics and nominal forward velocity of 33.5 m/sec (110 ft/sec), a predictor symbol predicting the vehicle position 4 to 7 sec in advance yields the best compromise between positional accuracy and system damping.

4. The predictor/director display performs well in trajectory following. However, the use of this display is limited to the narrow range about the trajectory in which the director is visible.

5. The tunnel plus predictor/director display outperforms the predictor/director display when the predictor is badly adjusted, or in situations in which the director is out of the visible range.

6. A prediction time of 4 to 7 sec, which yields the best compromise for the lateral control, yields vertical predictor motions which are too rapid. A vertical prediction based on 20 percent of the actual vertical acceleration yields the best pilot acceptance.

7. A vehicle axis cross, superimposed on the tunnel image does not contribute to better tracking. The error between vehicle axis cross and director square does not provide the correct control cues in trajectory following in a fixed-base simulator.

8. The roll and roll-stabilized versions of the tunnel display perform equally well in trajectory following and entries. This leaves the option open, for applying the roll version to head-up displays, in which the image has to be conformal with the visual world.

9. The tunnel plus predictor/director display performs very satisfactorily in the detection and correction of failures in automatic flight.

Langley Research Center
National Aeronautics and Space Administration
Hampton, VA 23665
October 1, 1980

APPENDIX A

VEHICLE MODEL

Vehicle Model and Stability Augmentation System

All equations of motion comply with the north-east-down sign convention. The lateral equations of motion, for small deviations from the nominal trim condition are given by

$$\begin{bmatrix} \dot{p} \\ \dot{\phi} \\ \dot{r} \\ \dot{v} \end{bmatrix} = \begin{bmatrix} \left(\frac{I_1 L_p}{I_{xx}} + \frac{I_3 N_p}{I_{zz}}\right) & 0 & \left(\frac{I_1 L_r}{I_{xx}} + \frac{I_3 N_r}{I_{zz}}\right) & \left(\frac{I_1 L_v}{I_{xx}} + \frac{I_3 N_v}{I_{zz}}\right) \\ 1 & 0 & \tan\theta_N & 0 \\ \left(\frac{I_2 L_p}{I_{xx}} + \frac{I_1 N_p}{I_{zz}}\right) & 0 & \left(\frac{I_2 L_r}{I_{xx}} + \frac{I_1 N_r}{I_{zz}}\right) & \left(\frac{I_2 L_v}{I_{xx}} + \frac{I_1 N_v}{I_{zz}}\right) \\ \left(w_N + \frac{Y_p}{m}\right) & g\cos\theta_N & \left(\frac{Y_r}{m} - u_N\right) & \frac{Y_v}{m} \end{bmatrix} \begin{bmatrix} p \\ \phi \\ r \\ v \end{bmatrix}$$

$$+ \begin{bmatrix} \left(\frac{I_1 L_{\delta_s}}{I_{xx}} + \frac{I_3 N_{\delta_s}}{I_{zz}}\right) & \left(\frac{I_1 L_{\delta_r}}{I_{xx}} + \frac{I_3 N_{\delta_r}}{I_{zz}}\right) \\ 0 & 0 \\ \left(\frac{I_2 L_{\delta_s}}{I_{xx}} + \frac{I_1 N_{\delta_s}}{I_{zz}}\right) & \left(\frac{I_2 L_{\delta_r}}{I_{xx}} + \frac{I_1 N_{\delta_r}}{I_{zz}}\right) \\ \frac{Y_{\delta_s}}{m} & \frac{Y_{\delta_r}}{m} \end{bmatrix} \begin{bmatrix} \delta_{s,a} \\ \delta_{r,a} \end{bmatrix} + \begin{bmatrix} \left(\frac{I_1 L_v}{I_{xx}} + \frac{I_3 N_v}{I_{zz}}\right) \\ 0 \\ \left(\frac{I_2 L_v}{I_{xx}} + \frac{I_1 N_v}{I_{zz}}\right) \\ \frac{Y_v}{m} \end{bmatrix} v_g \qquad \text{(A1)}$$

where

$$I_1 = \frac{I_{xx}I_{zz}}{I_{xx}I_{zz} - I_{xz}^2} \qquad I_2 = \frac{I_{xx}I_{xz}}{I_{xx}I_{zz} - I_{xz}^2} \qquad I_3 = \frac{I_{zz}I_{xz}}{I_{xx}I_{zz} - I_{xz}^2} \tag{A2}$$

For small angles of θ, the horizontal coordinates of the vehicle location in the inertial reference system, x_i and y_i, are obtained by integration of

$$\dot{x}_i = V \cos\left(\psi + \frac{v}{V}\right) \tag{A3}$$

and

$$\dot{y}_i = V \sin\left(\psi + \frac{v}{V}\right) \tag{A4}$$

The longitudinal equations of motion, for small deviations from the nominal trim condition, are given by

$$\begin{bmatrix} \dot{u} \\ \dot{w} \\ \dot{q} \\ \dot{\theta} \end{bmatrix} = \begin{bmatrix} \frac{X_u}{m} & \frac{X_w}{m} & \left(\frac{X_q}{m} - w_N\right) & -g\cos\theta_N \\ \frac{Z_u}{m} & \frac{Z_w}{m} & \left(u_N + \frac{Z_q}{m}\right) & -g\sin\theta_N \\ \frac{M_u}{I_{yy}} & \frac{M_w}{I_{yy}} & \frac{M_q}{I_{yy}} & 0 \\ 0 & 0 & 1 & 0 \end{bmatrix} \begin{bmatrix} u \\ w \\ q \\ \theta \end{bmatrix} + \begin{bmatrix} \frac{X_{\delta_b}}{m} & \frac{X_{\delta_c}}{m} \\ \frac{Z_{\delta_b}}{m} & \frac{Z_{\delta_c}}{m} \\ \frac{M_{\delta_b}}{I_{yy}} & \frac{M_{\delta_c}}{I_{yy}} \\ 0 & 0 \end{bmatrix} \begin{bmatrix} \delta_{b,a} \\ \delta_{c,a} \end{bmatrix} + \begin{bmatrix} \frac{X_w}{m} \\ \frac{Z_w}{m} \\ \frac{M_w}{I_{yy}} \\ 0 \end{bmatrix} w_g \tag{A5}$$

or written shortly as

$$\dot{\vec{x}}_v = A_v\vec{x}_v + B_v\vec{\delta}_{v,a} + W_v w_g \tag{A6}$$

The altitude z_i is obtained by integration of

$$\dot{z}_i = V \sin\left(\frac{w}{V} - \theta\right) \tag{A7}$$

A block diagram of the lateral SAS is shown in figure 36(a). The sideslip feedback is given by

$$g_v = f_v v \tag{A8}$$

The yaw-rate feedback is given by

$$g_r = f_r\left(r - g_1\right) \tag{A9}$$

$$\dot{g}_1 = -0.312g_1 + 0.312r \tag{A10}$$

The roll rate on differential cyclic (rudder) feedback is given by

$$g_{pr} = g_2 \tag{A11}$$

$$\dot{g}_2 = -0.243g_2 + 0.243f_{pr}p \tag{A12}$$

and the roll rate on cyclic feedback is given by

$$g_p = f_p p \tag{A13}$$

With the SAS engaged, the cyclic and differential-cyclic actuator inputs $\delta_{s,a}$ and $\delta_{r,a}$ are given by

$$\delta_{s,a} = \delta_s - g_p \tag{A14}$$

$$\delta_{r,a} = \delta_r + g_{pr} - g_r + g_v \tag{A15}$$

where δ_s and δ_r are the lateral-control stick and rudder-pedal commands, respectively.

State equation (A1) can be augmented, in order to incorporate the SAS dynamics. The lateral, augmented open-loop (SAS disengaged) state equation becomes

APPENDIX A

$$\begin{bmatrix} \dot{p} \\ \dot{\phi} \\ \dot{r} \\ \dot{v} \\ \dot{g}_1 \\ \dot{g}_2 \end{bmatrix} = \left[\begin{array}{cccc:cc} & & A_\ell \text{ - Matrix} & & 0 & 0 \\ & & & & 0 & 0 \\ & & & & 0 & 0 \\ & & & & 0 & 0 \\ \hdashline 0 & 0 & 0.312 & 0 & -0.312 & 0 \\ 0.243f_{pr} & 0 & 0 & 0 & 0 & -0.243 \end{array}\right] \begin{bmatrix} p \\ \phi \\ r \\ v \\ g_1 \\ g_2 \end{bmatrix}$$

$$+ \left[\begin{array}{cc} B_\ell \text{ - Matrix} & \\ & \\ \hdashline 0 & 0 \\ 0 & 0 \end{array}\right] \begin{bmatrix} \delta_{s,a} \\ \delta_{r,a} \end{bmatrix} + \left[\begin{array}{cc} W_\ell \text{ - Matrix} & \\ & \\ \hdashline 0 & 0 \\ 0 & 0 \end{array}\right] v_g \qquad \text{(A16)}$$

or written shortly as

$$\dot{\bar{x}}'_\ell = A'_\ell \bar{x}'_\ell + B'_\ell \bar{\delta}_{s,a} + W'_\ell v_g \qquad \text{(A17)}$$

The lateral, augmented closed-loop (SAS engaged) system is given by

$$\dot{\bar{x}}'_\ell = \hat{A}_\ell \bar{x}'_\ell + B'_\ell \bar{\delta}_\ell + W'_\ell v_g \qquad \text{(A18)}$$

where $\hat{A}_\ell$ is the lateral closed-loop system matrix given by

$$\hat{A}_\ell = \left[A'_\ell - B'_\ell F_\ell\right] \qquad \text{(A19)}$$

and F_ℓ is the lateral feedback matrix given by

APPENDIX A

$$F_\ell = \begin{bmatrix} f_p & 0 & 0 & 0 & 0 & 0 \\ 0 & 0 & f_r & -f_v & -f_r & -1 \end{bmatrix} \tag{A20}$$

and

$$\vec{\delta}_\ell = \begin{bmatrix} \delta_s \\ \delta_r \end{bmatrix} \tag{A21}$$

The lateral SAS can be easily altered or disengaged by altering or nullifying the matrix F_ℓ.

A block diagram of the longitudinal SAS is shown in figure 36(b). It consists of a pitch-rate feedback

$$g_q = f_q q \tag{A22}$$

a pitch-angle feedback

$$g_\theta = f_\theta \theta \tag{A23}$$

and a perturbed forward-velocity feedback

$$g_u = f_u u \tag{A24}$$

The vertical closed-loop system is given by

$$\dot{\vec{x}}_v = \hat{A}_v \vec{x}_v + B_v \vec{\delta}_v + W_v w_g \tag{A25}$$

where $\hat{A}_v$ is the closed-loop system matrix given by

$$\hat{A}_v = \left[A_v - B_v F_v \right] \tag{A26}$$

and F_v is the vertical feedback matrix, given by

APPENDIX A

$$F_v = \begin{bmatrix} -f_u & 0 & f_q & f_\theta \\ 0 & 0 & 0 & 0 \end{bmatrix} \tag{A27}$$

It is clear from the lateral stability derivatives that the not-augmented vehicle had very poor directional stability and poor yaw and roll damping. The lateral stability augmentation system (SAS) was derived from reference 5 and is shown in figure 36(a). It consists of a sideslip feedback, which provides the directional stability; a yaw-rate feedback, which provides the necessary yaw damping; a roll rate on differential cyclic (rudder) feedback, which minimizes the effect of roll-induced yaw; and a roll rate (on cyclic) feedback, to provide the necessary roll damping. With the SAS engaged, lateral control is accomplished by a lateral stick command only, without using the rudders, while the turn coordination is accomplished automatically by the feedback on the sideslip.

The not-augmented longitudinal vehicle dynamics had an unstable pole at $s = 0.519$ rad/sec. The longitudinal SAS was specially designed for this study and is shown in figure 36(b). The system had to provide longitudinal stability and had to keep the forward velocity constant. This was accomplished by a pitch-rate, pitch-attitude, and perturbed-forward-velocity feedback on the differential collective input (pitch). Thus, a forward stick command resulted in a proportional increase or decrease of the forward velocity. Vertical control was accomplished by a collective command. The rotor speed was assumed to remain constant, and the stability derivatives were assumed to be invariant with the engine torque.

The pole-zero location of the transfer function $H_{\delta_s}^{d_\ell}(s)$, relating the linearized lateral vehicle displacement with a cyclic control input, is shown in figure 37(a) for the SAS disengaged and in figure 37(b) for the SAS engaged. Shown in figures 38(a) and (b) are the locations for the $H_{\delta_c}^{d_v}(s)$ transfer function, relating the linearized vertical displacement with a collective input. As shown in figure 37(b), the lateral vehicle dynamics with SAS engaged were dominated by the three poles at the origin. The effect of the pair of complex poles with a natural frequency $\omega_n = 0.32$ rad/sec and a damping factor of $\zeta = 0.43$ is less dominant, because of the closely located pair of complex zeros, with $\omega_n = 0.25$ rad/sec and $\zeta = 0.43$.

The longitudinal dynamics with SAS engaged, shown in figure 38(b), were dominated by one pole at the origin and one at $s = -0.462$ rad/sec. The effect of the well damped pair of complex poles, with $\omega_n = 0.73$ rad/sec and $\zeta = 0.67$, was masked by the closely located pair of complex zeros, with $\omega_n = 0.63$ rad/sec and $\zeta = 0.76$.

APPENDIX A

Control Task Definition and Candidate Loop Closures

The control task was to minimize the lateral and vertical deviations from a specified reference trajectory, with minimum control effort.

The horizontal situation for following an arbitrarily curved trajectory is shown in figure 39. The lateral deviation from the trajectory is denoted by d_ℓ, the intercept angle of velocity vector and trajectory direction by d_γ, and the curvature of the trajectory at the approximate vehicle location by $f(t) = 1/R_t(t)$. The centripetal acceleration a_t for following a curve with radius R_t is given by

$$a_t(t) = \frac{V^2}{R_t(t)} = V^2 f(t) \tag{A28}$$

where V is the ground speed. For small deviations, d_γ and d_ℓ are given by

$$d_\gamma(t) = \frac{1}{V} \int \left[a_\ell(t) - a_t(t) \right] dt \tag{A29}$$

$$d_\ell(t) = V \int d_\gamma(t)\, dt \tag{A30}$$

where a_ℓ is the acceleration of the vehicle in lateral direction and with respect to an inertial reference system.

It has been shown in figure 37(b) that the transfer function $H_{\delta_s}^{d_\ell}(s)$ of the lateral augmented vehicle dynamics was dominated by three poles at the origin. It is clear that adequate rate information is required in order to stabilize the system. It is shown in references 1 and 2 that rate cues can originate from the visual field by deriving the control error a distance D ahead of the vehicle. It is also shown that the pilot was able to obtain a rough estimate of the predicted vehicle path from the apparent motion of conspicuous objects in the visual field (texture points). In figure 39 this circular, predicted vehicle path is shown. Point A is the predicted vehicle position at a distance D, or $T_p = D/V$ sec, ahead of the vehicle. The control error ϵ_ℓ is defined as the deviation of point A from the reference trajectory. It follows from the geometry of figure 39 that, for small $d_\ell d_\gamma$ and D/R_t, the following linearized expression for ϵ_ℓ can be derived:

$$\epsilon_\ell = d_\ell + D d_\gamma + \frac{1}{2}\left(a_\ell - a_t\right) + d_p \tag{A31}$$

or, with equations (2) and (3) and after Laplace transformation,

$$\epsilon_\ell(s) = \left(1 + T_p s + \frac{1}{2} T_p{}^2 s^2\right) d_\ell(s) + d_p(s) \tag{A32}$$

The term d_p constitutes a preview of the trajectory and accounts for changes in curvature $d_p(t)$ given by

$$d_p(t) = \int_0^{\sigma=T_p}\int \left[a_t(t) - a_t(\sigma)\right] d^2\sigma \tag{A33}$$

It follows from equation (A33) that, for straight trajectories or trajectories with a constant curvature, d_p will be zero.

A block diagram of this linearized system is shown in figure 40(a). The curvature $f(t)$ is the forcing function of the system.

A control error, based on the predicted vehicle position, yields the following advantages:

(1) A pair of complex zeros with a fixed damping factor of $\zeta = 0.707$ and a natural frequency ω_n which can be adjusted to the requirements of the system by varying the prediction time T_p.

(2) For straight trajectories or trajectories with a constant curvature, a zero value of ϵ_ℓ will yield a zero steady-state value of d_ℓ, as can be seen by setting ϵ_ℓ, s, and d_p to zero in equation (A32).

An alternative loop closure can be formulated by considering a point B on the vehicle direction of motion T_p seconds ahead of the vehicle. (See fig. 39.) The control error is then defined as the deviation of point B from the trajectory and, for small deviations, is given by

$$\epsilon_\ell(t) = d_\ell(t) + D d_\gamma(t) + \frac{1}{2} T_p{}^2 a_t + d_p(t) \tag{A34}$$

or

$$\epsilon_\ell(s) = \left(1 + T_p s\right) d_\ell + \frac{1}{2} T_p{}^2 a_t(s) \tag{A35}$$

A block diagram of this system is shown in figure 40(b). Unlike the control error of equation (A32), equation (A35) provides only a single zero. It also follows from equation (A35) that, in following a constant curve, d_ℓ will maintain a steady-state error after bringing ϵ_ℓ to zero.

APPENDIX A

Vertical loop closures can be formulated in a way similar to that used for the lateral loop closures. The control error in this situation is based on either the vertical path or on the vertical direction of motion of the vehicle. The vertical path and vertical direction of motion are defined as the projection of the velocity vector on the $x_b z_b$ vertical plane of symmetry of the vehicle.

It has been shown in figure 38(b) that the transfer function $H_{\frac{\delta}{c}}^{d_v}(s)$ of the vertical, augmented vehicle dynamics is effectively of a lower order than the corresponding transfer function of the lateral dynamics. This softens the demand on the amount of rate information necessary to stabilize the system. Thus, a control error based on the vertical direction might yield a satisfactory vertical loop closure, since the single zero might be sufficient. Furthermore, the vertical trajectory profile does not have sections with constant curvature, so that the problem of a steady-state error in d_v does not occur.

APPENDIX B

TUNNEL DISPLAY AND GENERATION

Tunnel Display

The basic principle, underlying the tunnel display, is shown in figure 41. The trajectory to be followed is presented as a perspective tunnel image with a constant square cross section. The perspective appearance of the tunnel changes with the vehicle position. Positional cues are derived from this perspective appearance, while rate cues are derived from the rate of change in the appearance. In figure 41, the line AA represents the horizon and point C the center of the image, which represents the vehicle axis. Point C is not explicitly displayed, but the pilot can estimate its location by using the monitor frame as a reference. The trajectory is curved to the left, as shown in the corresponding plan view (fig. 42). The bank angle ϕ is determined from the inclination of the horizon with respect to the reference frame. Point F indicates the tunnel direction and is not explicitly displayed. However, it is assumed that the location of point F can be estimated by the pilot, by extending the four tunnel corner lines nearest to the vehicle, to a focal point at infinity. Point S is the center of the nearest square and is to be estimated as well. The centerline FS constitutes the tunnel direction at the approximate position of the vehicle. When defining the F_y-axis to be parallel and the F_z-axis to be perpendicular to the horizon, the lateral and vertical deviations of the vehicle from the trajectory can be estimated from the distance between F and S in F_y- and F_z-directions, respectively.

Attitude information can be estimated from the deviation of focal point F from the center of the image C. Thus, the lateral intercept angle d_ψ of the vehicle axis with the tunnel direction is estimated from the distance between F and C in F_y-direction, and the vertical intercept angle d_θ of the vehicle axis with the tunnel direction is estimated from the distance between F and C in F_z-direction. The downslope of the trajectory θ_t is determined by the distance point F is under the horizon AA.

Rate cues originate from the rate of change of the above mentioned quantities. A relative impression of forward motion is derived from the "passing by" of tunnel segments. Note that this velocity impression can be augmented by presenting the corner lines of the tunnel as separate line segments, rather than solid lines.

A preview of the trajectory to be followed is obtained by considering a centerpoint T on the trajectory, a distance D ahead of the vehicle. Point R is a point on FS and is also a distance D ahead. Unlike R which is to be estimated, the tunnel section at T is explicitly shown. The distance between T and R in F_y-direction provides an indication of the trajectory curvature, while the distance between T and R in F_z-direction indicates changes in the slope.

APPENDIX B

Predictor Display

The lateral as well as the vertical vehicle paths are assumed to be circular and tangential to the velocity vector $\vec{V}$. The lateral and vertical curvatures are given by

$$\frac{1}{R_\ell} = \frac{a_\ell(t)}{V^2} \tag{B1}$$

$$\frac{1}{R_v} = \frac{a_v(t)}{V^2} \tag{B2}$$

where a_ℓ and a_v are the lateral (in y_b body-axis direction) and vertical (in z_b body-axis direction) accelerations with respect to the inertial reference system. The predictor symbol P indicates a point on the predicted vehicle path, a distance D ahead of the vehicle. When defining C_y and C_z as the lateral and vertical screen axes (see fig. 41), the deviation of P from the center of the monitor in the C_y-direction is given by

$$\lambda_\ell = \frac{v}{V} + \frac{D/R_\ell}{1 + \sqrt{1 - \left(D/R_\ell\right)^2}} \tag{B3}$$

and in the C_z direction by

$$\lambda_v = \frac{w}{V} + \frac{D/R_v}{1 + \sqrt{1 - \left(D/R_v\right)^2}} \tag{B4}$$

where v and w are the components of $\vec{V}$ in y_b- and z_b-directions, respectively, and V is the ground speed. The values of λ_ℓ and λ_v are in fractional screen coordinates (screen limits are ± 1), for a $\pm 45^o$ horizontal-and-vertical field of view.

A valid control strategy for the tunnel plus predictor/director display is to minimize the error between the predictor P and tunnel section T. The linearized control error is then given by equation (A32) of appendix A. A prediction time T_p is chosen which yields the best compromise between positional accuracy and system damping for the given vehicle dynamics and airspeed.

Since the vertical dynamics are of a higher bandwidth than the lateral dynamics, a prediction time T_p which yields the best results for the lateral control will probably be too large for the vertical control. An excessively large prediction time will result in a

sluggish response in the vertical control. Furthermore, rapid vertical predictor motions will occur, since the vertical disturbances are less "filtered" by the vehicle dynamics. This problem is solved by choosing a value of T_p which is the most appropriate for the lateral control on one hand and by reducing the vertical acceleration in computing the vertical curvature on the other hand. Thus, the vertical curvature is computed from

$$\frac{1}{R_v} = k_{pv} \frac{a_v}{V^2} \tag{B5}$$

where k_{pv} is a gain and $0 \leqq k_{pv} \leqq 1$. It is clear that for $k_{pv} = 0$ the predictor symbol deteriorates into a velocity vector symbol.

Where the lateral acceleration a_ℓ is not measured or available, the curvature of the lateral path can be approximated from the bank angle ϕ according to

$$\frac{1}{R_\ell} = g \frac{\phi}{V^2} \tag{B6}$$

Since equation (B6) only yields the correct curvature in the steady state when following constant curves, system performance is expected to be less good than with the predictor based on the lateral acceleration. However, the steady-state error in d_ℓ in following constant curves with this simplified predictor will be zero as well.

Variables Necessary To Drive the Display

The variables necessary to display the tunnel image are the coordinates of the vehicle position in the inertial reference system, x_i, y_i, and z_i, and the attitude angles of the vehicle, ψ, θ, and ϕ. The variables x_i, y_i, and z_i can only be obtained by, or with the help of, ground-based equipment, such as a microwave landing system. The accuracy with which the desired trajectory can be followed directly depends on the accuracy with which the vehicle position can be estimated. The attitude angles ψ, θ, and ϕ can be obtained with standard vertical and heading gyros.

The variables necessary to display the predictor symbol are the velocities v, w, and V, as well as the accelerations a_ℓ and a_v. The accelerations a_ℓ and a_v can be measured directly with onboard accelerometers. The velocities v, w, and V can be estimated from the sideslip, angle of attack, and airspeed, measured at the vehicle. However, these variables are calculated with respect to the air mass rather than to an inertial reference system so that the appropriate corrections for the steady-state wind components have to be made.

APPENDIX B

An alternative method of obtaining v, w, and V is by a rotational transformation of $\dot{x}_i$, $\dot{y}_i$, and $\dot{z}_i$ through ψ, θ, and ϕ. The velocities $\dot{x}_i$, $\dot{y}_i$, and $\dot{z}_i$ can be derived by differentiation of x_i, y_i, and z_i or derived from estimates using position and accelerometer data. These computations can be carried out with onboard equipment.

REFERENCES

1. Grunwald, Arthur J.; and Merhav, S. J.: Vehicular Control by Visual Field Cues – Analytical Model and Experimental Validation. IEEE Trans. Syst., Man, & Cybern., vol. SMC-6, no. 12, Dec. 1976, pp. 835-845.

2. Grunwald, Arthur J.; and Merhav, S. J.: Effectiveness of Basic Display Augmentation in Vehicular Control by Visual Field Cues. IEEE Trans. Syst., Man, & Cybern., vol. SMC-8, no. 9, Sept. 1978, pp. 679-690.

3. Ostroff, Aaron J.; Downing, David R.; and Rood, William J.: A Technique Using a Nonlinear Helicopter Model for Determining Trims and Derivatives. NASA TN D-8159, 1976.

4. Hatfield, Jack J.; Elkins, Henry C.; Batson, Vernon M.; and Poole, William L.: A Flexible Flight Display Research System Using a Ground-Based Interactive Graphics Terminal. Applications of Computer Graphics in Engineering, NASA SP-390, 1975, pp. 387-418.

5. Davis, J. M.: Stability and Control Analysis. No. 114-AD-603 (Contract DA23-204-AMC-04366 (Y)), Vertol Div., Boeing Co., Nov. 28, 1966.

TABLE 1.- STABILITY DERIVATIVES FOR LEVEL FLIGHT OF CH-47C HELICOPTER

Lateral dynamics		Longitudinal dynamics	
Parameter	Value	Parameter	Value
Y_v/m	$-0.0779\ sec^{-1}$	X_u/m	$-0.0219\ sec^{-1}$
Y_p/m	$-0.6246\ m \cdot sec^{-1}$	X_w/m	$0.0358\ sec^{-1}$
Y_r/m	$-0.0679\ m \cdot sec^{-1}$	X_q/m	$0.7146\ m \cdot sec^{-1}$
Y_{δ_s}/m	$0.1343\ m \cdot sec^{-2}\ cm^{-1}$	X_{δ_b}/m	$0.0159\ m \cdot sec^{-2}\ cm^{-1}$
Y_{δ_r}/m	$-0.0068\ m \cdot sec^{-2}\ cm^{-1}$	X_{δ_c}/m	$0.0461\ m \cdot sec^{-2}\ cm^{-1}$
L_v/I_{xx}	$-0.01804\ msec^{-1}$	Z_u/m	$-0.0589\ sec^{-1}$
L_p/I_{xx}	$-0.8210\ sec^{-1}$	Z_w/m	$-0.5727\ sec^{-1}$
L_r/I_{xx}	$-0.0675\ sec^{-1}$	Z_q/m	$-0.3357\ m \cdot sec^{-1}$
L_{δ_s}/I_{xx}	$0.1597\ sec^{-2}\ cm^{-1}$	Z_{δ_b}/m	$0.0562\ m \cdot sec^{-2}\ cm^{-1}$
L_{δ_r}/I_{xx}	$-0.0533\ sec^{-2}\ cm^{-1}$	Z_{δ_c}/m	$-1.1518\ m \cdot sec^{-2}\ cm^{-1}$
N_v/I_{zz}	$-0.0007\ (m/sec^{-1})^{-1}$	M_u/I_{yy}	$-0.0138\ (m/sec^{-1})^{-1}$
N_p/I_{zz}	$-0.0169\ sec^{-1}$	M_w/I_{yy}	$0.0571\ msec^{-1}$
N_r/I_{zz}	$-0.0391\ sec^{-1}$	M_q/I_{yy}	$-1.6959\ sec^{-1}$
N_{δ_s}/I_{zz}	$0.0034\ sec^{-2}\ cm^{-1}$	M_{δ_b}/I_{yy}	$0.1568\ sec^{-2}\ cm^{-1}$
N_{δ_r}/I_{zz}	$0.0776\ sec^{-2}\ cm^{-1}$	M_{δ_c}/I_{yy}	$0.0622\ sec^{-2}\ cm^{-1}$
m	$14\,968.6\ kg$	I_{yy}	$273\,536.0\ kg \cdot m^2$
I_{xx}	$50\,386.3\ kg \cdot m^2$	u_N	$33.53\ m \cdot sec^{-1}$
I_{zz}	$257\,685.0\ kg \cdot m^2$	w_N	$1.72\ m \cdot sec^{-1}$
I_{xz}	$19\,838.3\ kg \cdot m^2$	θ_N	$0.05122\ rad$

TABLE 2.- BACKGROUND OF TEST SUBJECTS

Subject	Occupation	Age	Total flight time, hr	Percent of total flight time in helicopters	Aircraft	Previous simulator experience
1	Physical scientist	43	360	15	Cessna 150 and 172 Piper Cherokee Bell 47	Some
2	Aeronautical engineer	30	0	---	----------	Extensive
3	Research pilot	36	2200	30	All types	Extensive
4	Research pilot	43	5200	20	All types	Extensive

TABLE 3.- RESULTS OF TRAJECTORY FOLLOWING EXPERIMENT: SUBJECT 1

	Basic tunnel (no roll)	EADI/map	Tunnel plus vehicle axis cross/director (no roll), D = 305 m (1000 ft)	Vehicle axis cross/director (no roll), D = 305 m (1000 ft)	Tunnel plus predictor/director, k_{pv} = 0.2 D = 229 m (750 ft)		Tunnel plus simplified predictor (no roll), D = 229 m (750 ft)	Simplified predictor/director (no roll), D = 229 m (750 ft)
					No roll	Roll		
No. of runs	7	10	12	10	6	6	15	3
$cov(d_f)$, m^2	578.6 ±320.5	3663.8 ±2687.5	745.5 ±494.4	1840.9 ±272.6	100.0 ±12.3	114.8 ±23.7	173.3 +51.0	189.8 ±19.6
$cov(d_v)$, m^2	205.8 ±141.7	1089.8 ±746.7	186.5 ±145.6	1775.9 ±605.2	28.2 ±13.6	37.8 ±10.4	22.3 ±6.8	21.4 ±3.3
$cov(\epsilon_f)$, m^2	NR[a]	NR	4689.3 ±1092.5	1621.5 ±650.9	146.3 ±27.6	209.8 ±67.3	227.0 ±102.0	158.1 ±22.6
$cov(\epsilon_v)$, m^2	NR	NR	412.6 ±97.1	577.7 ±376.3	100.0 ±29.5	137.7 ±59.2	105.3 ±42.4	81.3 ±2.2
$cov(\dot{\epsilon}_f)$, $(m/sec)^2$	NR	NR	158.8 ±43.9	80.0 ±19.9	251.4 ±17.1	223.3 ±20.6	88.1 ±22.9	60.7 ±6.3
$cov(\dot{\epsilon}_v)$, $(m/sec)^2$	NR	NR	41.8 ±13.7	33.3 ±9.0	112.2 ±13.7	117.0 ±18.5	90.4 ±39.8	49.9 ±5.6
$cov(d_\psi)$, $10^{-3} rad^2$	11.7 ±3.1	51.4 ±21.7	13.6 ±3.9	13.9 ±3.9	4.33 ±.55	4.52 ±1.23	7.18 ±2.50	5.17 ±.99
cov(p), 10^{-3} $(rad/sec)^2$	8.12 ±2.78	7.71 ±3.89	8.69 ±3.99	5.47 ±1.32	2.51 ±.33	2.27 ±.31	1.63 ±.36	1.14 ±.07
$cov(\delta_s)$, cm^2 (roll)	2.66 ±.70	2.76 ±1.29	3.03 ±1.16	1.99 ±.38	1.61 ±.18	1.30 ±.23	1.16 ±.17	0.96 ±.08
$cov(\delta_c)$, cm^2 (collective)	10.53 ±4.10	6.23 ±2.59	11.92 3.01	7.30 ±3.16	6.67 ±2.32	7.60 ±4.00	5.99 ±1.90	4.53 ±.09

[a]Not relevant for this display configuration.

TABLE 4.- RESULTS OF TRAJECTORY FOLLOWING EXPERIMENT; SUBJECT 2

	Basic tunnel (no roll)	EADI/map	Tunnel plus vehicle axis cross/director (no roll), D = 305 m (1000 ft)	Vehicle axis cross/director (no roll), D = 305 m (1000 ft)	Tunnel plus predictor/director, D = 229 m (750 ft)		Tunnel plus simplified predictor (no roll), D = 229 m (750 ft)	Simplified predictor/director (no roll), D = 229 m (750 ft)
					No roll	Roll		
No. of runs	6	10	12	8	5	7	4	2
$cov(d_\ell)$, m^2	270.2 ±147.0	1969.4 ±1401.5	326.4 ±111.0	2485.3 ±293.1	90.0 ±14.2	83.6 ±11.0	214.6 ±29.0	155.8 ±3.4
$cov(d_v)$, m^2	112.4 ±22.7	797.6 ±538.3	135.6 ±43.0	1255.1 ±311.8	22.9 ±4.1	16.2 ±3.7	20.5 ±4.9	25.2 ±.8
$cov(\epsilon_\ell)$, m^2	NR[a]	NR	4947.1 ±975.4	1808.0 ±539.3	177.9 ±21.3	202.0 ±37.6	274.1 ±57.3	58.0 ±.6
$cov(\epsilon_v)$, m^2	NR	NR	324.3 ±87.2	444.0 ±243.3	59.4 ±8.2	65.0 ±11.7	75.7 ±17.5	52.4 ±1.2
$cov(\dot{\epsilon}_\ell)$, $(m/sec)^2$	NR	NR	134.4 ±48.7	148.4 ±66.7	241.5 ±29.4	224.5 ±20.6	114.9 ±12.1	105.6 ±8.4
$cov(\dot{\epsilon}_v)$, $(m/sec)^2$	NR	NR	22.3 ±5.0	65.8 ±18.3	151.1 ±13.2	134.2 ±20.7	59.1 ±7.3	62.4 ±14.9
$cov(d_\psi)$, $10^{-3}rad^2$	8.40 ±1.90	38.48 ±13.25	8.03 ±2.72	13.55 ±3.36	4.69 ±.65	4.62 ±.48	8.38 ±.71	5.13 ±.21
cov(p), 10^{-3} $(rad/sec)^2$	9.30 ±1.50	16.07 ±4.24	16.60 ±7.19	12.58 ±5.58	3.62 ±.41	2.38 ±.36	2.12 ±.12	2.07 ±.12
$cov(\delta_s)$, cm^2 (roll)	3.42 ±.62	5.07 ±1.20	5.89 ±2.08	4.12 ±1.54	2.08 ±.23	1.51 ±.26	1.40 ±.06	1.63 ±.16
$cov(\delta_c)$, cm^2 (collective)	14.67 ±3.25	8.68 ±3.03	15.84 ±3.33	48.64 ±17.64	8.65 ±2.78	8.57 ±3.25	5.07 ±.41	4.92 ±.21

[a]Not relevant for this display configuration.

TABLE 5.- RESULTS OF TRAJECTORY FOLLOWING EXPERIMENT; SUBJECTS 3 AND 4

	Subject 3			Subject 4		
	Tunnel plus predictor/director (no roll), k_{pv} = 0.2 D = 229 m (750 ft)	Basic tunnel (no roll)	EADI/map	Tunnel plus predictor/director (no roll), k_{pv} = 0.2 D = 229 m (750 ft)	Basic tunnel (no roll)	EADI/map
No. of runs	7	6	7	7	8	8
$cov(d_\ell)$, m^2	124.7 ±35.2	353.2 ±286.7	3850.4 ±3965.5	138.9 ±29.1	650.3 ±516.1	1652.1 ±840.3
$cov(d_v)$, m^2	33.7 ±16.8	142.7 ±50.6	313.7 ±99.1	41.2 ±17.5	328.8 ±213.8	923.4 ±494.5
$cov(\epsilon_\ell)$, m^2	216.2 ±59.0	NR[a]	NR	209.7 ±42.1	NR	NR
$cov(\epsilon_v)$, m^2	131.6 ±44.3	NR	NR	122.1 ±33.8	NR	NR
$cov(\dot{\epsilon}_\ell)$, $(m/sec)^2$	230.0 ±58.9	NR	NR	239.7 ±22.0	NR	NR
$cov(\dot{\epsilon}_v)$, $(m/sec)^2$	115.7 ±21.0	NR	NR	114.7 ±13.5	NR	NR
$cov(d_\psi)$, $10^{-3}rad^2$	5.07 ±.29	12.25 ±6.17	42.42 ±16.67	3.66 ±.96	17.98 ±7.69	37.90 ±19.32
cov(p), 10^{-3} $(rad/sec)^2$	1.63 ±.20	4.30 ±.60	3.84 ±.52	1.99 ±.13	9.82 ±2.02	5.08 ±.87
$cov(\delta_s)$, cm^2 (roll)	1.14 ±.16	1.66 ±.31	1.41 ±.22	1.27 ±.10	3.32 ±.68	1.94 ±.47
$cov(\delta_c)$, cm^2 (collective)	7.64 ±2.33	10.13 ±1.96	5.34 ±1.47	6.66 ±2.14	11.79 ±2.22	9.84 ±2.69

[a]Not relevant for this display configuration.

TABLE 6.- RESULTS OF TRAJECTORY FOLLOWING EXPERIMENT; EFFECT OF D AND COMPARISON OF TUNNEL PLUS PREDICTOR/DIRECTOR WITH PREDICTOR/DIRECTOR; SUBJECT 1

	Tunnel plus predictor/director (no roll), k_{pv} = 1				Predictor/director (no roll), k_{pv} = 1		
	D = 91.4 m (300 ft)	D = 137 m (450 ft)	D = 229 m (750 ft)	D = 305 m (1000 ft)	D = 91.4 m (300 ft)	D = 229 m (750 ft)	D = 305 m (1000 ft)
No. of runs, n	4	5	5	8	5	5	4
$cov(d_\ell)$, m^2	[a]49.2 [b]±5.7	68.2 ±3.7	107.3 ±26.7	173.6 ±39.6	67.0 ±4.1	138.1 ±48.5	276.3 ±41.3
$cov(d_v)$, m^2	11.9 ±1.5	17.4 ±4.2	59.2 ±40.8	46.4 ±17.7	12.9 ±2.4	53.9 ±10.5	71.0 ±10.7
$cov(\epsilon_\ell)$, m^2	37.4 ±6.9	60.7 ±4.7	260.2 ±47.7	937.5 ±102.2	62.1 ±4.8	229.1 ±54.7	515.4 ±91.7
$cov(\epsilon_v)$, m^2	23.2 ±2.2	41.0 ±11.2	250.3 ±88.5	1 289.0 ±566.2	22.0 ±2.7	302.2 ±34.0	1 036.2 ±129.4
$cov(\dot{\epsilon}_\ell)$, $(m/sec)^2$	13.4 ±.8	64.5 ±19.6	380.7 ±87.4	1 080.0 ±442.8	18.2 ±3.7	437.5 ±146.4	694.8 ±236.5
$cov(\dot{\epsilon}_v)$, $(m/sec)^2$	23.8 ±30.0	160.0 ±300.0	2121.7 ±1719.3	14 963.7 ±4 250.6	91.6 ±8.0	4897.7 ±3190.0	12 159.1 1 654.0
$cov(d_\psi)$, $10^{-3} rad^2$	3.69 ±.46	4.40 ±.29	4.67 ±1.53	6.98 ±1.11	5.04 ±.46	4.86 ±1.85	5.74 ±1.05
cov(p), 10^{-3} $(rad/sec)^2$	3.58 ±.37	2.44 ±.24	2.24 ±.46	1.48 ±.37	4.39 ±.44	1.57 ±.19	0.89 ±.16
$cov(\delta_s)$, cm^2 (roll)	1.68 ±.14	1.37 ±.07	1.36 ±.24	1.03 ±.20	1.79 ±.14	1.09 ±.08	0.71 ±.16
$cov(\delta_c)$, cm^2 (collective)	5.50 ±.27	4.02 ±.68	5.59 ±1.07	4.92 ±1.00	5.32 ±.56	4.37 ±.39	5.54 ±1.86

[a]Average of n runs.

[b]Standard deviation of n runs.

TABLE 7.- RESULTS OF TRAJECTORY FOLLOWING EXPERIMENT; EFFECT OF D AND COMPARISON OF TUNNEL PLUS PREDICTOR/DIRECTOR WITH PREDICTOR/DIRECTOR; SUBJECT 2

	Tunnel plus predictor/director (no roll), k_{pv} = 1				Predictor/director (no roll), k_{pv} = 1		
	D = 91.4 m (300 ft)	D = 137 m (450 ft)	D = 229 m (750 ft)	D = 305 m (1000 ft)	D = 91.4 m (300 ft)	D = 229 m (750 ft)	D = 305 m (1000 ft)
No. of runs, n	4	4	8	4	4	4	4
$cov(d_\ell)$, m^2	47.4 ±6.2	47.0 ±3.6	102.1 ±9.9	111.8 ±11.7	47.8 ±4.4	110.6 ±14.9	227.1 ±50.3
$cov(d_v)$, m^2	9.0 ±1.3	13.5 ±1.8	26.7 ±5.1	33.9 ±2.9	12.2 ±2.8	74.9 ±15.5	61.2 ±15.9
$cov(\epsilon_\ell)$, m^2	36.3 ±5.9	42.5 ±3.5	253.5 ±44.2	1 272.8 ±235.9	41.4 ±5.5	125.8 ±15.9	235.3 ±48.4
$cov(\epsilon_v)$, m^2	19.6 ±1.6	56.0 ±5.2	342.9 ±47.4	1 192.4 ±275.4	22.9 ±5.1	420.4 ±38.5	812.2 ±11.4
$cov(\dot{\epsilon}_\ell)$, $(m/sec)^2$	12.3 ±2.0	76.5 ±8.2	279.5 ±67.0	1 144.4 ±154.2	11.9 ±1.0	204.3 ±26.1	648.6 ±62.0
$cov(\dot{\epsilon}_v)$, $(m/sec)^2$	202.5 ±95.7	862.9 ±184.1	7570.3 ±3586.1	21 140.0 ±5 593.0	420.3 ±513.7	11 280.0 ±792.0	20 498.0 ±5 820.0
$cov(d_\psi)$, $10^{-3} rad^2$	4.18 ±.21	3.34 ±.23	4.48 ±.74	5.78 ±.86	4.38 ±.43	3.66 ±.31	3.91 ±.40
cov(p), 10^{-3} $(rad/sec)^2$	4.14 ±.46	3.19 ±.18	2.29 ±.30	4.38 ±.82	5.13 ±.65	1.84 ±.21	1.93 ±.26
$cov(\delta_s)$, cm^2 (roll)	1.89 ±.11	1.73 ±.08	1.32 ±.14	2.12 ±.44	2.06 ±.21	1.16 ±.11	1.20 ±.22
$cov(\delta_c)$, cm^2 (collective)	5.85 ±.24	5.11 ±.43	4.75 ±.16	6.78 ±1.32	5.81 ±.33	4.62 ±.13	5.95 ±1.86

TABLE 8.- RESULTS OF TRAJECTORY ENTRY EXPERIMENT; SUBJECT 1

	Tunnel plus predictor/director (no roll), k_{pv} = 0.2				Predictor/director (no roll), k_{pv} = 0.2		Tunnel plus predictor/director (roll), k_{pv} = 0.2 D = 137 m (450 ft)	Basic tunnel (roll)	EADI/map
	D = 91.4 m (300 ft)	D = 137 m (450 ft)	D = 229 m (750 ft)	D = 305 m (1000 ft)	D = 229 m (750 ft)	D = 305 m (1000 ft)			
No. of series of 6 entries	4	4	4	4	4	4	4	4	5
$sc(d_f)$, m	10.8 ±.6	11.4 ±.9	11.7 ±.7	14.8 ±.8	13.3 ±.5	20.8 ±2.5	12.1 ±1.0	19.4 ±2.1	34.4 ±3.0
$sc(d_v)$, m	3.0 ±.2	3.6 ±.2	4.8 ±.3	4.7 ±.5	5.7 ±.2	7.2 ±.5	3.3 ±.2	6.9 ±.4	19.1 ±1.6
T_{sf}, sec	16.3 ±.6	16.8 ±1.0	16.2 ±.4	22.1 ±4.0	23.4 ±1.4	36.0 ±1.3	17.1 ±1.4	28.3 ±5.6	46.5 ±2.9
T_{sv}, sec	10.2 ±.5	10.5 ±.6	12.9 ±2.3	14.6 ±2.4	18.1 ±1.7	24.2 ±3.7	10.6 ±.2	31.3 ±2.1	44.6 ±2.3
$cov(\epsilon_f)$, 10^2 m^2	64.0 ±1.3	48.0 ±1.1	21.6 ±.5	17.0 ±2.0	20.3 ±.5	11.1 ±3.5	47.9 ±1.9	NR[a]	NR
$cov(\epsilon_v)$ 10^2 m^2	1.20 ±.10	0.91 ±.04	0.80 ±.06	1.30 ±.20	1.17 ±.14	0.91 ±.19	0.94 ±.06	NR	NR
$cov(\dot{\epsilon}_f)$, 10^2(m/sec)^2	1.03 ±.03	0.94 ±.04	1.17 ±.18	2.64 ±.88	1.11 ±.07	2.56 ±.67	0.99 ±.04	NR	NR
$cov(\dot{\epsilon}_v)$, 10^2(m/sec)^2	0.09 ±.01	0.22 ±.01	0.91 ±.33	1.96 ±.38	0.97 ±.63	2.97 ±.69	0.20 ±.04	NR	NR
cov(p), 10^{-3} (rad/sec)^2	3.39 ±.15	2.37 ±.23	1.96 ±.27	1.91 ±.23	1.96 ±.15	1.57 ±.17	2.72 ±.33	6.02 ±1.55	9.40 ±2.36
$cov(\delta_s)$, cm^2 (roll)	1.26 ±.05	0.94 ±.09	0.85 ±.10	0.81 ±.09	0.86 ±.06	0.70 ±.05	1.15 ±.12	1.94 ±.48	3.15 ±.73
$cov(\delta_c)$, cm^2 (collective)	2.92 ±.10	2.72 ±.05	2.46 ±.04	2.50 ±.21	2.21 ±.09	2.08 ±.06	2.52 ±.10	5.69 ±.75	4.39 ±1.71

[a]Not relevant for this display configuration.

TABLE 9.- RESULTS OF TRAJECTORY ENTRY EXPERIMENT; SUBJECT 2

	Tunnel plus predictor/director (no roll), k_{pv} = 0.2				Predictor/director (no roll), k_{pv} = 0.2		Tunnel plus predictor/director (roll), k_{pv} = 0.2 D = 137 m (450 ft)	Basic tunnel (roll)	EADI/map
	D = 91.4 m (300 ft)	D = 137 m (450 ft)	D = 229 m (750 ft)	D = 305 m (1000 ft)	D = 229 m (750 ft)	D = 305 m (1000 ft)			
No. of series of 6 entries	4	4	4	4	4	4	5	6	4
$sc(d_f)$, m	13.0 ±1.2	13.9 ±.6	13.5 ±1.8	16.8 ±.5	13.9 ±.9	19.9 ±1.5	11.9 ±1.5	18.0 ±.9	35.9 ±9.2
$sc(d_v)$, m	3.72 ±.21	4.09 ±.21	4.54 ±.45	5.30 ±.22	7.56 ±.81	8.05 ±.92	3.97 ±.30	7.14 ±1.11	18.29 ±3.84
T_{sf}, sec	17.4 ±.6	18.0 ±.2	18.2 ±.2	33.7 ±3.9	24.8 ±1.1	35.8 ±2.9	16.0 ±.8	34.6 ±6.2	47.3 ±2.4
T_{sv}, sec	12.2 ±1.3	11.5 ±.2	11.5 ±.4	15.4 ±1.9	25.4 ±1.3	26.5 ±.9	11.6 ±1.4	39.7 ±3.5	43.5 ±3.6
$cov(\epsilon_f)$, 10^2 m^2	69.5 ±2.6	53.3 ±1.6	24.4 ±1.6	19.9 ±2.8	20.6 ±1.0	9.5 ±1.7	51.1 ±2.9	NR[a]	NR
$cov(\epsilon_v)$, 10^2 m^2	1.39 ±.06	1.00 ±.04	0.80 ±.10	1.21 ±.81	1.83 ±.28	1.29 ±.32	1.02 ±.17	NR	NR
$cov(\dot{\epsilon}_f)$, $10^2(m/sec)^2$	0.97 ±.04	0.82 ±.01	0.98 ±.12	2.69 ±.49	1.53 ±.30	2.37 ±.53	0.92 ±.04	NR	NR
$cov(\dot{\epsilon}_v)$, $10^2(m/sec)^2$	0.12 ±.04	0.20 ±.05	1.55 ±1.40	5.39 ±5.47	0.91 ±.39	4.18 ±2.40	0.29 ±.12	NR	NR
cov(p), 10-3 $(rad/sec)^2$	2.86 ±.14	2.10 ±.33	1.80 ±.28	2.20 ±.29	3.03 ±.78	2.47 ±.52	2.36 ±.40	5.89 ±1.02	12.20 ±1.59
$cov(\delta_s)$, cm^2 (roll)	1.11 ±.03	0.88 ±.14	0.79 ±.12	0.90 ±.08	1.26 ±.31	1.03 ±.18	0.96 ±.15	1.99 ±.32	3.84 ±.49
$cov(\delta_c)$, cm^2 (collective)	2.86 ±.21	2.54 ±.03	2.44 ±.13	2.42 ±.18	2.12 ±.04	1.94 ±.18	2.71 ±.22	12.85 ±2.27	3.74 ±.69

[a]Not relevant for this display configuration.

TABLE 10.- RESULTS OF TRAJECTORY ENTRY EXPERIMENT; SUBJECT 3

	Tunnel plus predictor/director (no roll), k_{pv} = 0.2			Predictor/director (no roll), k_{pv} = 0.2		Basic tunnel (roll)	EADI/map
	D = 137 m (450 ft)	D = 229 m (750 ft)	D = 305 m (1000 ft)	D = 229 m (750 ft)	D = 305 m (1000 ft)		
No. of series of 6 entries	3	3	3	3	3	3	4
$sc(d_f)$, m	11.3 ±.6	16.9 ±2.2	17.8 ±1.9	22.5 ±3.0	19.7 ±1.3	22.7 ±.9	39.7 ±14.0
$sc(d_v)$, m	5.27 ±.18	6.73 ±.50	8.45 ±.90	9.90 ±1.15	11.61 ±.81	6.82 ±.84	22.0 ±8.4
T_{sf}, sec	18.0 ±.6	19.4 ±.6	34.2 ±5.3	28.0 ±.6	40.7 ±3.6	29.0 ±.2	48.3 ±1.4
T_{sv}, sec	12.9 ±1.1	16.7 ±3.0	25.4 ±2.6	28.6 ±3.1	32.3 ±2.4	27.4 ±3.5	41.4 ±4.8
$cov(\epsilon_f)$, 10^2 m^2	47.6 ±1.3	26.7 ±.8	26.2 ±8.7	30.5 ±5.6	9.0 ±.5	NR[a]	NR
$cov(\epsilon_v)$, 10^2 m^2	1.37 ±.05	1.53 ±.18	2.62 ±.67	2.61 ±.54	2.87 ±.53	NR	NR
$cov(\dot{\epsilon}_f)$, $10^2(m/sec)^2$	1.05 ±.03	0.87 ±.08	4.28 ±1.80	1.43 ±.14	1.82 ±.14	NR	NR
$cov(\dot{\epsilon}_v)$, $10^2(m/sec)^2$	0.17 ±.04	0.47 ±.21	0.91 ±.50	0.15 ±.02	0.27 ±.06	NR	NR
cov(p), 10^{-3} $(rad/sec)^2$	2.31 ±.14	1.35 ±.19	3.18 ±1.18	2.24 ±.23	1.78 ±.02	5.51 ±.65	4.36 ±.63
$cov(\delta_s)$, cm^2 (roll)	0.92 ±.05	0.58 ±.07	1.11 ±.36	0.88 ±.07	0.70 ±.01	1.74 ±.18	1.48 ±.22
$cov(\delta_c)$, cm^2 (collective)	2.66 ±.14	2.10 ±.11	2.45 ±.30	1.72 ±.08	1.68 ±.02	5.96 ±.94	1.75 ±.29

[a]Not relevant for this display configuration.

TABLE 11.- RESULTS OF TRAJECTORY ENTRY EXPERIMENT; SUBJECT 4

	Tunnel plus predictor/director (no roll), k_{pv} = 0.2			Predictor/director (no roll), k_{pv} = 0.2	Basic tunnel (roll)	EADI/map
	D = 137 m (450 ft)	D = 229 m (750 ft)	D = 305 m (1000 ft)	D = 305 m (1000 ft)		
No. of series of 6 entries	2	4	4	3	3	4
$sc(d_f)$, m	17.5 ±2.0	18.7 ±2.1	24.5 ±2.2	26.8 ±2.2	25.5 ±4.5	39.7 ±14.0
$sc(d_v)$, m	4.26 ±.48	5.33 ±.28	6.11 ±.27	8.73 ±.53	12.05 ±1.69	22.00 ±8.26
T_{sf}, sec	20.6 ±1.4	24.4 ±2.0	38.8 ±2.9	36.8 ±2.2	42.5 ±2.0	48.3 ±1.4
T_{sv}, sec	12.0 ±1.5	15.4 ±3.3	19.0 ±4.0	27.6 ±1.8	42.8 ±1.4	41.4 ±4.8
$cov(\epsilon_f)$, 10^2 m^2	55.4 ±.3	25.5 ±1.6	21.9 ±7.0	16.3 ±3.0	NR[a]	NR
$cov(\epsilon_v)$, 10^2 m^2	1.29 ±.08	1.25 ±.36	1.43 ±.32	1.87 ±.31	NR	NR
$cov(\dot{\epsilon}_f)$, $10^2(m/sec)^2$	1.15 ±.02	1.16 ±.05	3.26 ±1.26	3.55 ±2.15	NR	NR
$cov(\dot{\epsilon}_v)$, $10^2(m/sec)^2$	0.19 ±.01	0.88 ±.54	2.26 ±1.24	0.79 ±.37	NR	NR
cov(p), 10^{-3} $(rad/sec)^2$	2.60 ±.37	1.78 ±.15	2.22 ±.74	1.27 ±.10	9.30 ±.34	4.36 ±.63
$cov(\delta_s)$, cm^2 (roll)	0.95 ±.10	0.72 ±.05	0.83 ±.27	0.54 ±.04	2.95 ±.18	1.48 ±.22
$cov(\delta_c)$, cm^2 (collective)	2.74 ±.11	2.74 ±.53	2.35 ±.19	1.97 ±.20	8.49 ±2.48	1.75 ±.29

[a]Not relevant for this display configuration.

TABLE 12.- RESULTS OF MONITORING EXPERIMENT; SUBJECTS 1 AND 2

	Subject 1			Subject 2		
	Tunnel plus predictor/director (no roll), k_{pv} = 0.2 D = 229 m (750 ft)	Predictor/director (no roll), k_{pv} = 0.2 D = 229 m (750 ft)	EADI/map	Tunnel plus predictor/director (no roll), k_{pv} = 0.2 D = 229 m (750 ft)	Predictor director (no roll), k_{pv} = 0.2 D = 229 m (750 ft)	EADI map
No. of series of 4	13	12	12	19	18	16
T_r, sec	8.3 ±1.8	9.0 ±1.6	11.2 ±1.5	7.5 ±1.4	8.1 ±1.6	8.6 ±1.5
T_c, sec	6.6 ±1.3	7.3 ±2.3	10.7 ±4.7	5.0 ±2.8	9.0 ±2.4	8.8 ±3.6
$cov(d_f)$, 10^2 m^2	2.04 ±.58	3.95 ±2.87	9.29 ±9.29	1.62 ±.26	3.81 ±1.77	4.88 ±5.03
$cov(d_v)$, 10^2 m^2	0.67 ±.14	0.90 ±.37	1.49 ±.48	0.60 ±.12	0.84 ±.26	0.96 ±.53
$cov(\epsilon_f)$, 10^2 m^2	1.72 ±.59	2.69 ±1.66	NR[a]	1.68 ±.63	3.16 ±1.57	NR
$cov(\epsilon_v)$, 10^2 m^2	0.87 ±.21	1.03 ±.39	NR	0.68 ±.17	0.84 ±.23	NR
$cov(d_\psi)$, 10^{-3}rad^2	9.70 ±3.20	14.47 ±9.39	27.65 ±16.32	6.83 ±1.76	12.44 ±5.65	20.07 ±9.63
cov(p), 10^{-3} (rad/sec)^2	2.25 ±.34	2.36 ±.62	6.75 ±3.36	2.39 ±.46	1.94 ±.34	8.00 ±2.59
$cov(\delta_s)$, cm^2 (roll)	1.44 ±.15	1.58 ±.35	2.96 ±1.05	1.46 ±.18	1.38 ±.26	3.15 ±.75
$cov(\delta_c)$, cm^2 (collective)	7.63 ±1.95	6.99 ±2.07	9.15 ±2.06	7.38 ±1.74	8.15 ±2.03	7.72 ±1.97

[a]Not relevant for this display configuration.

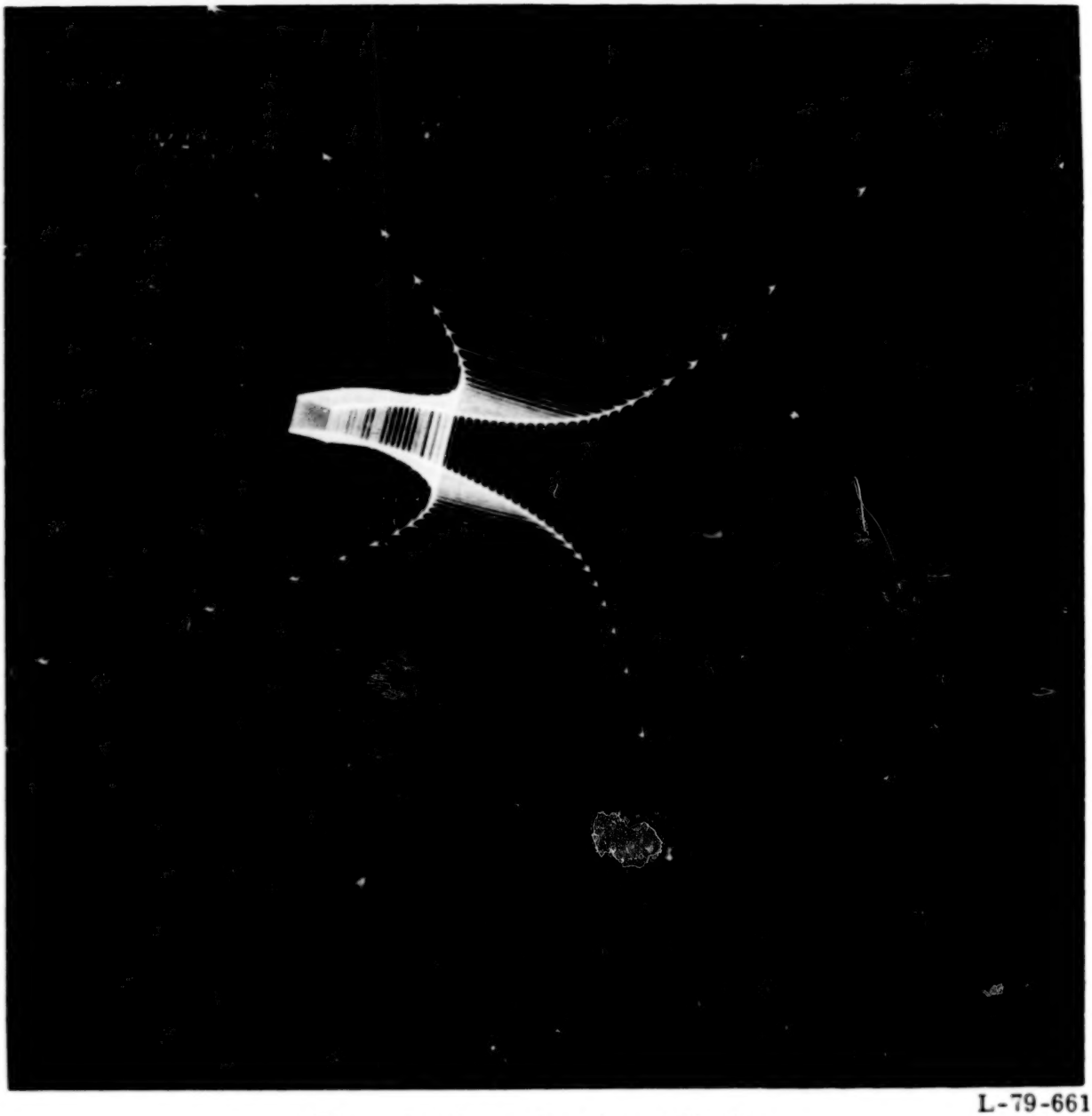

L-79-661

Figure 1.- Conceptual tunnel display.

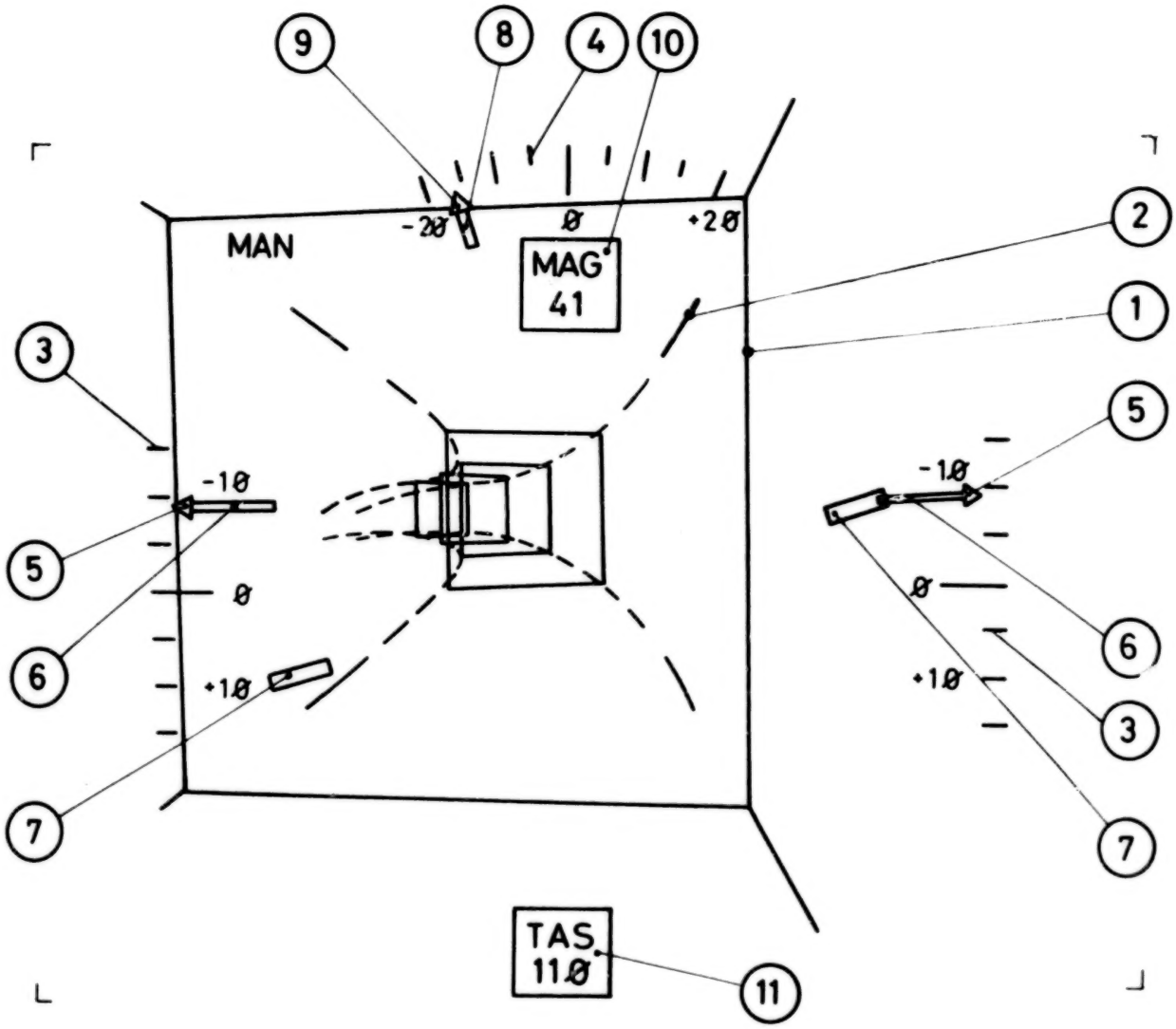

(a) Basic tunnel display, roll-stabilized version.

Figure 2.- Display configurations. Adage Graphics Terminal.

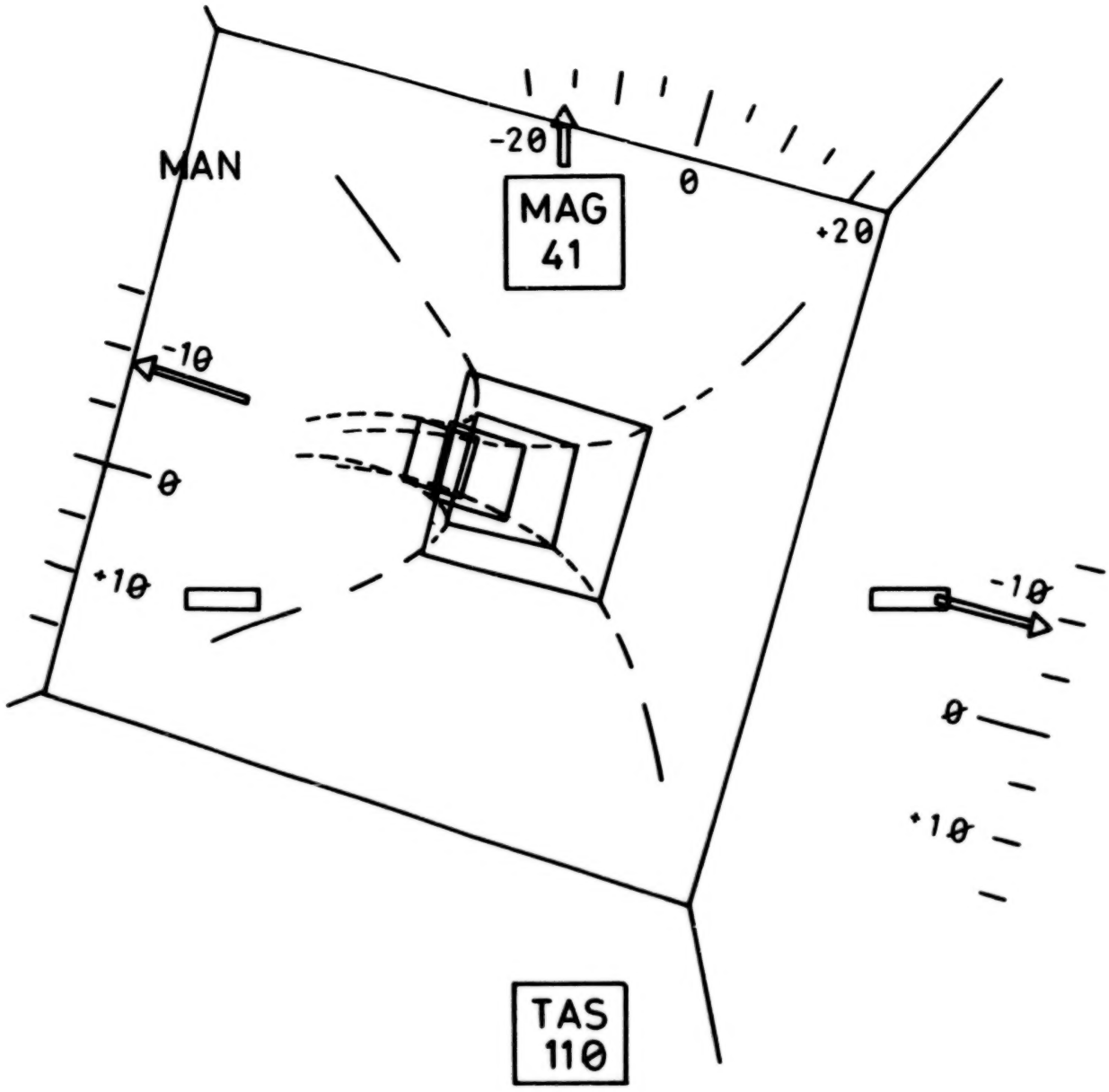

(b) Basic tunnel display, roll version.

Figure 2.- Continued.

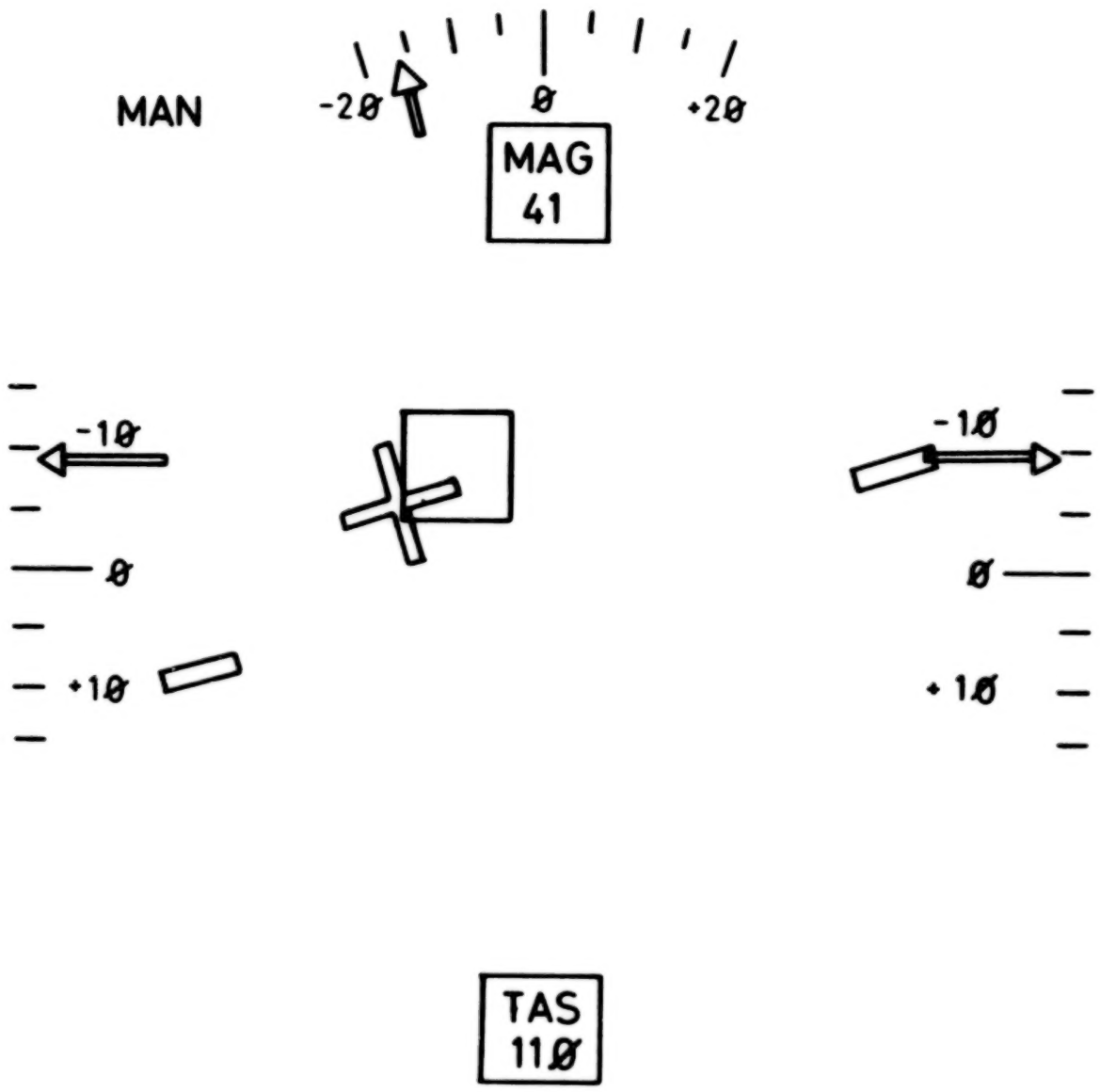

(c) Predictor/director display.

Figure 2.- Continued.

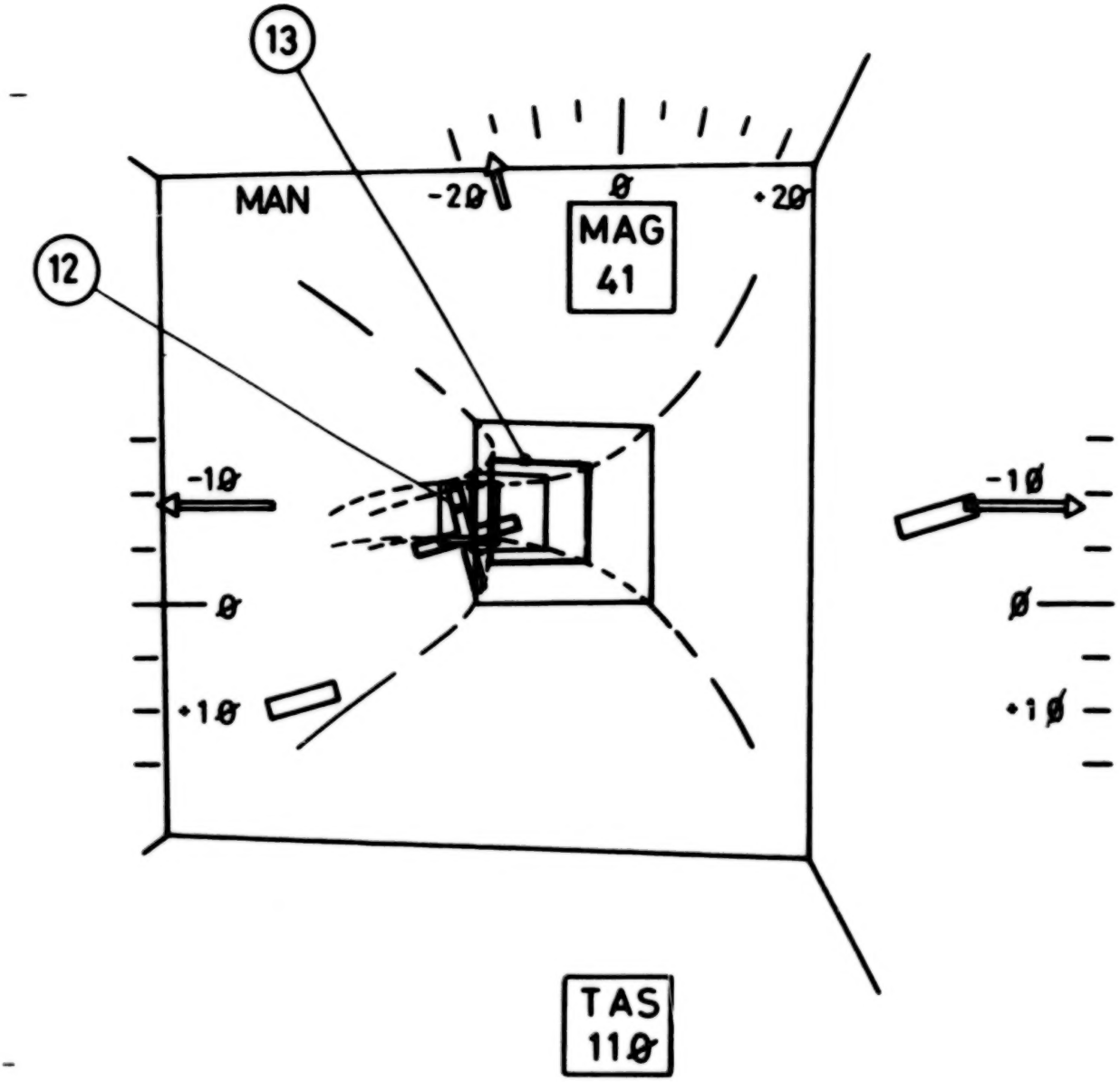

(d) Tunnel display with superimposed predictor symbol.

Figure 2.- Continued.

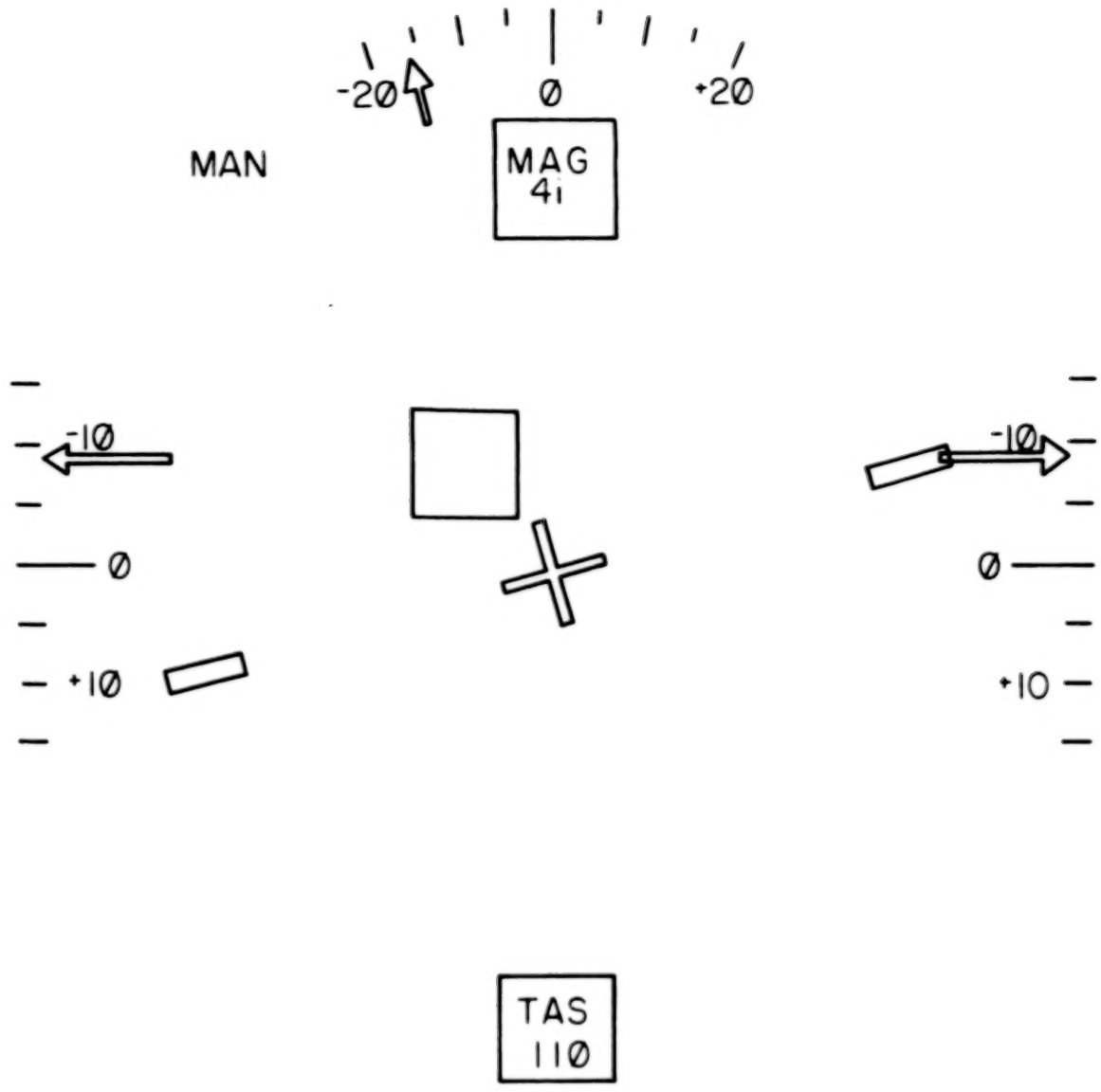

(e) Vehicle axis cross and director square display.

Figure 2.- Continued.

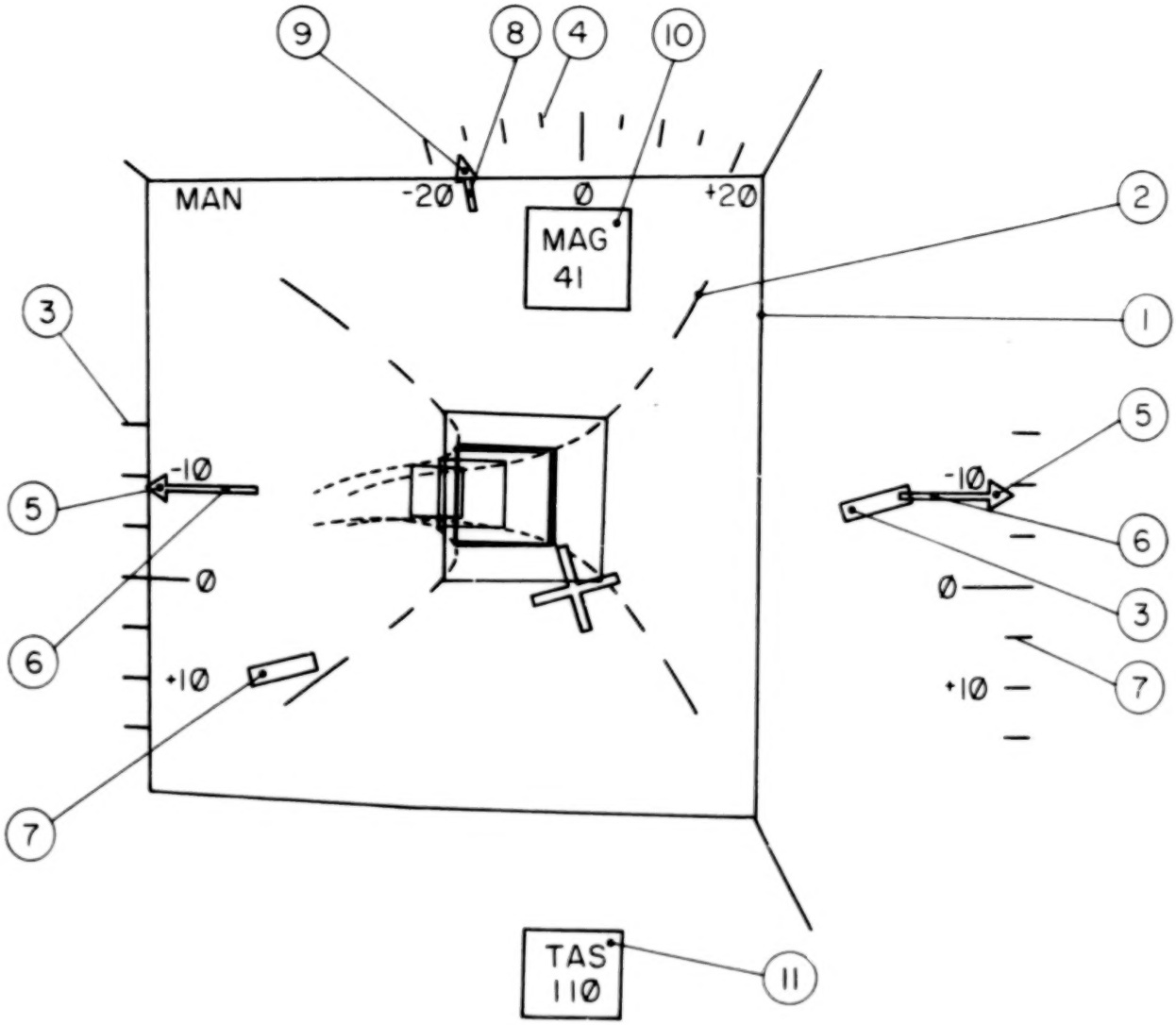

(f) Tunnel display with vehicle axis cross.

Figure 2.- Continued.

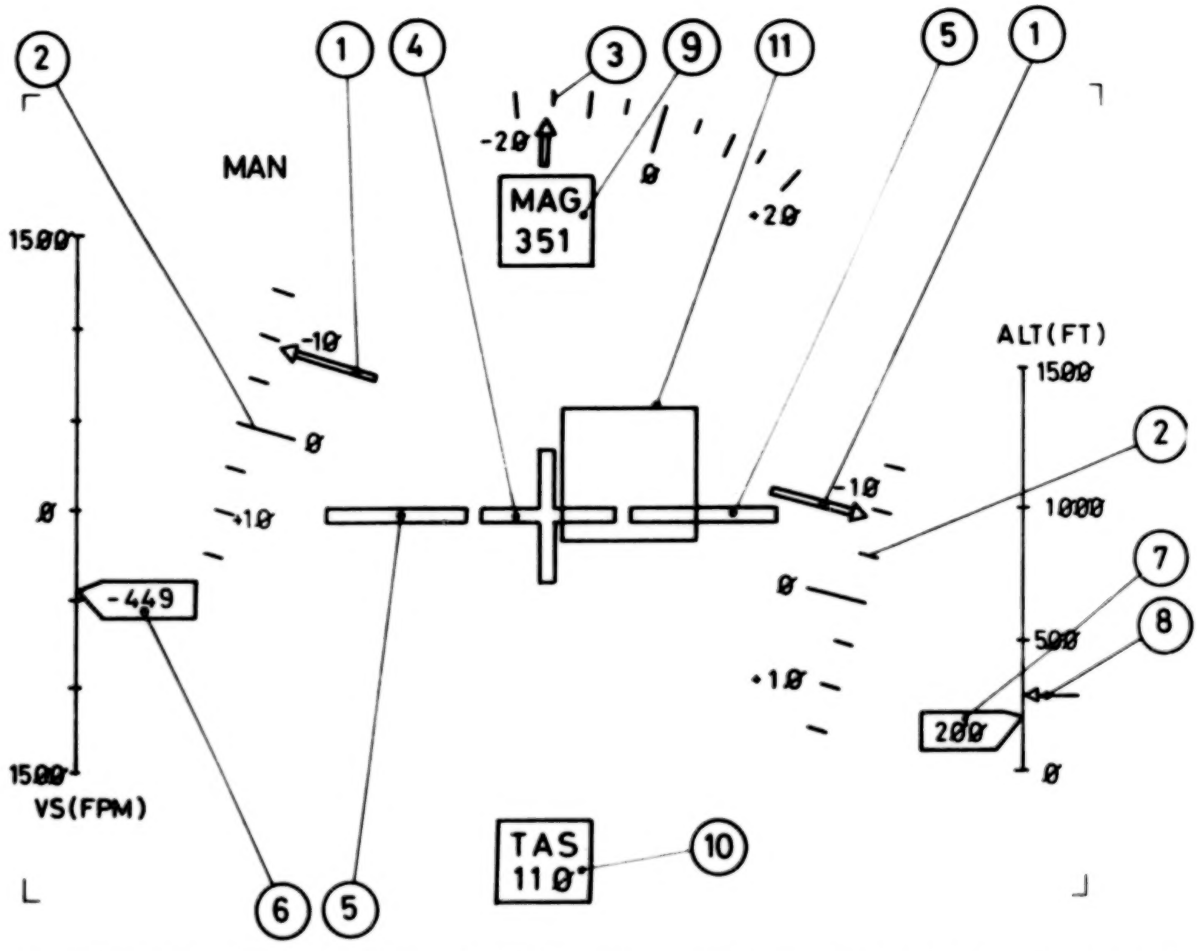

(g) Electronic attitude director indicator with vertical speed indicator and altimeter; 1 m = 3.28 ft and 1 m/sec = 197 ft/min.

Figure 2.- Continued.

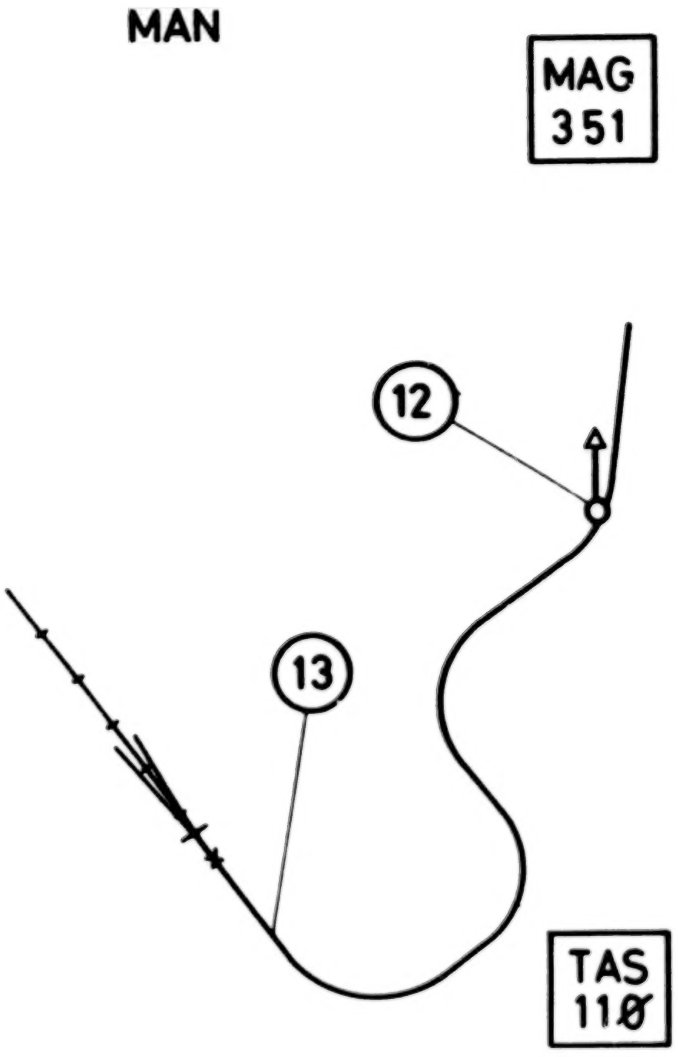

(h) Horizontal situation indicator (map display).

Figure 2.- Concluded.

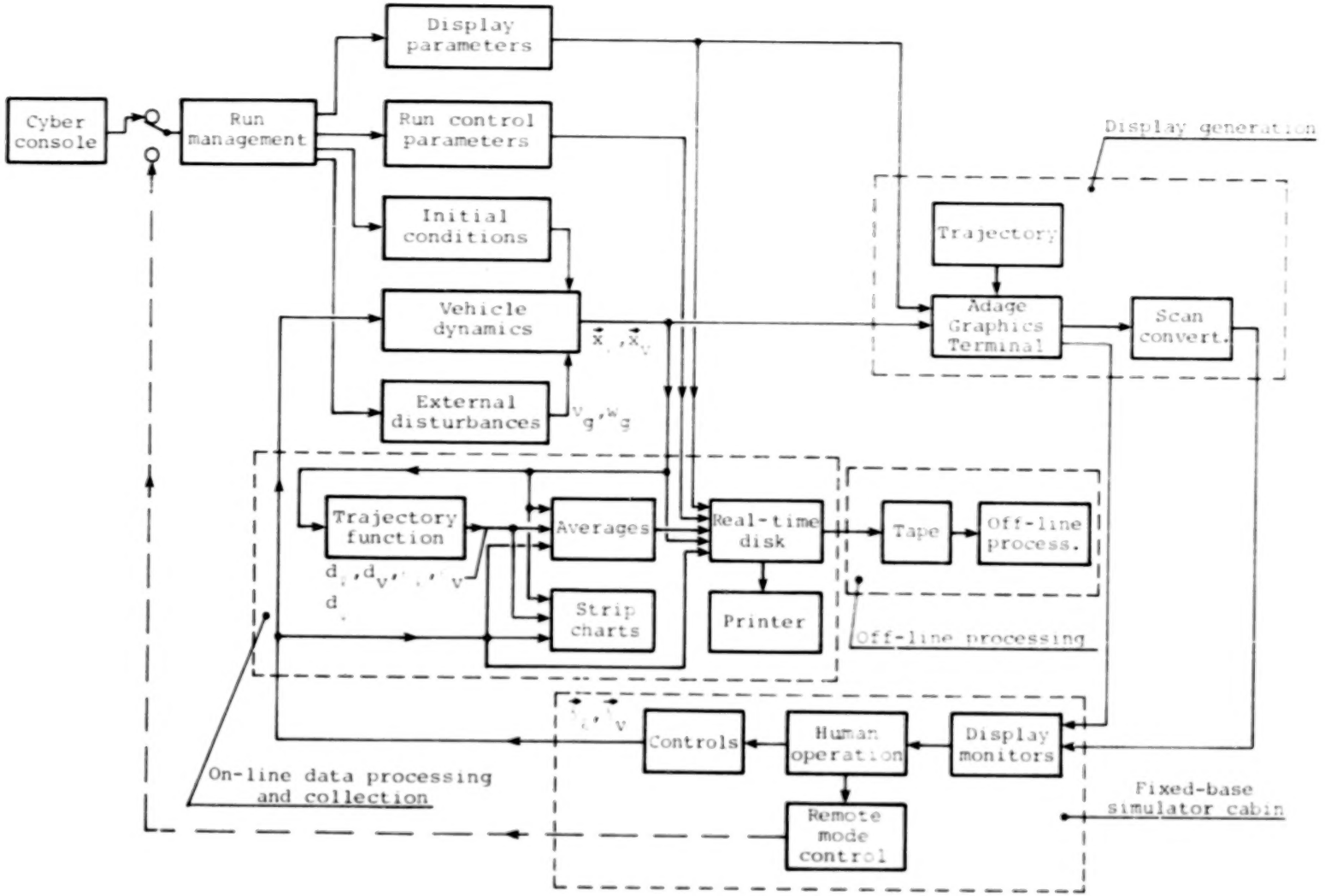

Figure 3.- Functional diagram of experimental system.

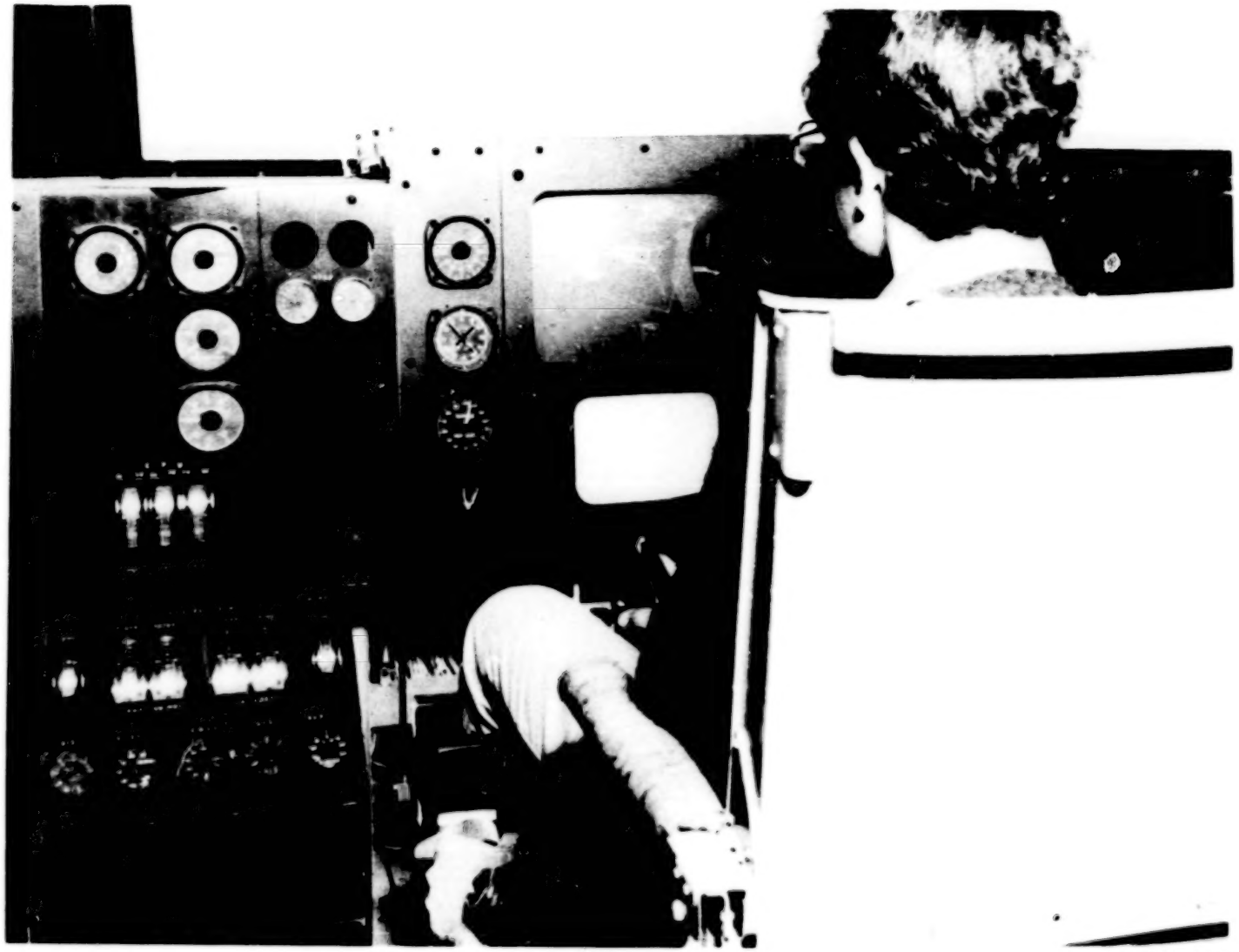

L-79-426

Figure 4.- Fixed-base simulator cabin.

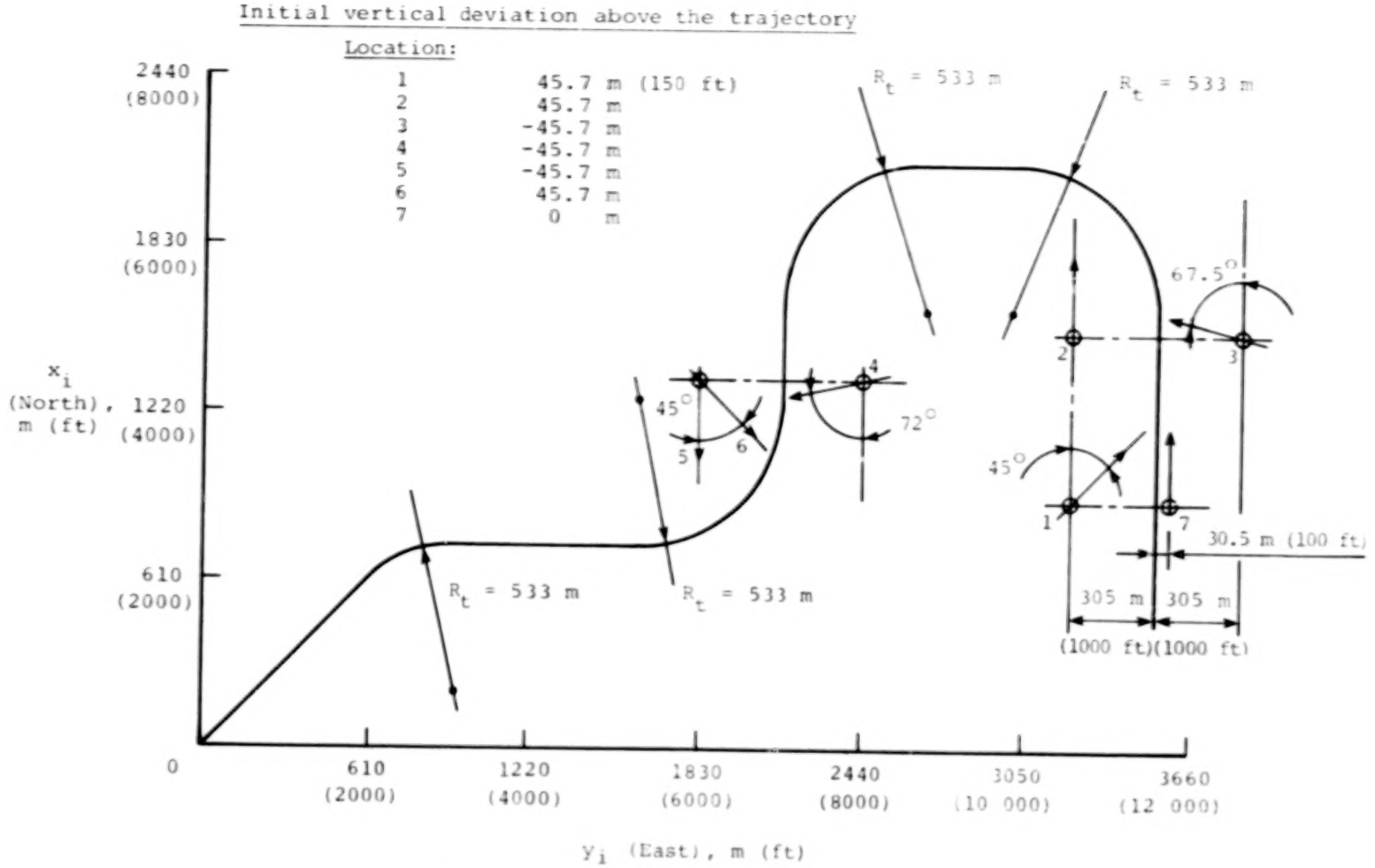

Figure 5.- Plan view of desired trajectory.

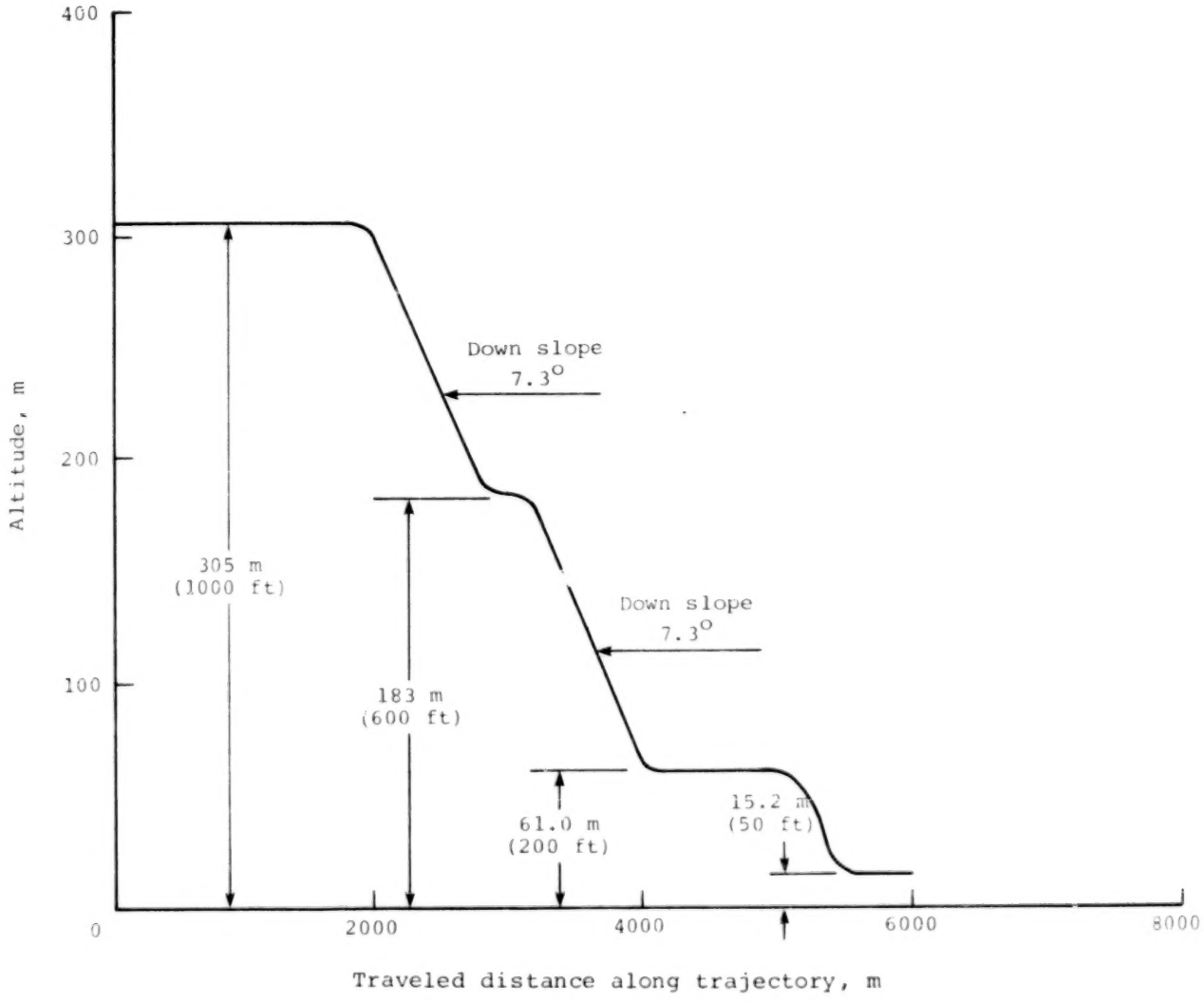

Figure 6.- Descent profile of desired trajectory.

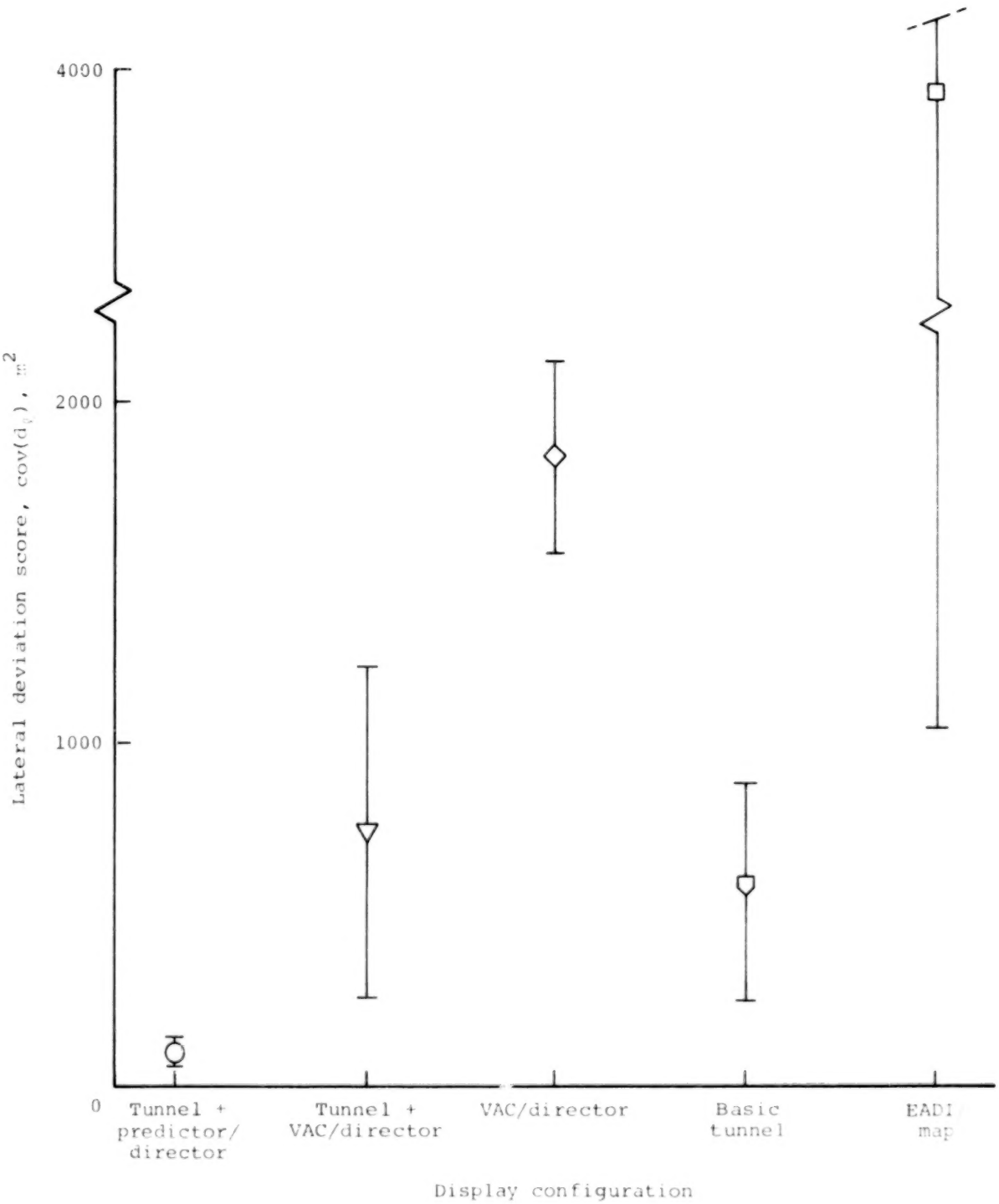

Figure 7.- Results of trajectory following experiment; lateral deviation score, subject 1.

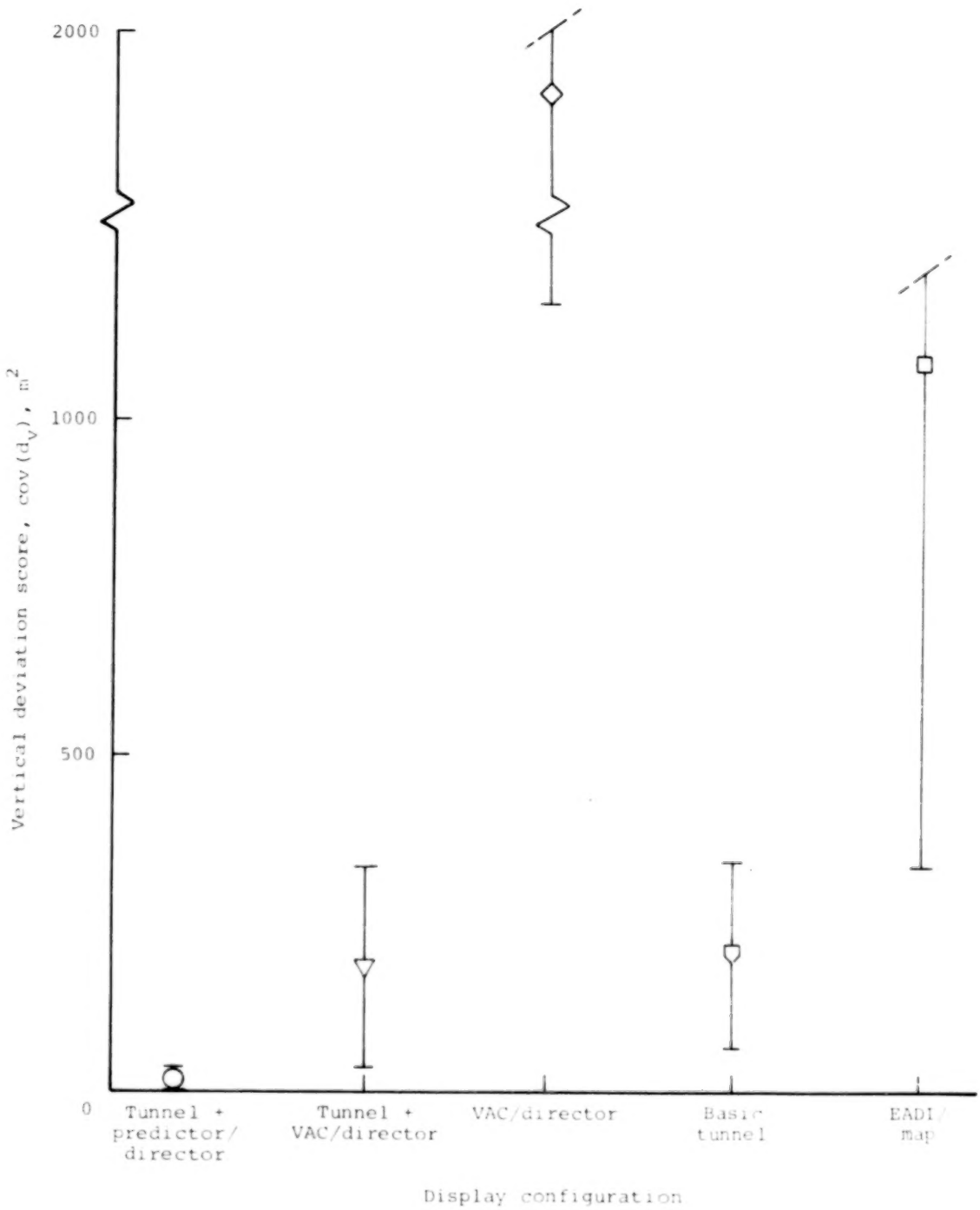

Figure 8.- Results of trajectory following experiment; vertical deviation score, subject 1.

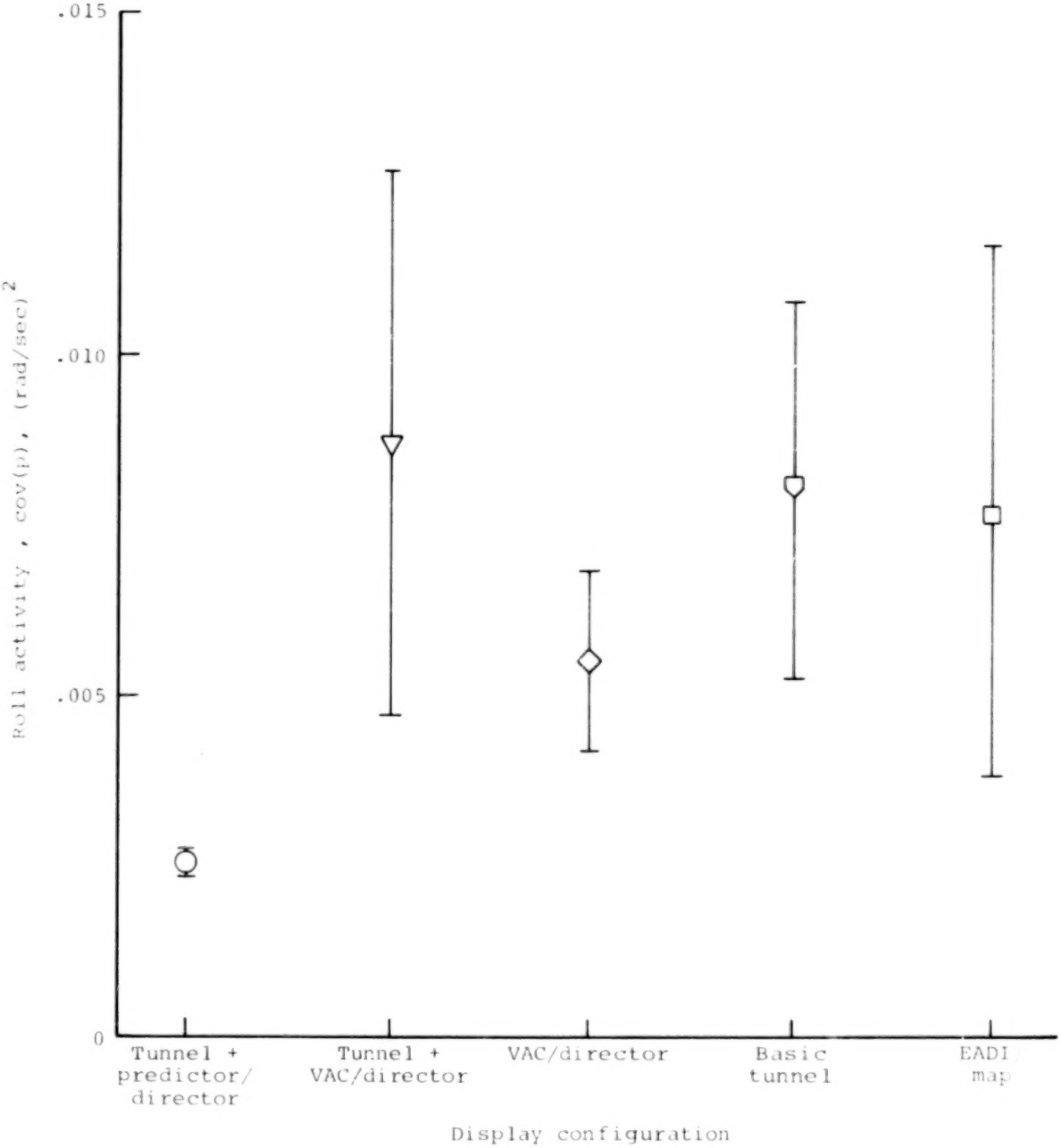

Figure 9.- Results of trajectory following experiment; roll activity, subject 1.

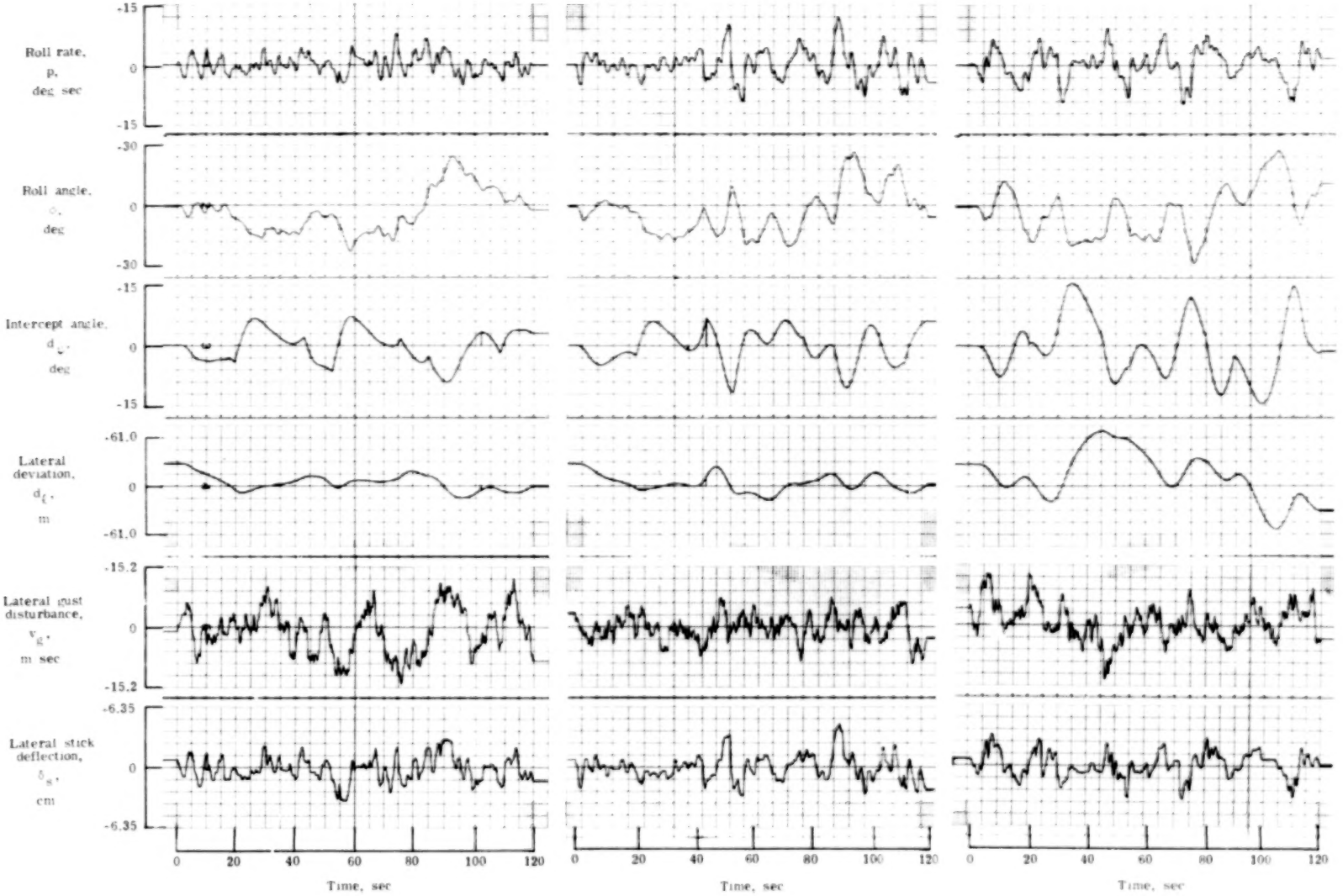

(a) Tunnel/predictor display, $k_{pv} = 0.2$, D = 305 m (1000 ft).

(b) Basic tunnel display.

(c) EADI/map.

Figure 10.- Time histories of lateral response for trajectory following; subject 1.

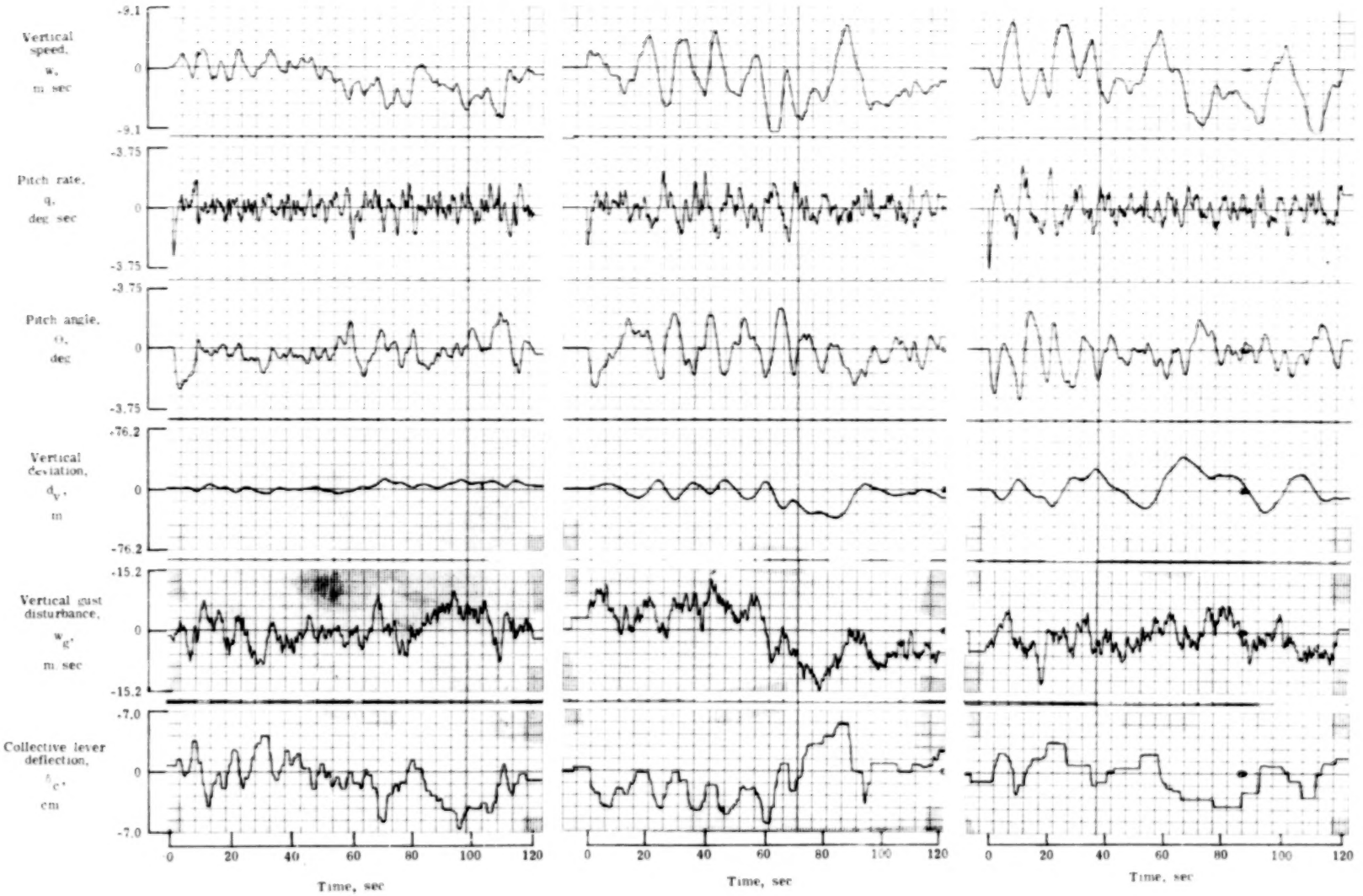

(a) Tunnel/predictor display, $k_{pv} = 0.2$, D = 305 m (1000 ft).

(b) Basic tunnel display.

(c) EADI/map.

Figure 11.- Time histories of vertical response for trajectory following; subject 1.

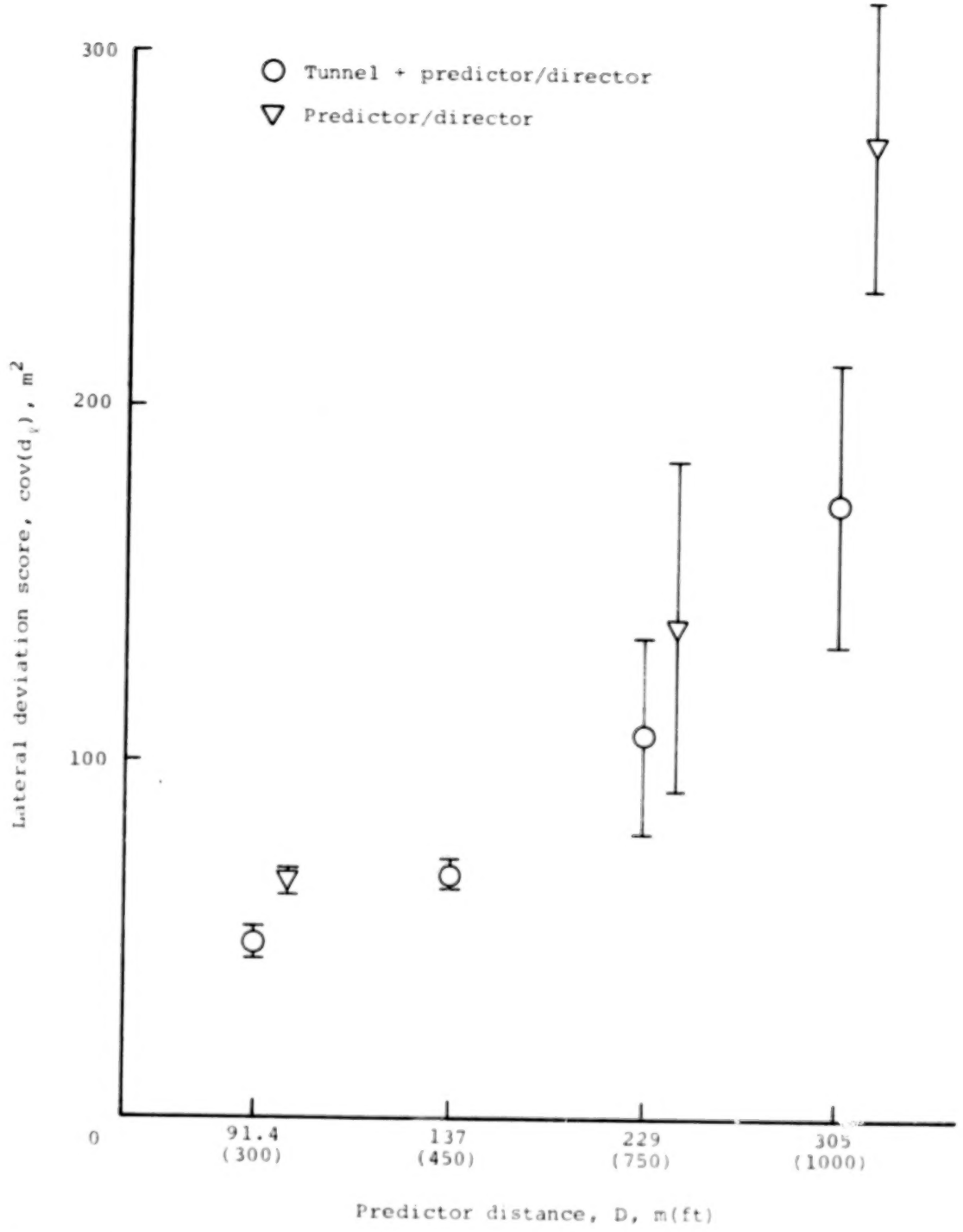

Figure 12.- Results of trajectory following experiment; effect of D on lateral deviation score, subject 1.

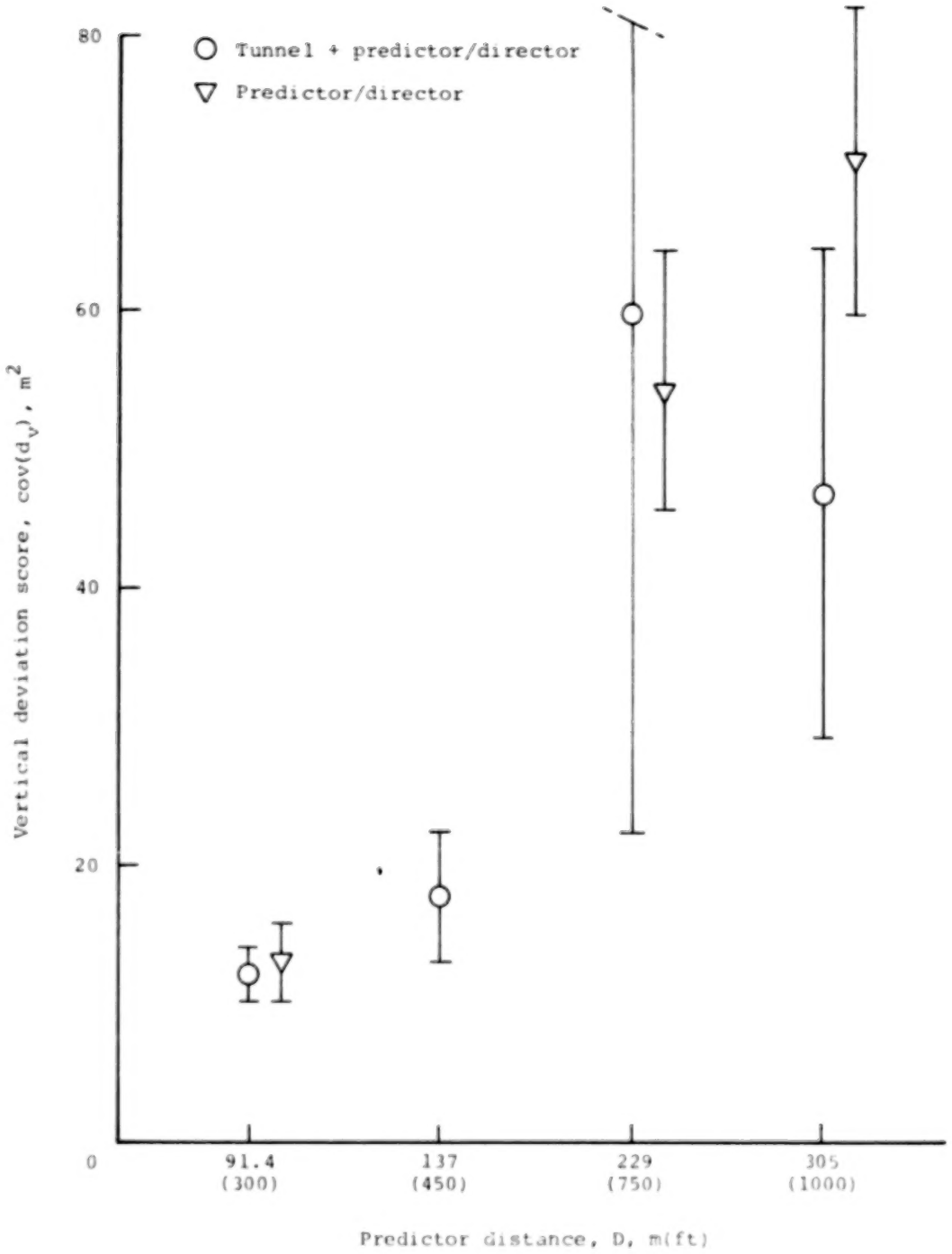

Figure 13.- Results of trajectory following experiment; effect of D on vertical deviation score, subject 1.

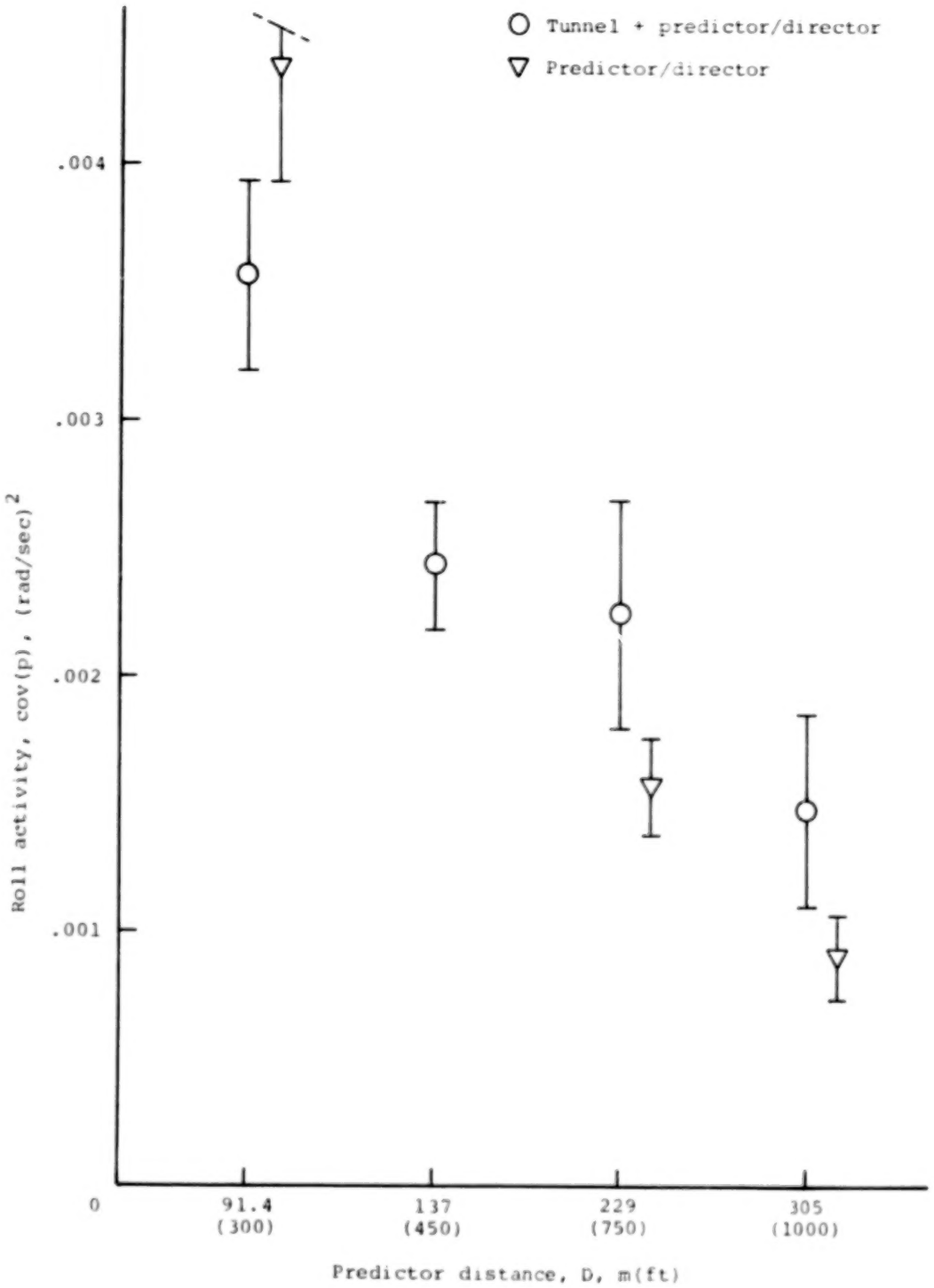

Figure 14.- Results of trajectory following experiment; effect of D on roll activity, subject 1.

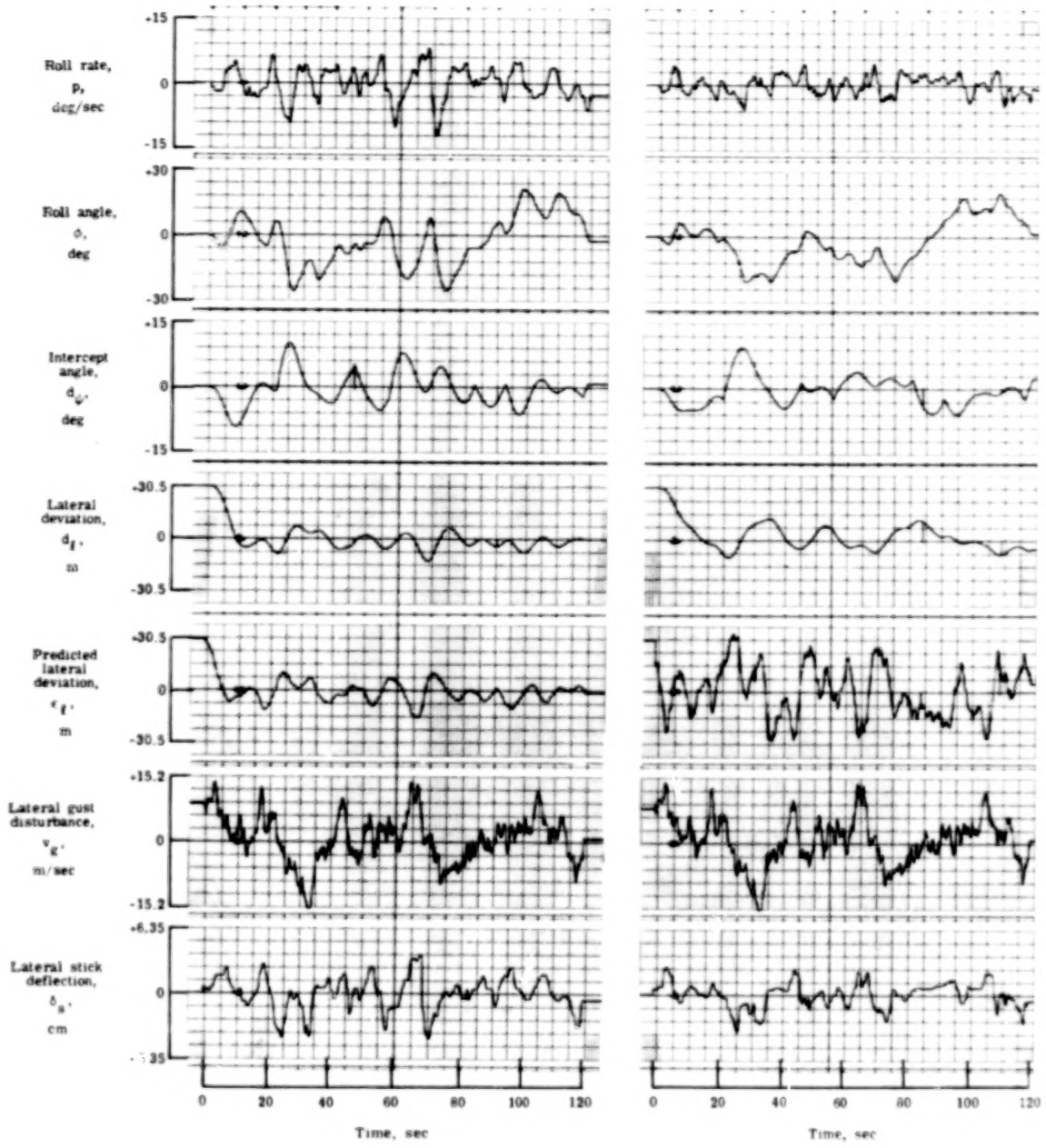

(a) Tunnel plus predictor/director; $k_{pv} = 1$, D = 91.4 m (300 ft).

(b) Tunnel plus predictor/director; $k_{pv} = 1$, D = 229 m (750 ft).

Figure 15.- Time histories of lateral response for trajectory following; effect of D, subject 1.

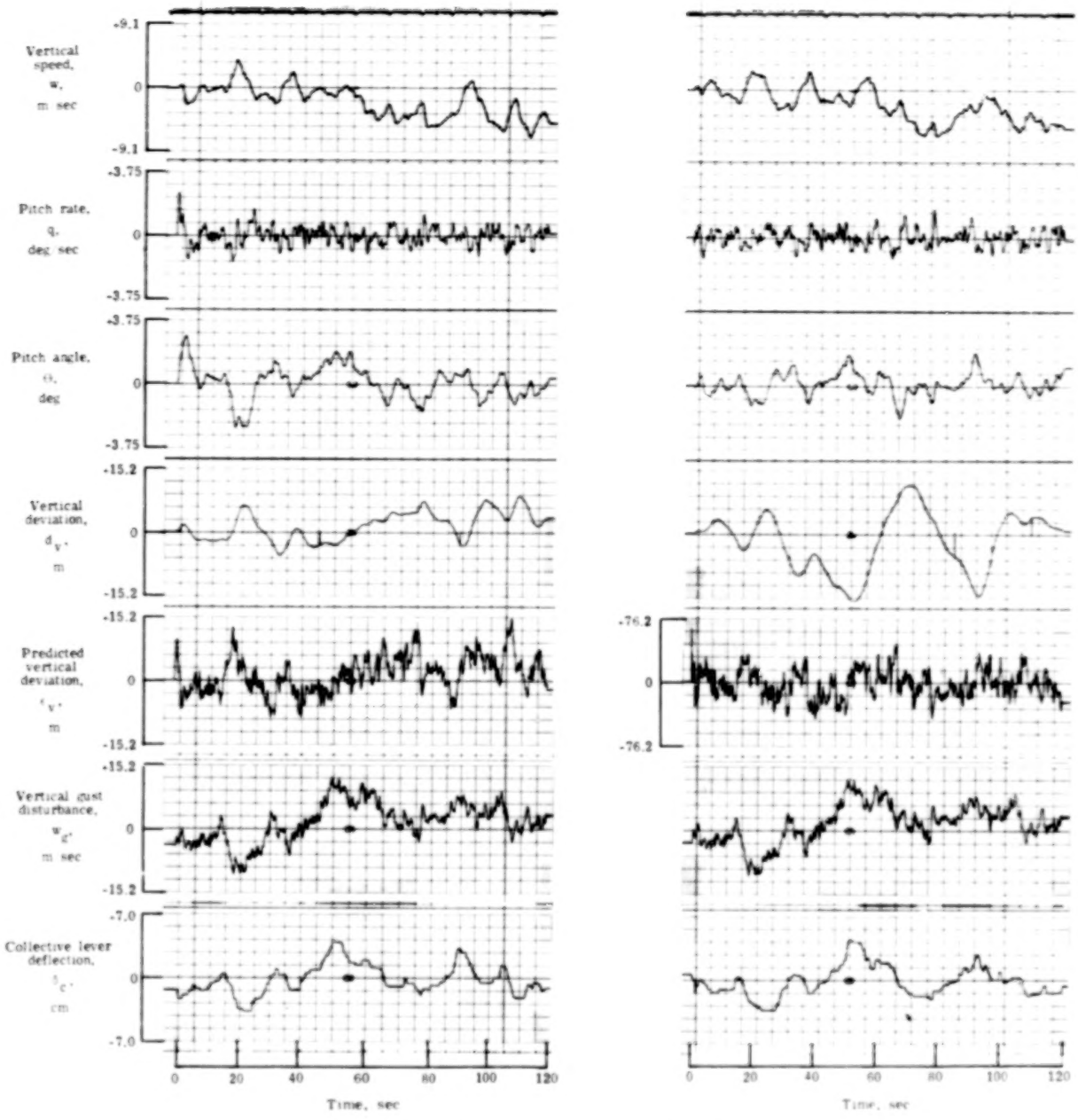

(a) Tunnel plus predictor/director; $k_{pv} = 1$, D = 91.4 m (300 ft).

(b) Tunnel plus predictor/director; $k_{pv} = 1$, D = 229 m (750 ft).

Figure 16.- Time histories of vertical response for trajectory following: effect of D, subject 1.

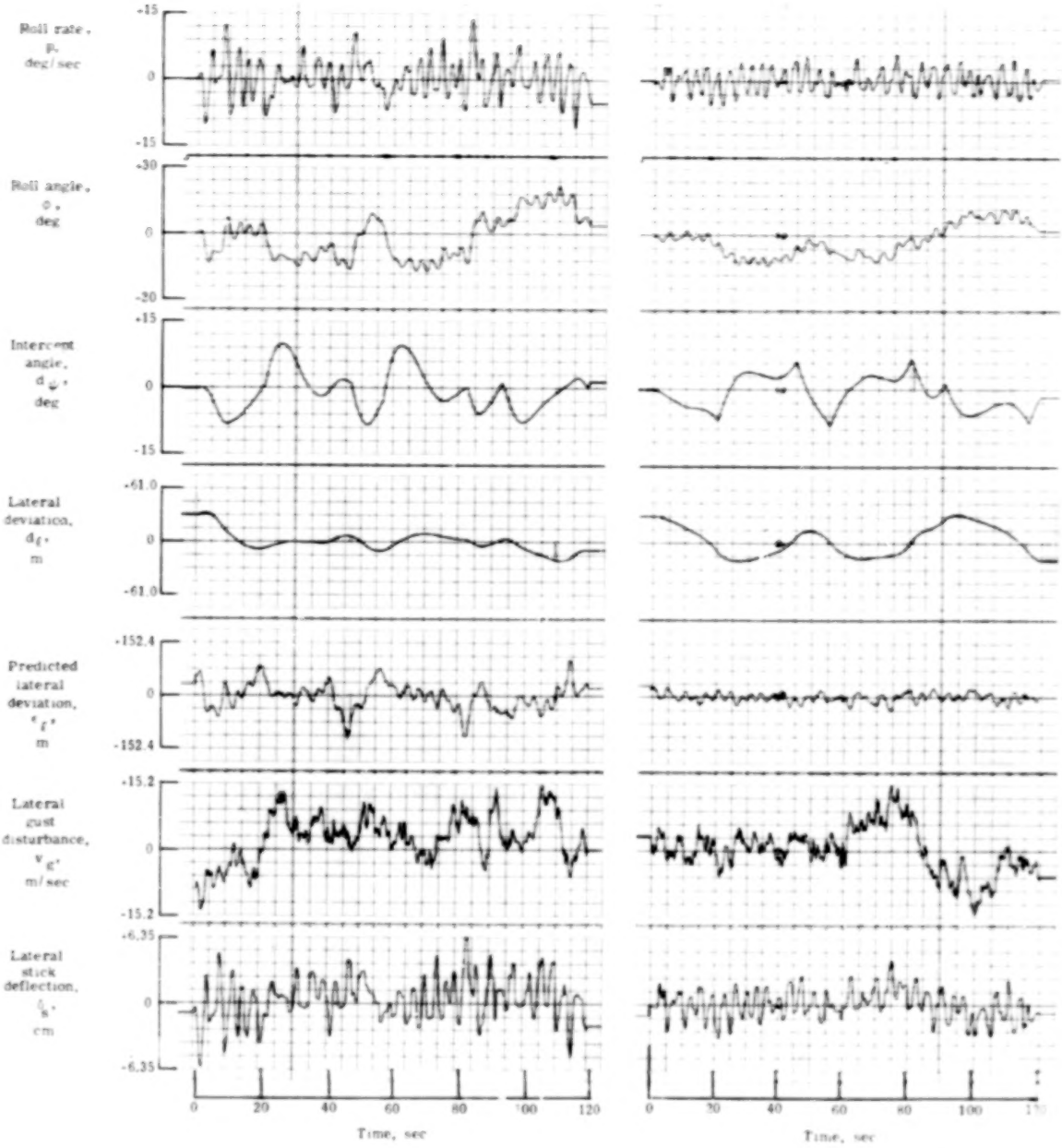

(a) Tunnel plus predictor/director; D = 305 m (1000 ft).

(b) Predictor/director; D = 305 m (1000 ft).

Figure 17.- Time histories of lateral response for trajectory following; comparison of tunnel plus predictor/director with predictor/director, subject 1.

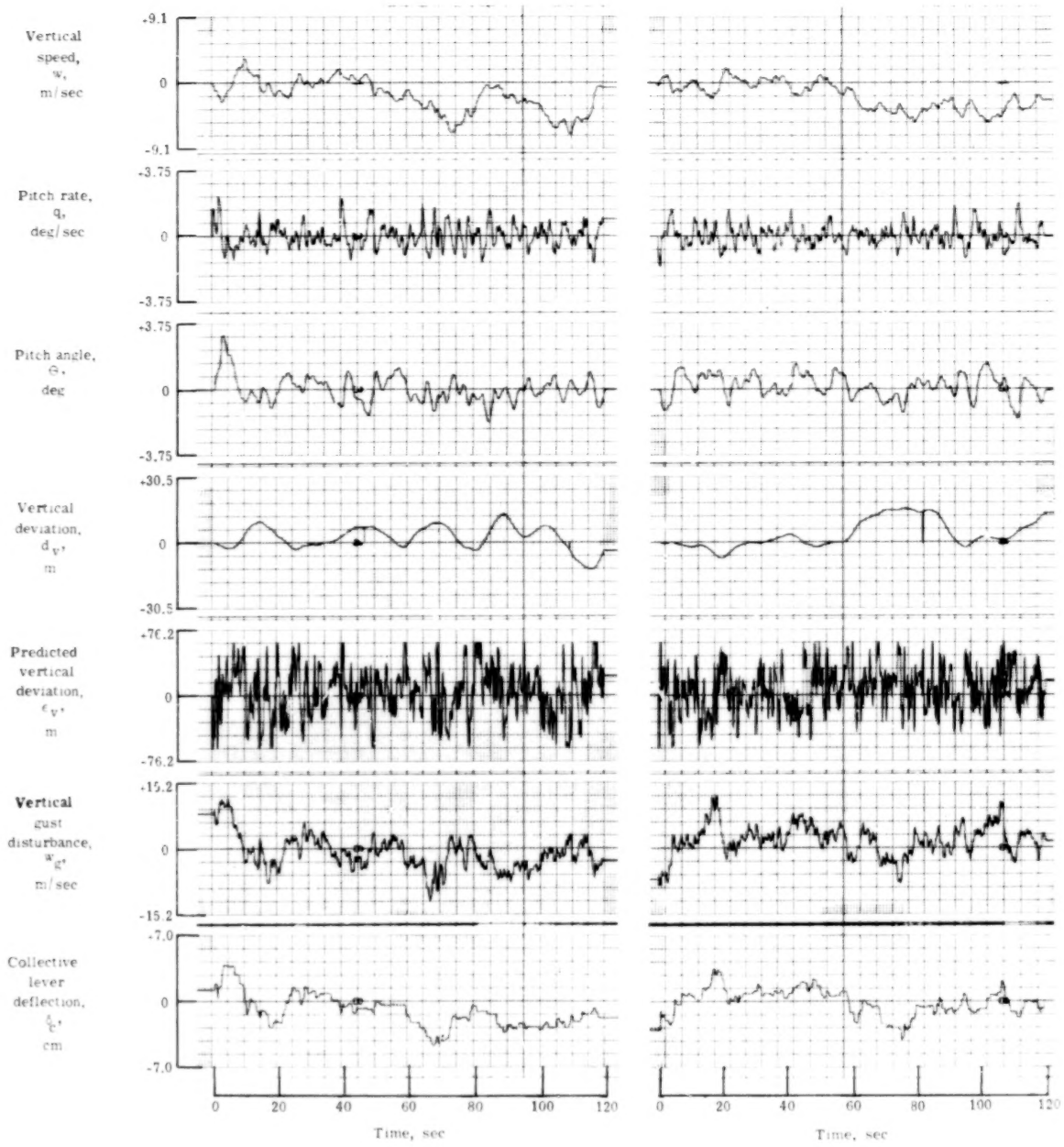

(a) Tunnel plus predictor/director; D = 305 m (1000 ft).

(b) Predictor/director; D = 305 m (1000 ft).

Figure 18.- Time histories of vertical response for trajectory following; comparison of tunnel plus predictor/director with predictor/director, subject 1.

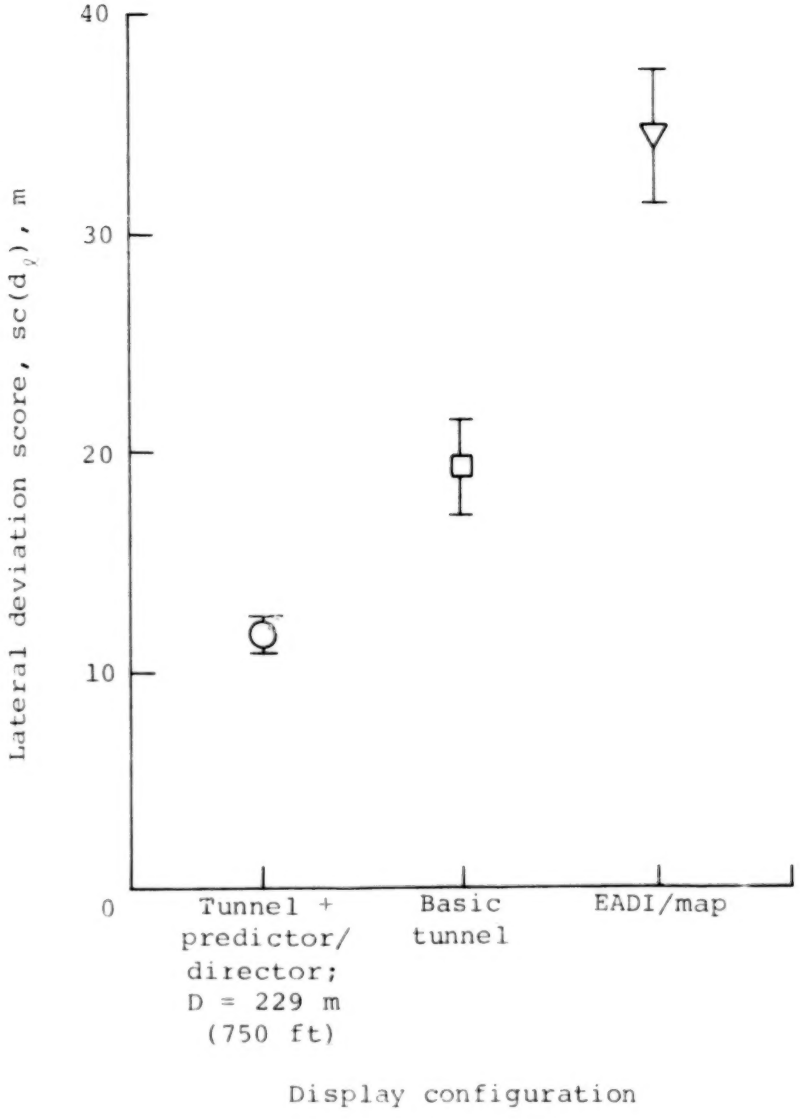

Figure 19.- Results of trajectory entry experiment; lateral deviation score, subject 1.

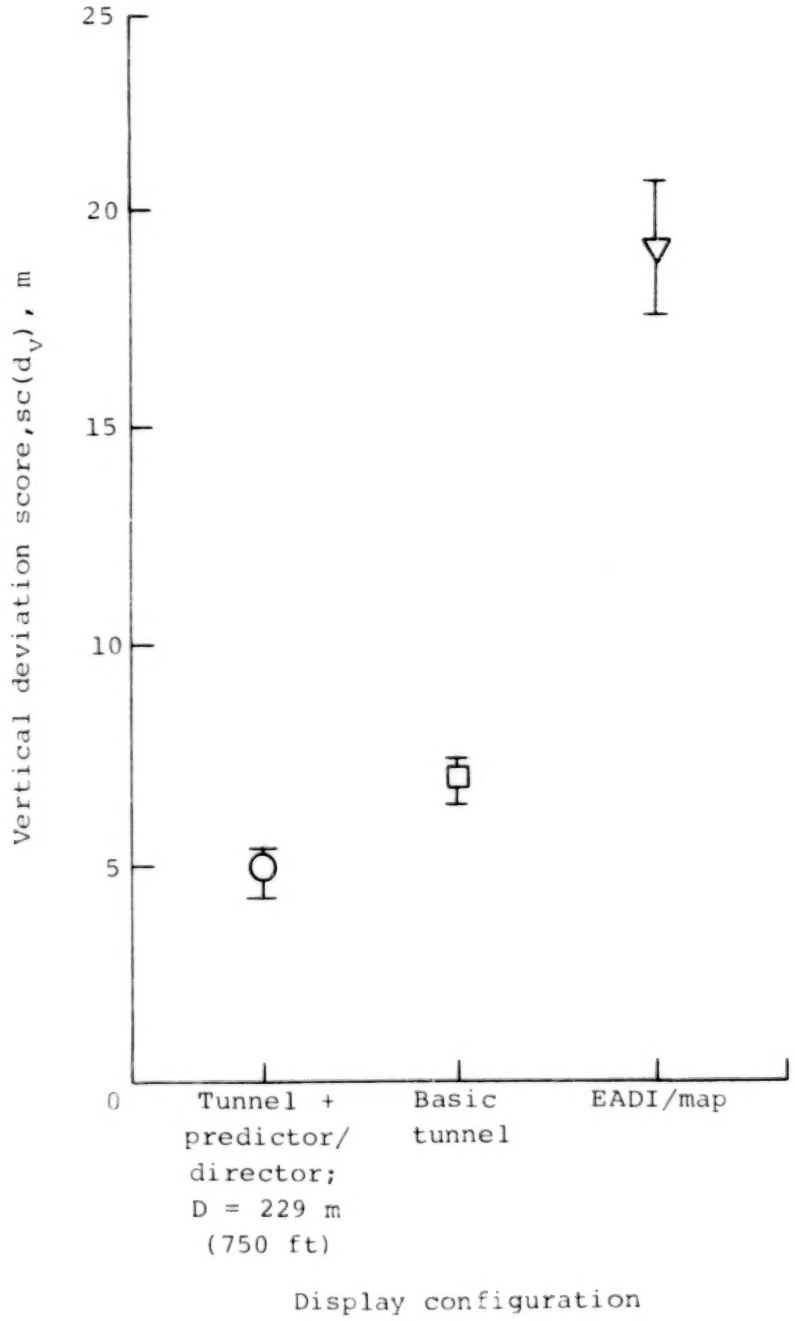

Figure 20.- Results of trajectory entry experiment; vertical deviation score, subject 1.

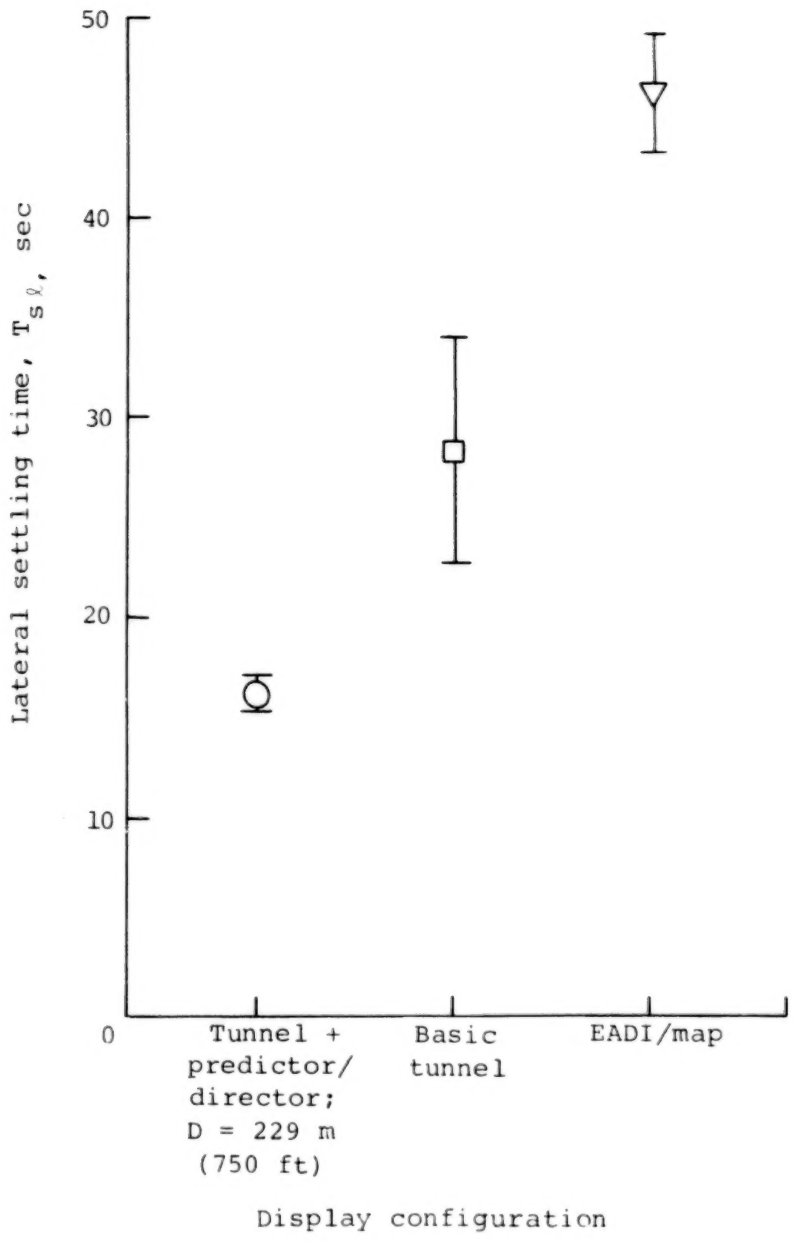

Figure 21.- Results of trajectory entry experiment; lateral settling time, subject 1.

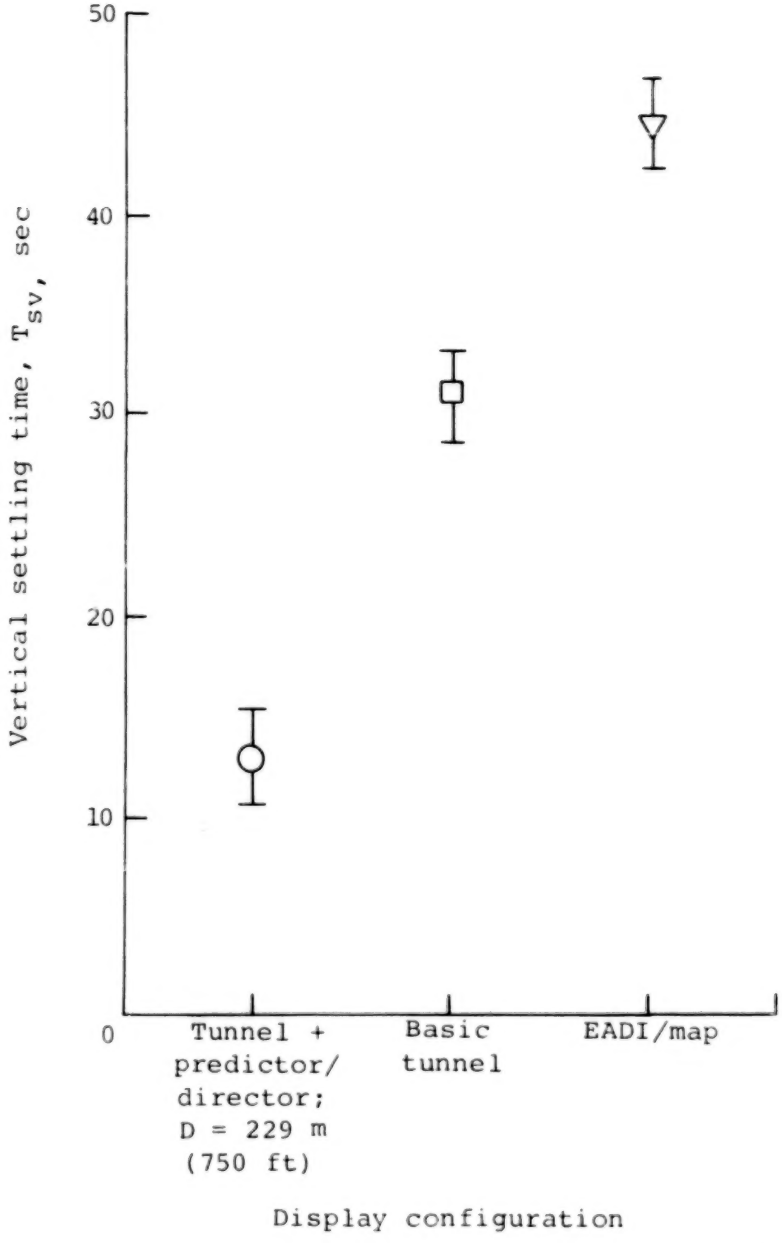

Figure 22.- Results of trajectory entry experiment; vertical settling time, subject 1.

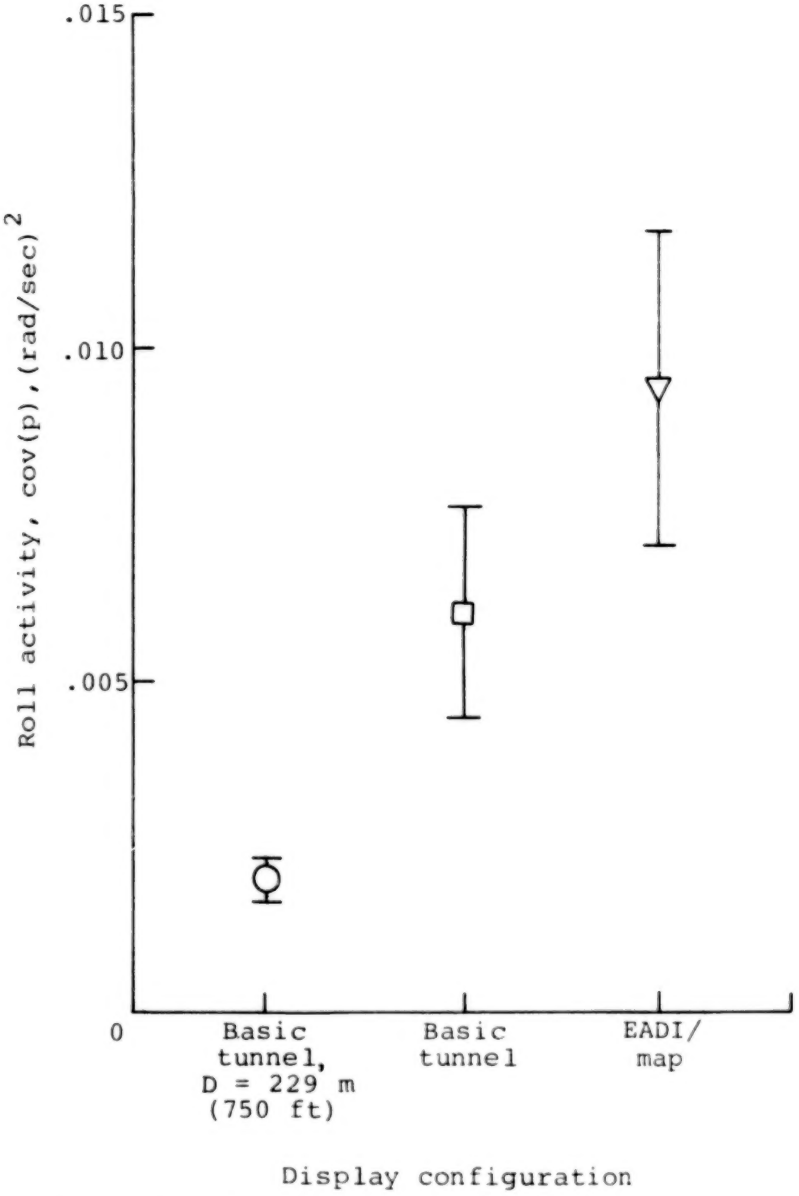

Figure 23.- Results of trajectory entry experiment; roll activity, subject 1.

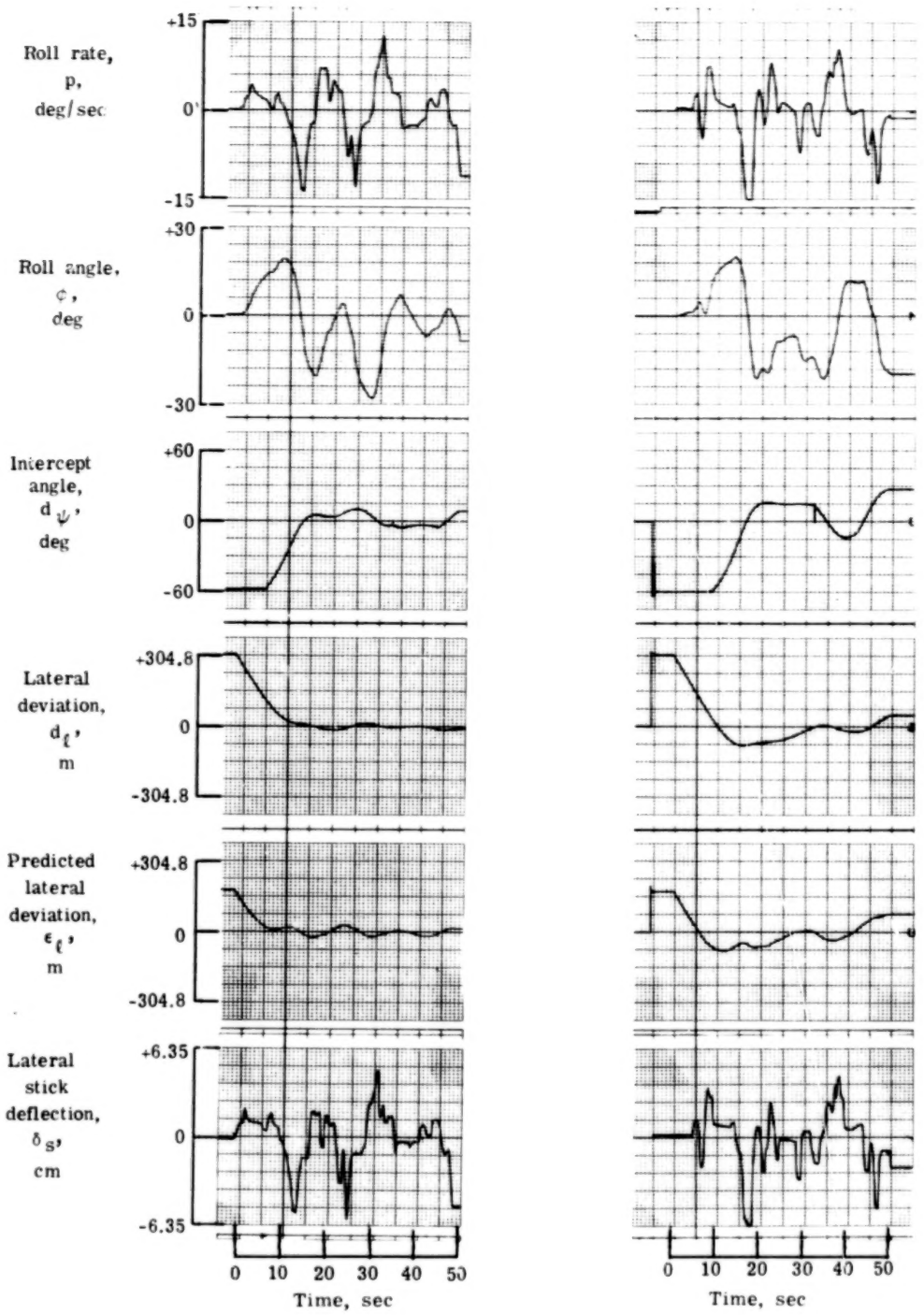

(a) Tunnel display.

(b) EADI/map display.

Figure 24.- Time histories of lateral response for entry maneuvers; comparison of basic tunnel display with EADI/map, subject 1, initial location 3.

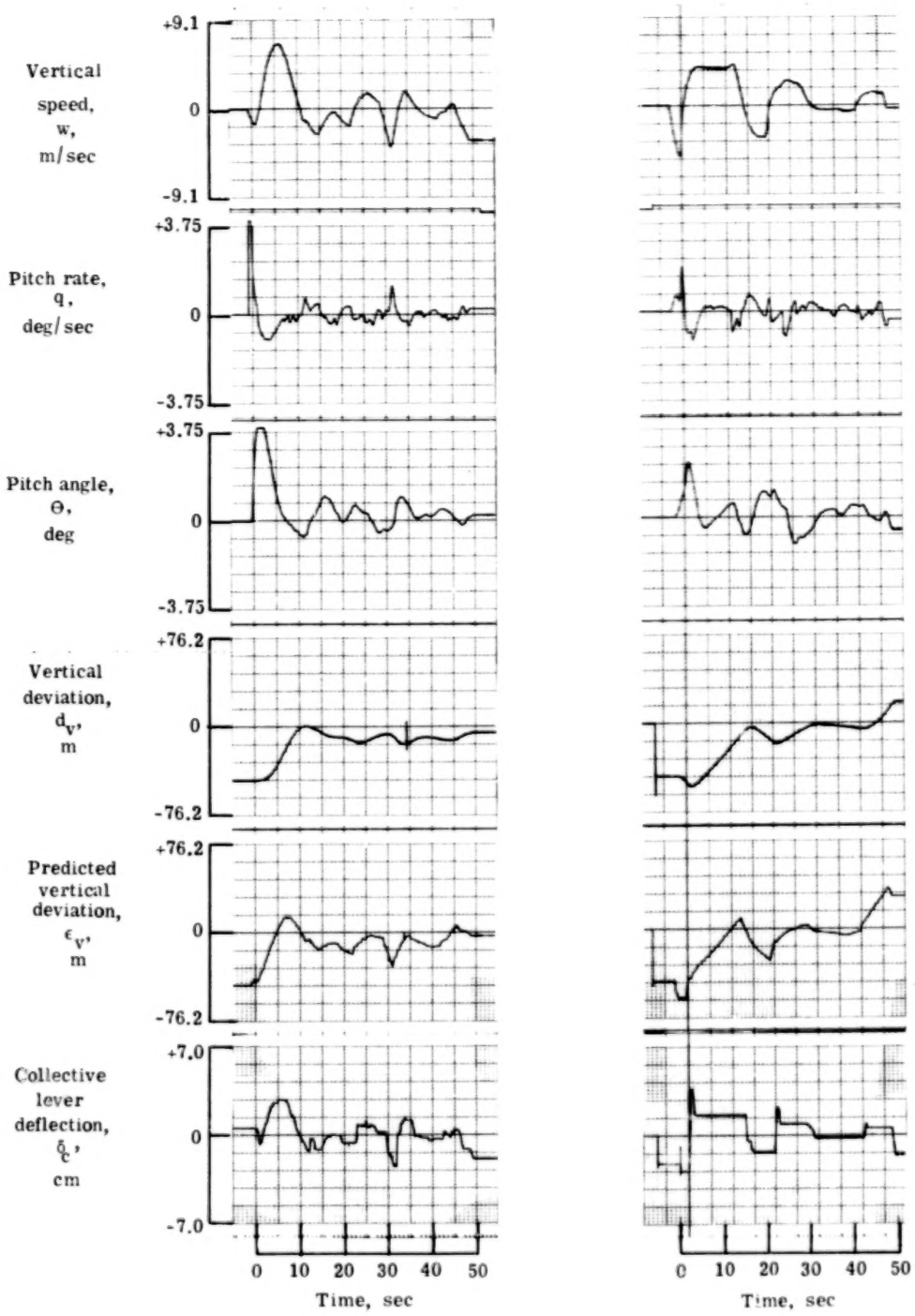

(a) Tunnel display. (b) EADI/map display.

Figure 25.- Time histories of vertical response for entry maneuvers; comparison of basic tunnel display with EADI/map, subject 1, initial location 3.

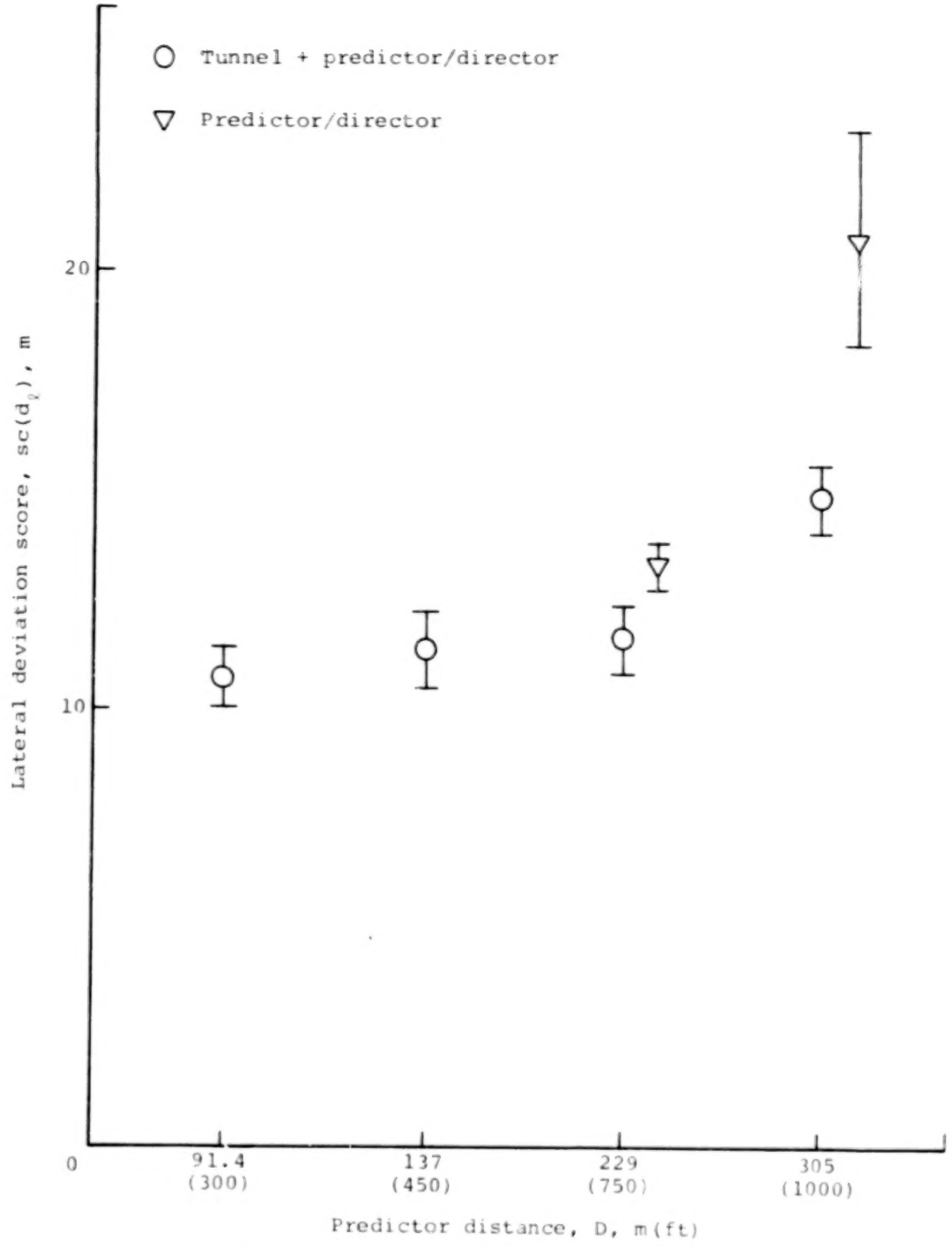

Figure 26.- Results of trajectory entry experiment; effect of D on lateral deviation score, subject 1.

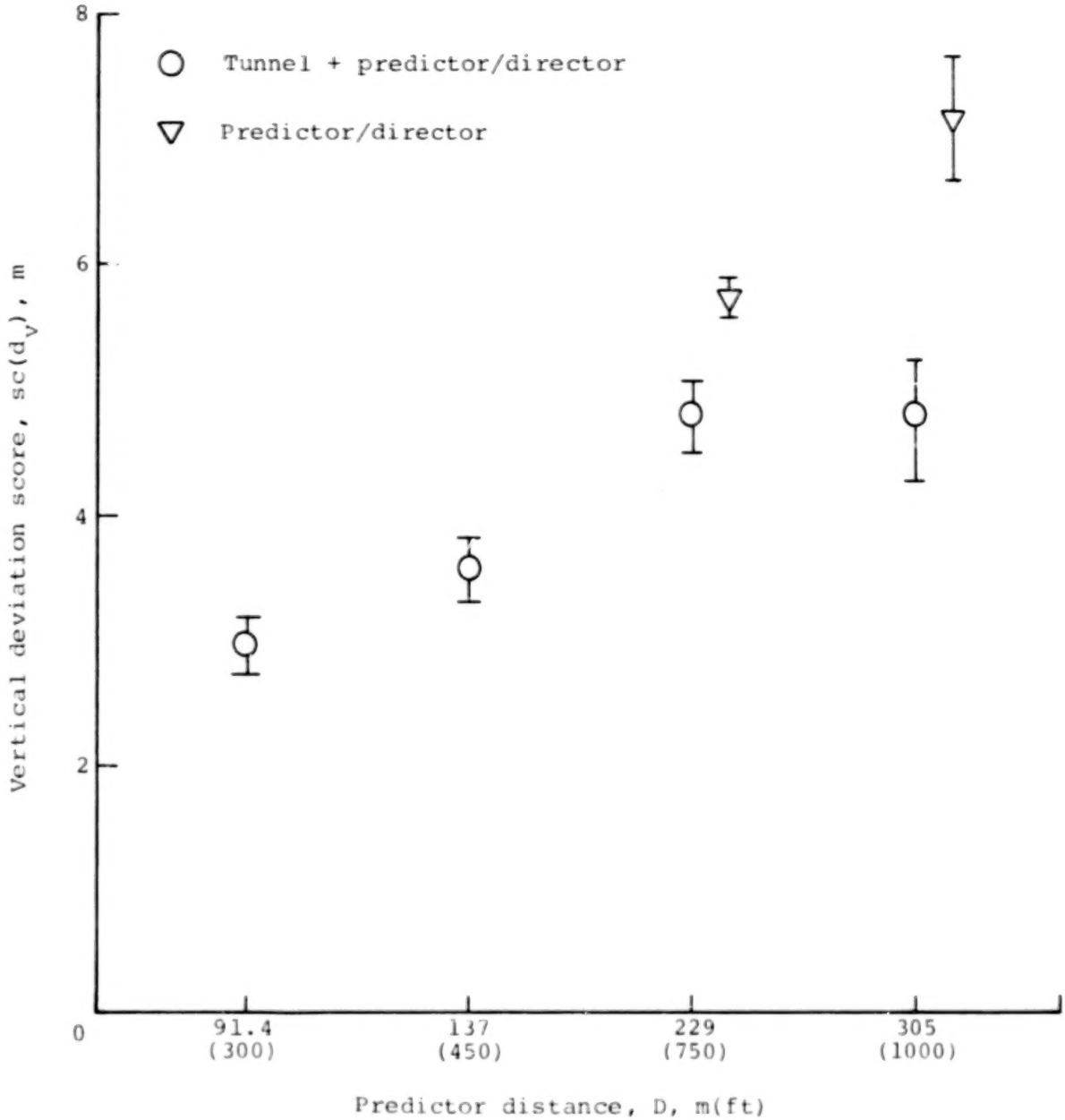

Figure 27.- Results of trajectory entry experiment; effect of D on vertical deviation score, subject 1.

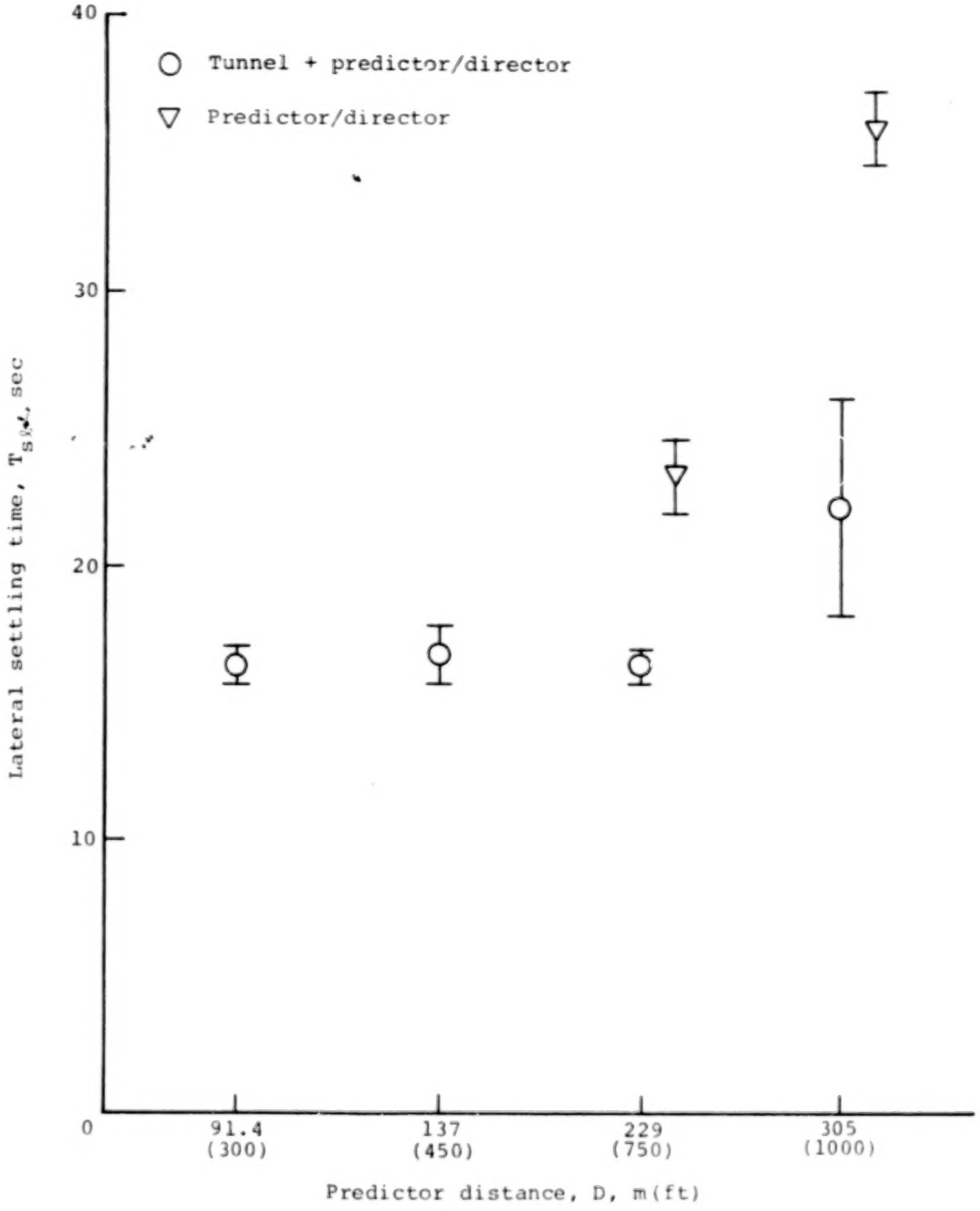

Figure 28.- Results of trajectory entry experiment; effect of D on lateral settling time, subject 1.

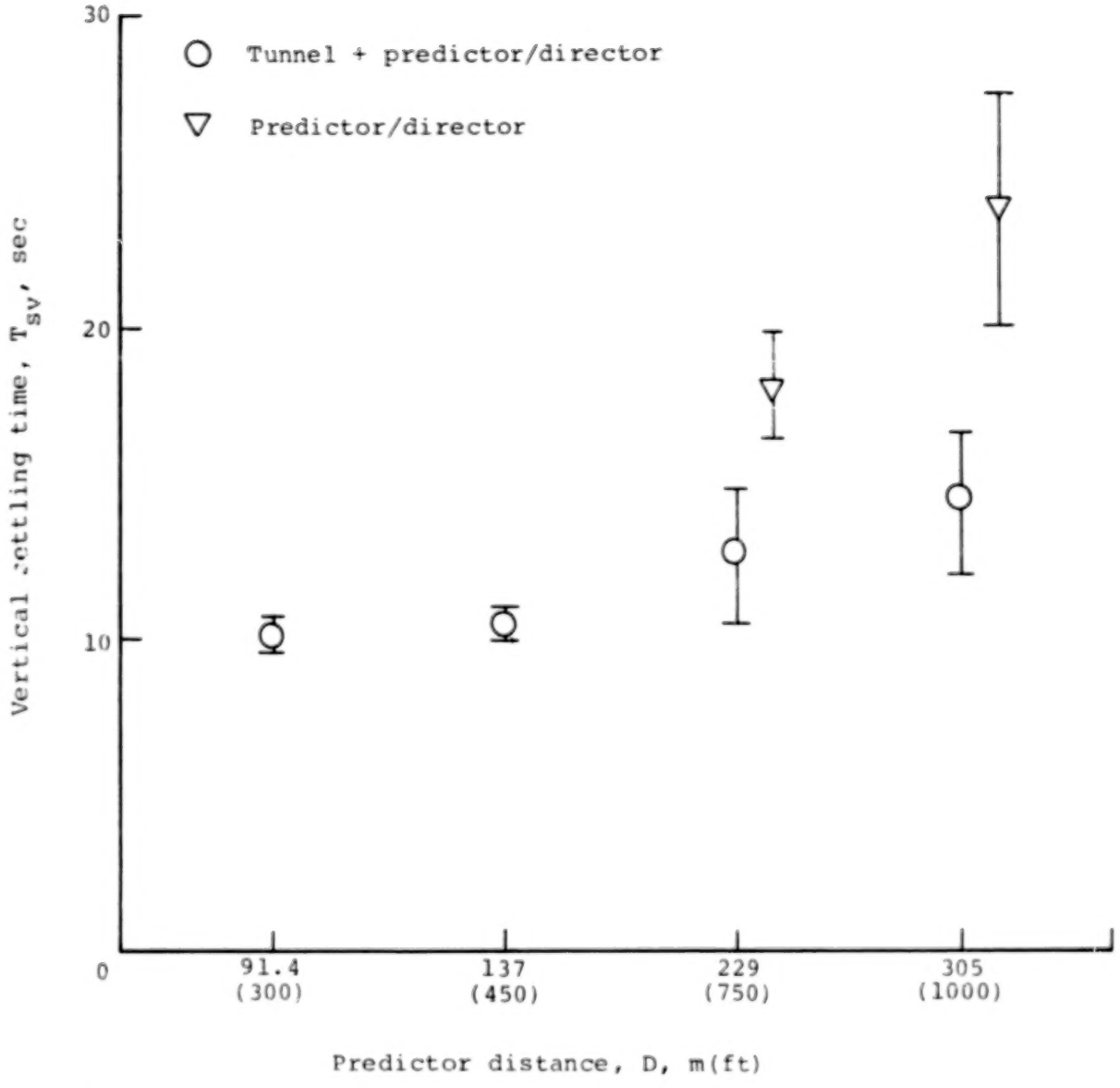

Figure 29.- Results of trajectory entry experiment; effect of D on vertical settling time, subject 1.

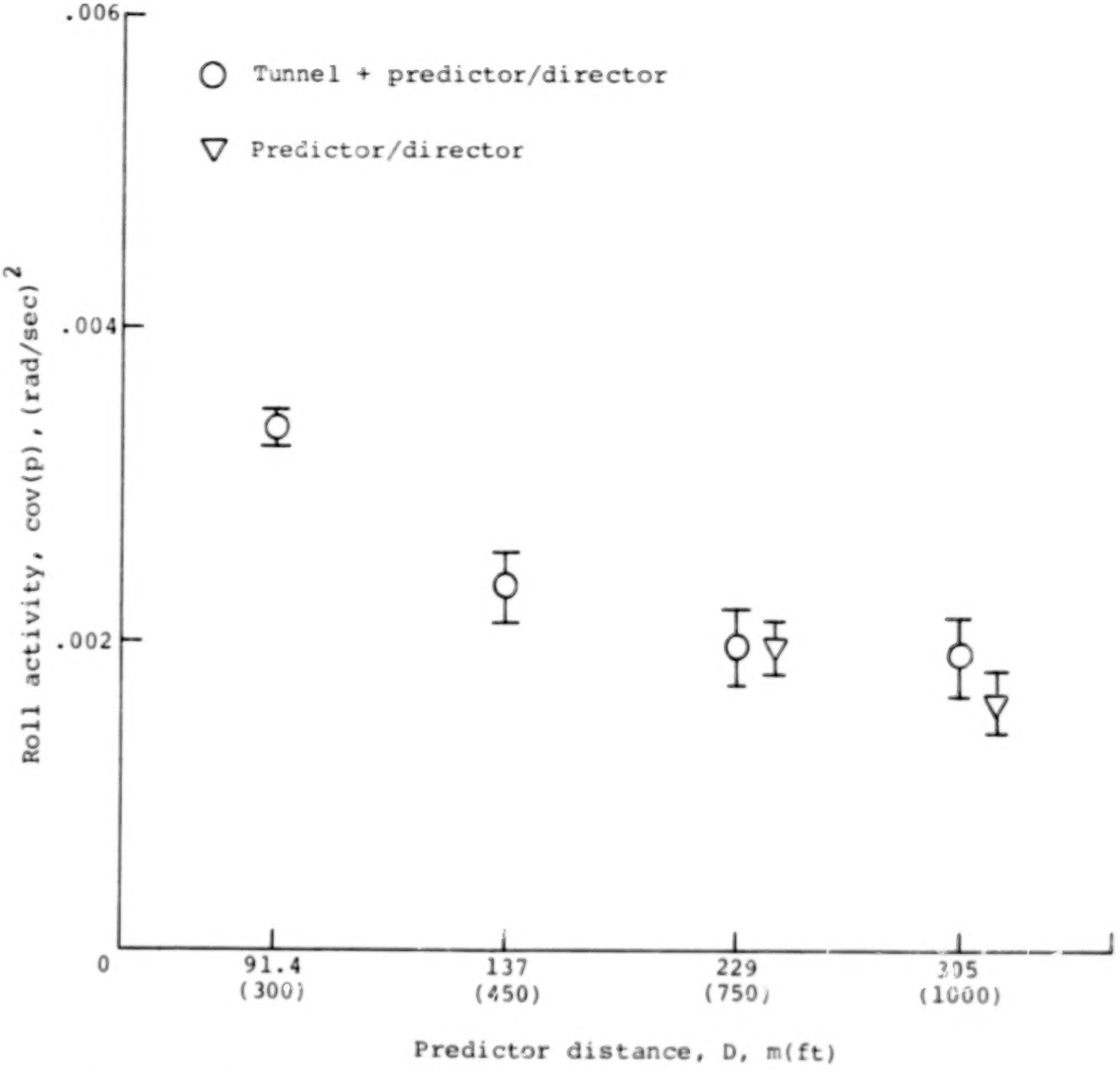

Figure 30.- Results of trajectory entry experiment; effect of D on roll activity, subject 1.

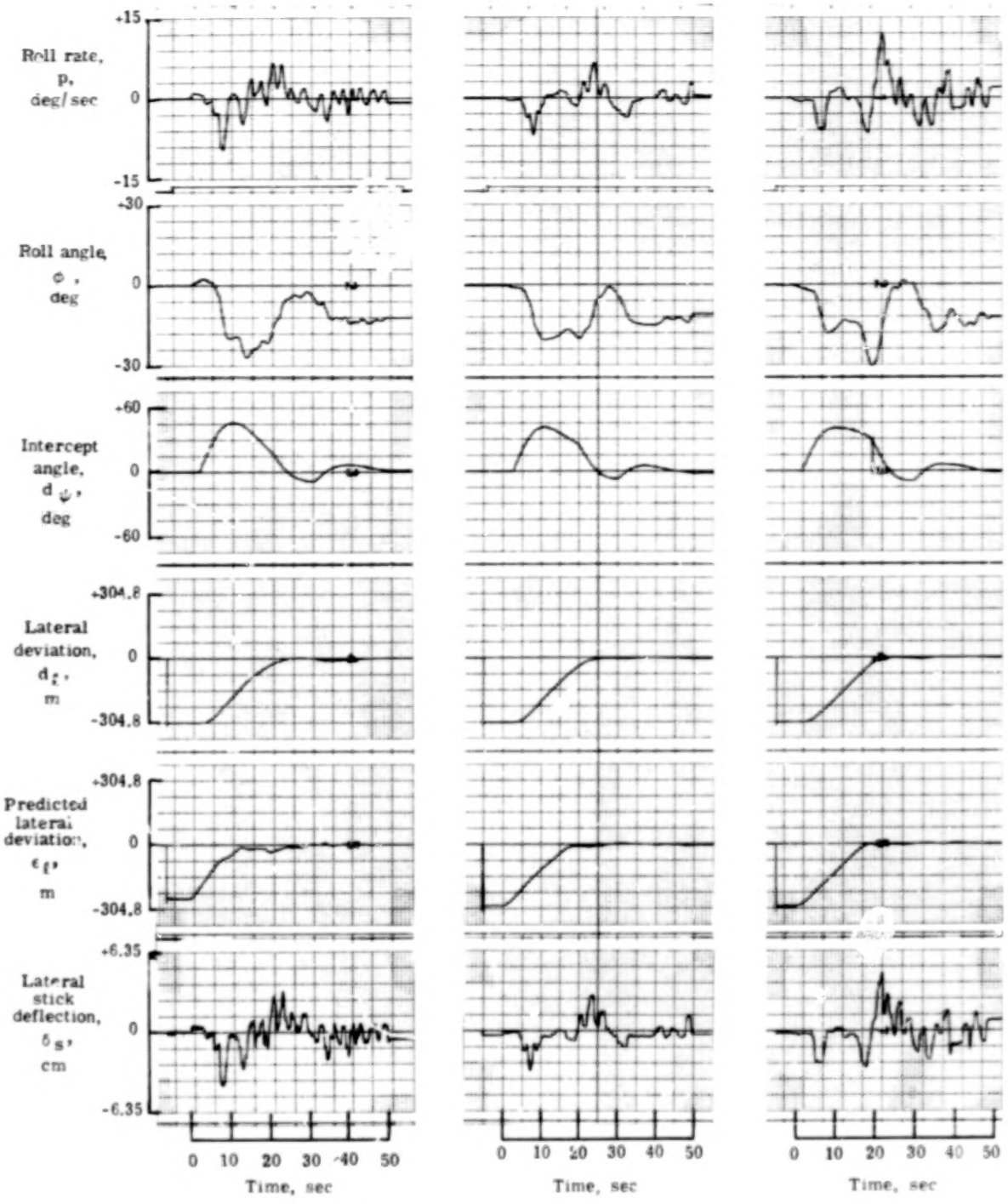

(a) Tunnel plus predictor/director; D = 229 m (750 ft).

(b) Tunnel plus predictor/director; D = 137 m (450 ft).

(c) Tunnel plus predictor/director; D = 91.4 m (300 ft).

Figure 31.- Time histories of lateral response for entry maneuvers; effect of D, initial location 2.

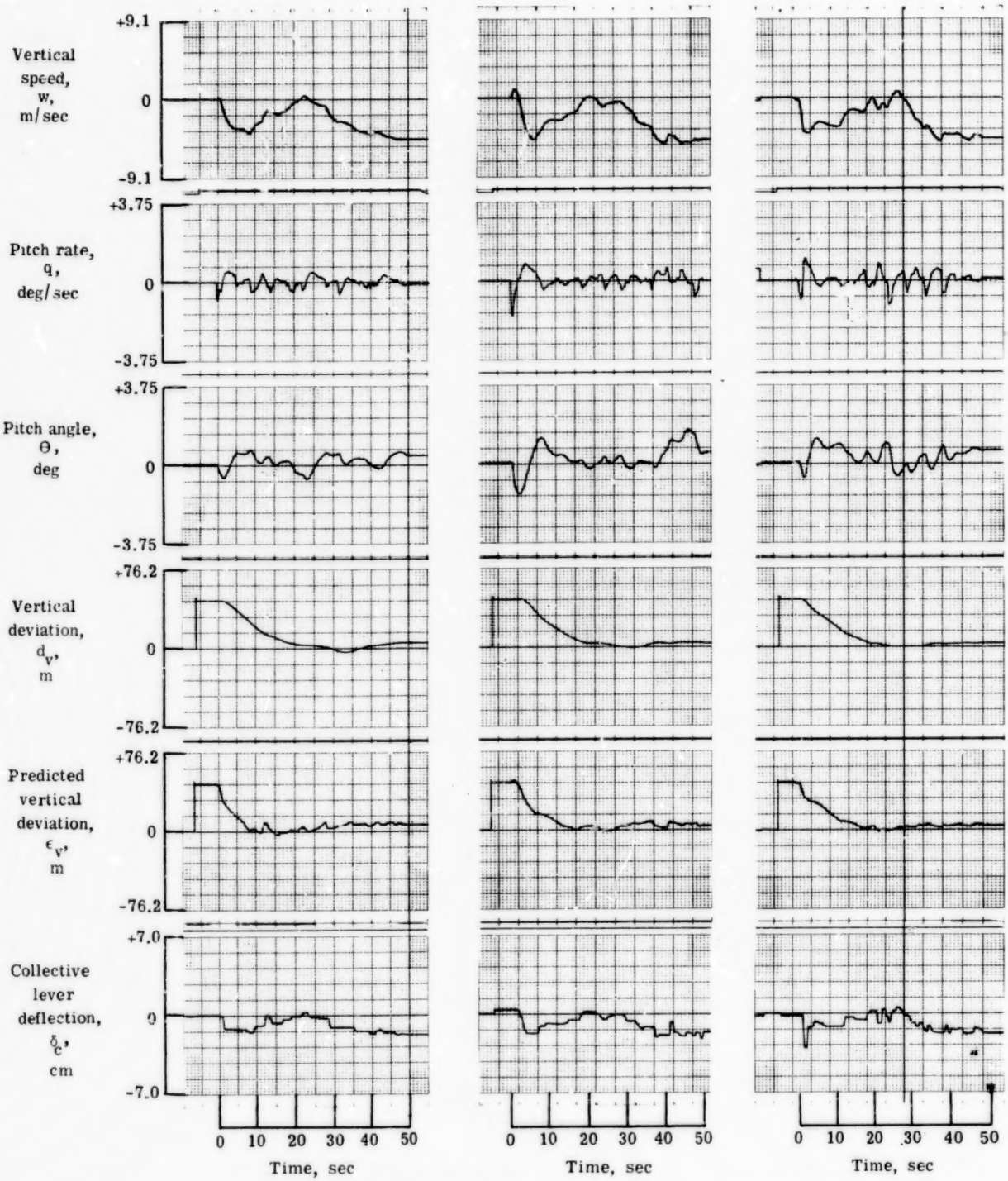

(a) Tunnel plus predictor/director; D = 229 m (750 ft).

(b) Tunnel plus predictor/director; D = 137 m (450 ft).

(c) Tunnel plus predictor/director; D = 91.4 m (300 ft).

Figure 32.- Time histories of vertical response for entry maneuvers; effect of D, initial location 2.

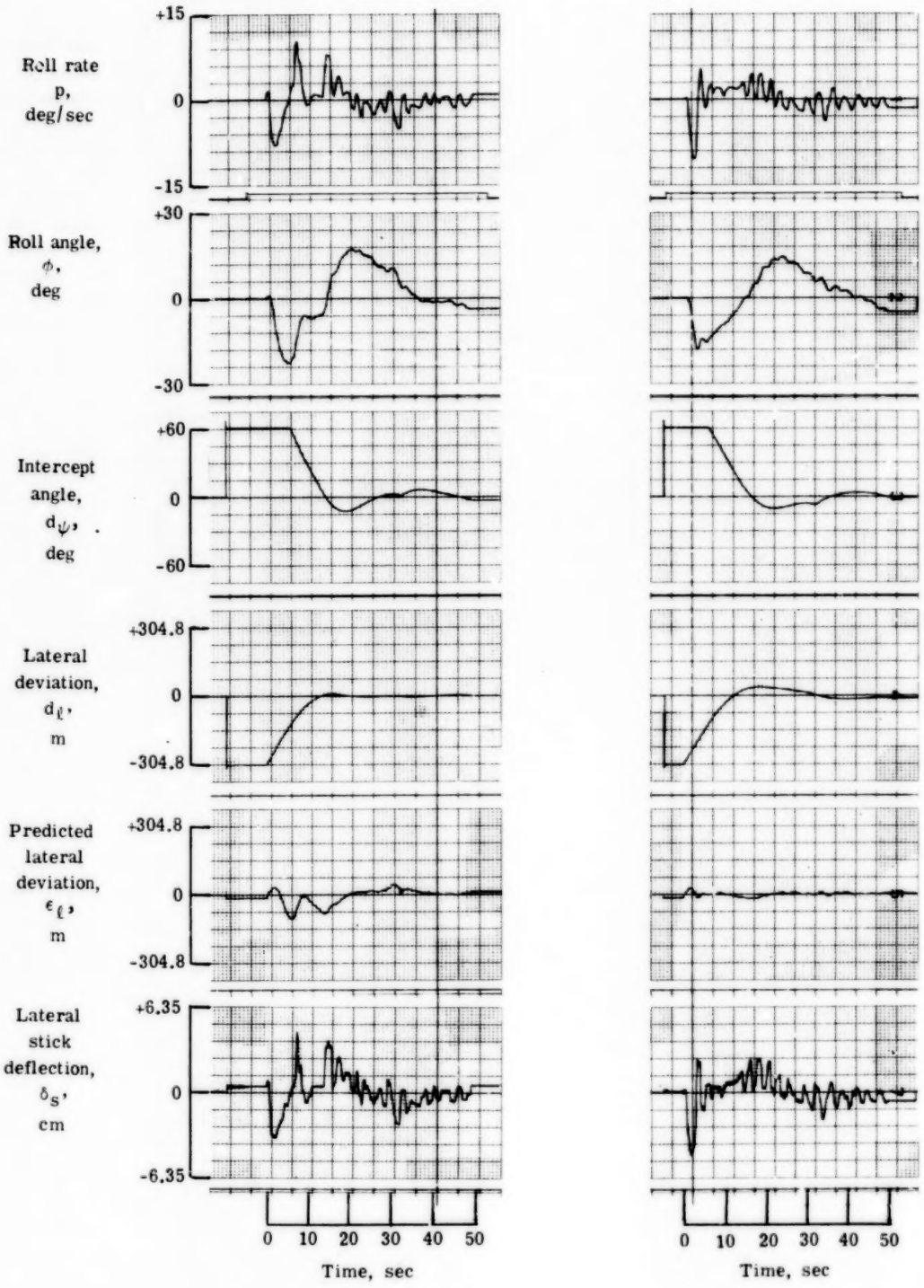

(a) Tunnel plus predictor/director; D = 305 m (1000 ft).

(b) Predictor/director; D = 305 m (1000 ft).

Figure 33.- Time histories of lateral response for entry maneuvers; comparison of tunnel plus predictor/director with predictor/director; initial location 4.

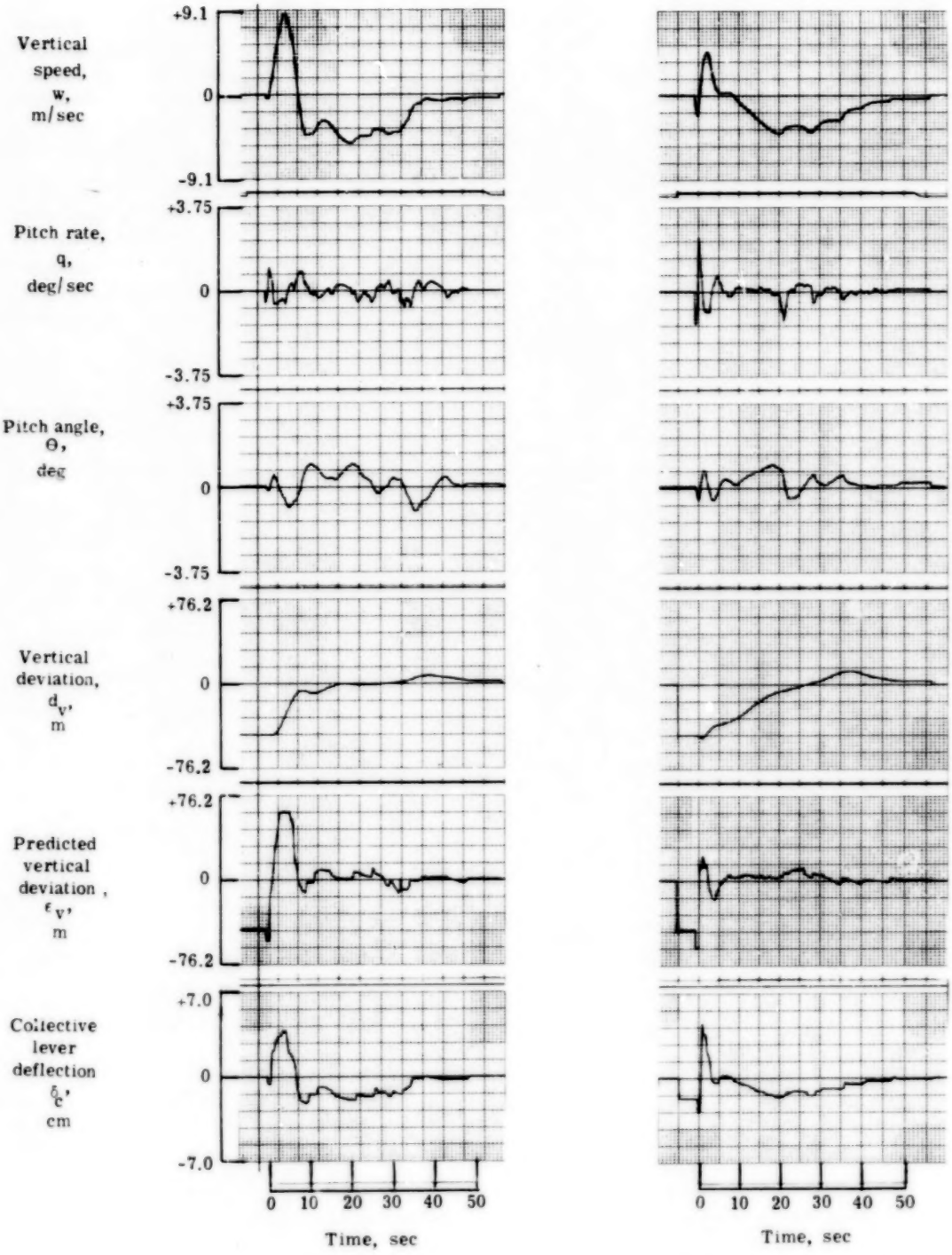

(a) Tunnel plus predictor/director; D = 305 m (1000 ft).

(b) Predictor/director; D = 305 m (1000 ft).

Figure 34.- Time histories of vertical response for entry maneuvers; comparison of tunnel plus predictor/director with predictor/director; initial location 4.

L-74-8035

Figure 35.- CH-47C helicopter – flight validation vehicle.

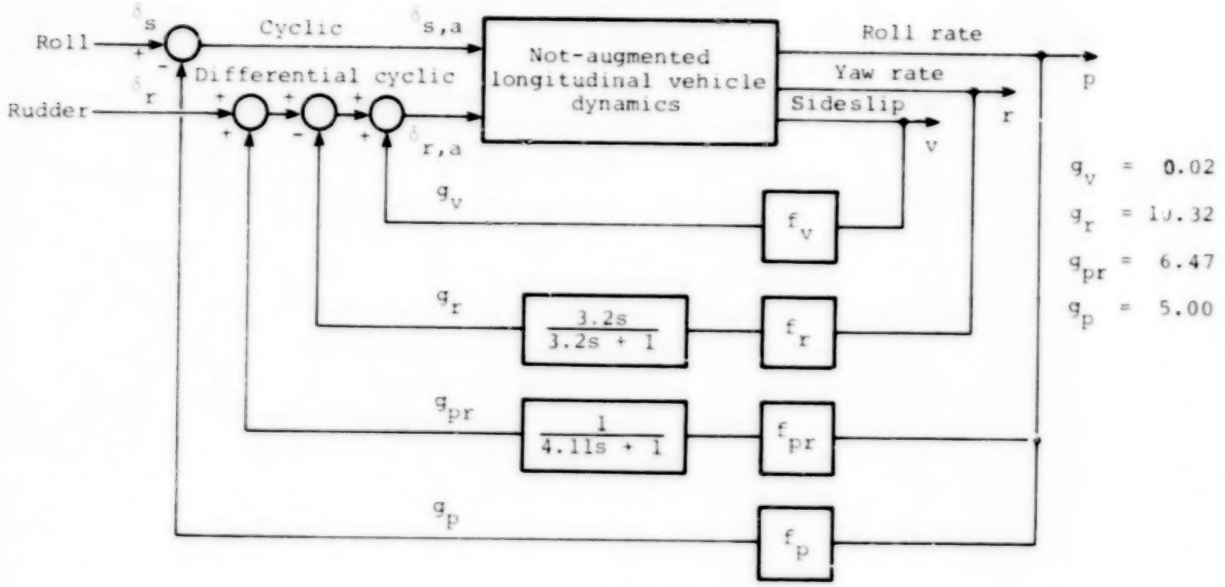

(a) Lateral.

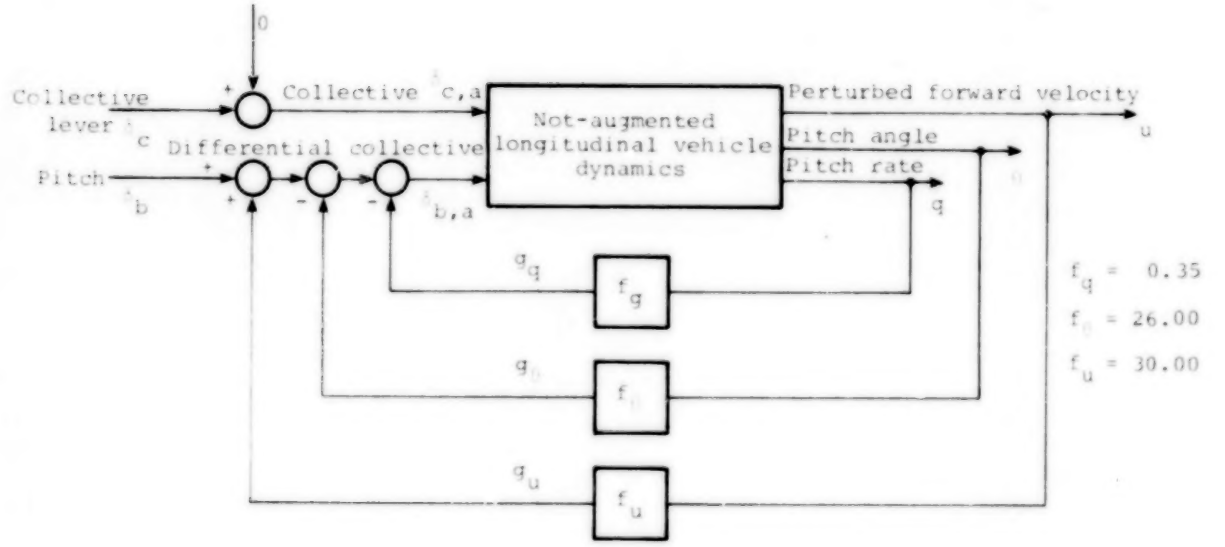

(b) Longitudinal.

Figure 36.- Block diagram of stability augmentation systems.

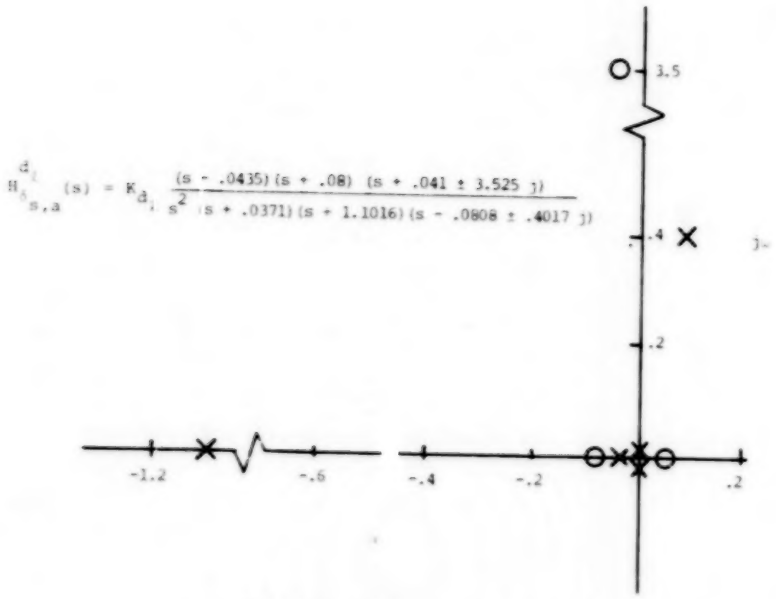

(a) SAS disengaged.

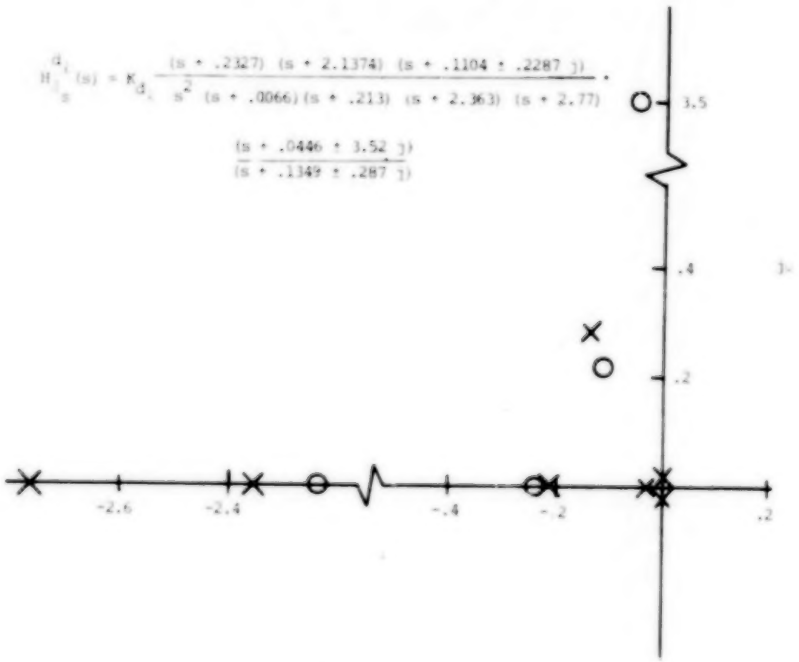

(b) SAS engaged.

Figure 37.- Complex-plane plot of pole-zero location of $H_{\delta_s}^{d_f}(s)$: j = imaginary axis, ω = frequency (rad/sec), and $\sigma = \zeta\omega_n$.

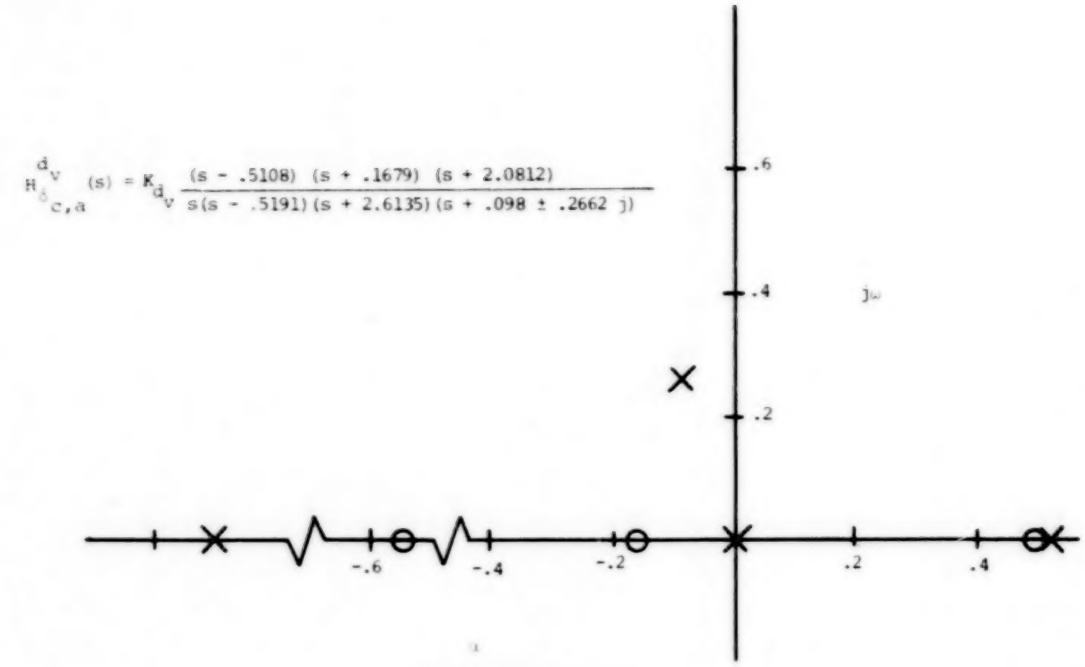

(a) SAS disengaged.

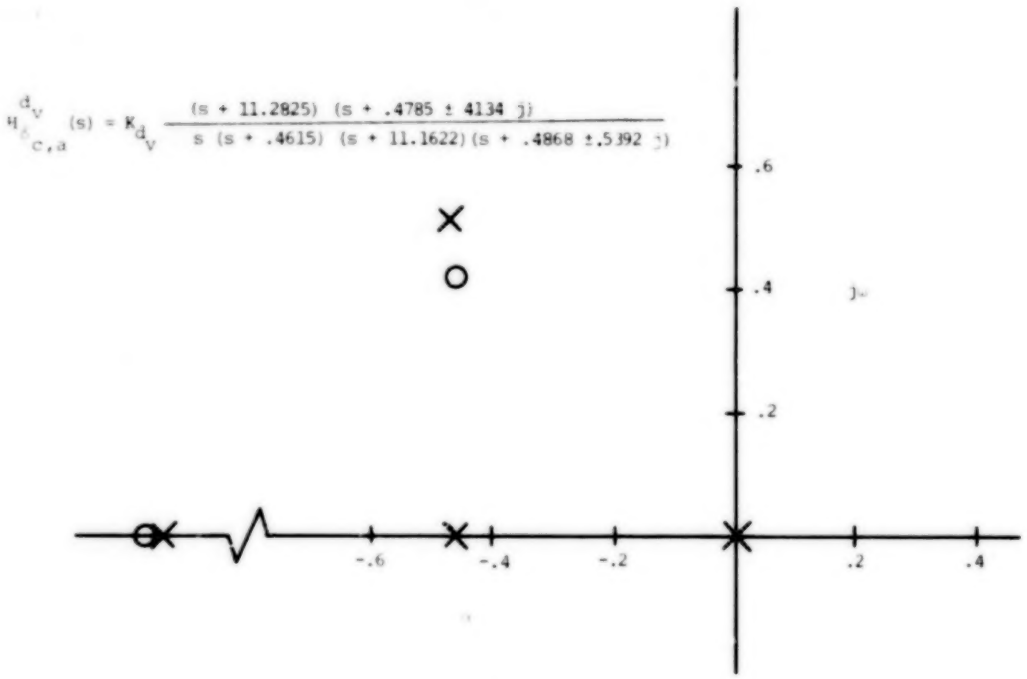

(b) SAS engaged.

Figure 38.- Complex-plane plot of pole-zero location of $H_{\delta_c}^{d_V}(s)$; j = imaginary axis, ω = frequency (rad/sec), and $\alpha = \zeta\omega_n$.

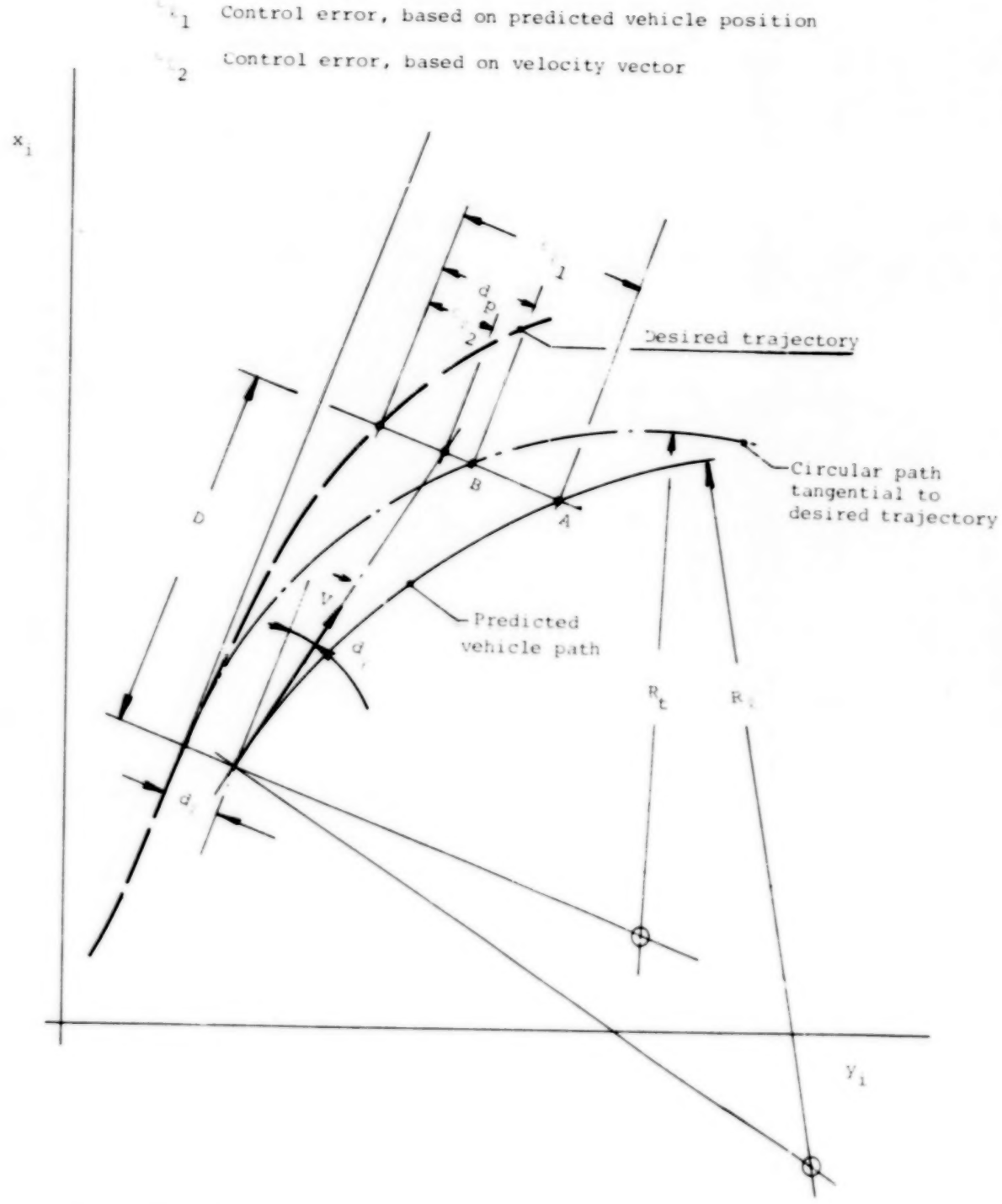

Figure 39.- Horizontal situation of following arbitrarily curved trajectory.

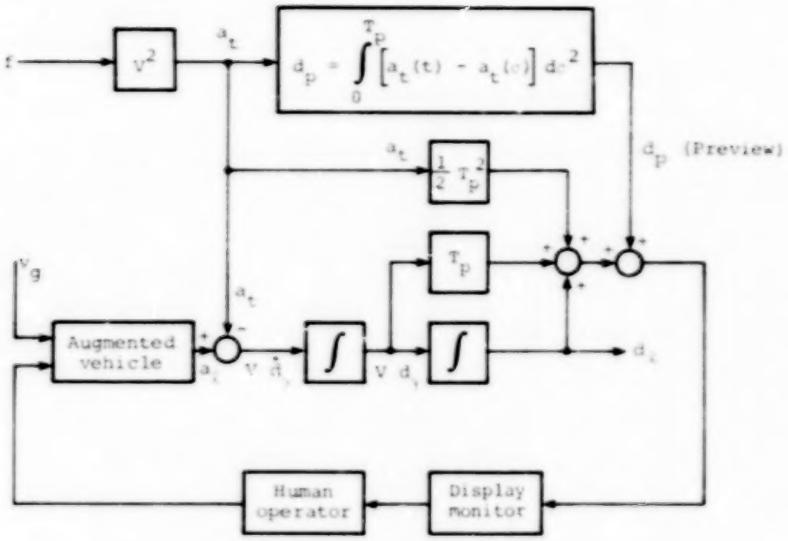

(a) Based on predicted vehicle position.

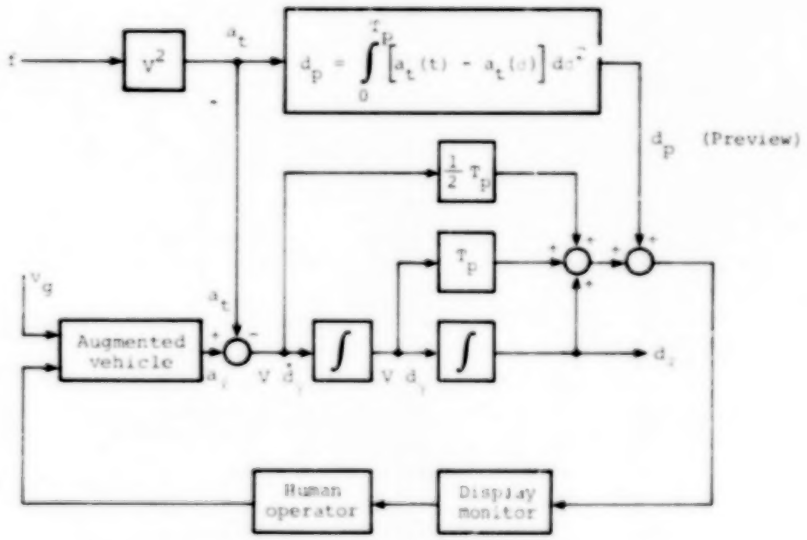

(b) Based on vehicle velocity vector.

Figure 40.- Block diagram of vehicular control.

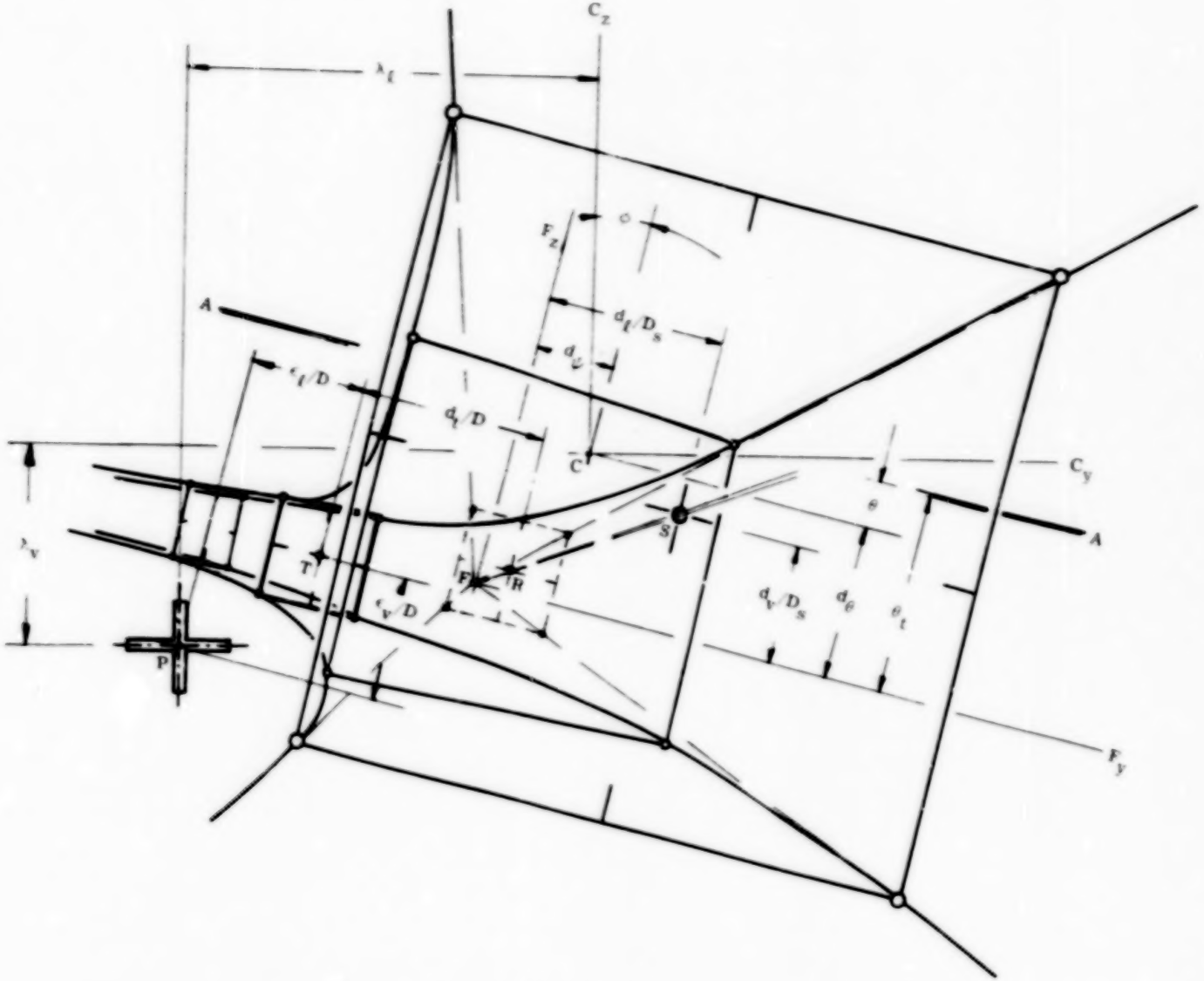

Figure 41.- Positional, rate, and directional cues derived from tunnel display.

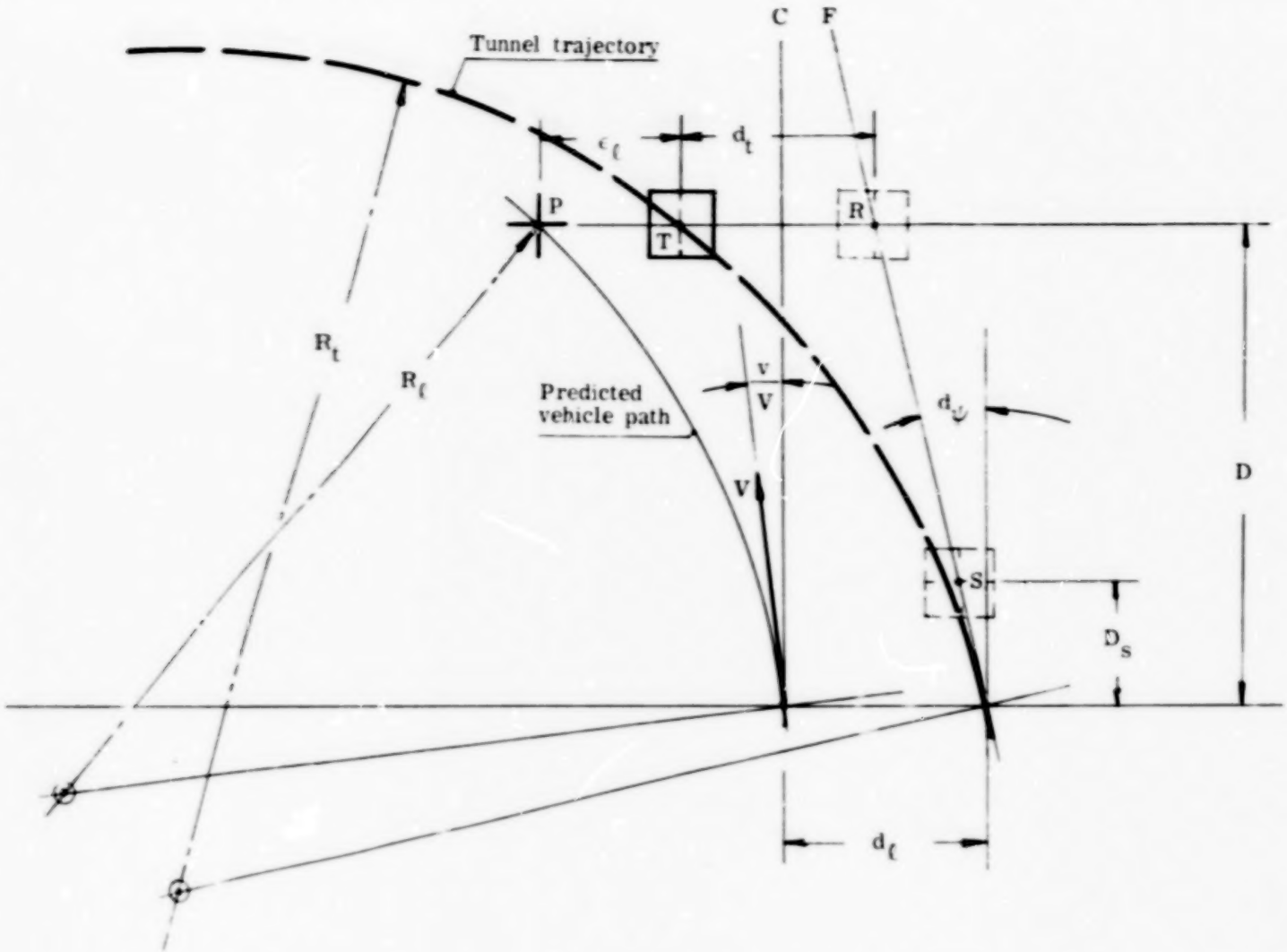

Figure 42. - Horizontal situation of figure 41.

1. Report No. NASA TP-1736	2. Government Accession No.	3. Recipient's Catalog No.
4. Title and Subtitle EVALUATION OF A COMPUTER-GENERATED PERSPECTIVE TUNNEL DISPLAY FOR FLIGHT-PATH FOLLOWING		5. Report Date December 1980 6. Performing Organization Code 505-34-23-01
7. Author(s) Arthur J. Grunwald, James B. Robertson, and Jack J. Hatfield		8. Performing Organization Report No. L-13253 10. Work Unit No.
9. Performing Organization Name and Address NASA Langley Research Center Hampton, VA 23665		11. Contract or Grant No. 13. Type of Report and Period Covered Technical Paper
12. Sponsoring Agency Name and Address National Aeronautics and Space Administration Washington, DC 20546		14. Sponsoring Agency Code

15. Supplementary Notes

Arthur J. Grunwald: NRC-NASA Resident Research Associate, now at Technion-Israel Institute of Technology, Haifa, Israel.
James B. Robertson and Jack J. Hatfield: Langley Research Center, Hampton, Virginia.

16. Abstract

The purpose of this study was to evaluate the use of a computer-generated perspective tunnel display for following a strongly curved flight path. The display was evaluated by monitoring pilot performance in a fixed-base simulator with the vehicle dynamics of a CH-47 tandem-rotor helicopter. Superposition of the predicted future vehicle position on the tunnel image was also investigated to determine whether, and to what extent, it contributes to better system performance (the best predicted future vehicle position was sought).

Three types of simulator experiments were conducted: following a desired trajectory in the presence of disturbances; entering the trajectory from a random position, outside the trajectory; detecting and correcting failures in automatic flight.

The tunnel display with superimposed predictor/director symbols was shown to be a very successful combination, which outperformed the other two displays in all three experiments. A prediction time of 4 to 7 sec was found to optimize trajectory tracking for the given vehicle dynamics and flight condition. Pilot acceptance of the tunnel plus predictor/director display was found to be favorable, and the time the pilot needed for familiarization with the display was found to be relatively short.

17. Key Words (Suggested by Author(s))	18. Distribution Statement
Integrated display format Fixed-base simulation Flight demonstration Predictive symbology Perspective tunnel display Real-world symbology	Unclassified – Unlimited Subject Category 06

19. Security Classif. (of this report)	20. Security Classif. (of this page)	21. No. of Pages	22. Price*
Unclassified	Unclassified	97	A05

* For sale by the National Technical Information Service, Springfield, Virginia 22161

NASA-Langley, 1980

END

March 4, 1981